



**POLITECNICO
DI TORINO**

DEPARTMENT OF ELECTRONICS AND TELECOMMUNICATIONS
Master's Degree in Electronic Engineering

Master's Degree Thesis

**Electrochemical processing, packaging and
characterization of high-density implantable
neural probes for in-vivo recording**

Supervisors:

Prof. Danilo Demarchi

Prof. Maysam Chamanzar

Candidate:

Andrea Bonaccorso

March, 2020

Abstract

Implantable neural probes represent one of the most revolutionary technologies of the last years, having experienced a large growth because of the wide range of applications in which they can be adopted, ranging from the treatment of neurological disease to the Internet of Things. They aim to record or stimulate the neurons activity using thin needles to be implanted into the brain cortex, with a depth and location depending on the particular device purpose.

The biggest challenge for a more massive use of human machine interfaces for biomedical applications is related to the capability of developing small devices with a high density of recording/stimulation sites, able to last long in a biological medium. That happens because unconventional materials for microfabrication processes have to be used, even if micromachining is not well developed for such materials. Thus, it is the case of stainless steel used to give robustness and flexibility to devices substrates, as well as Parylene C to ensure biocompatibility and good insulation performance: both of them have been adopted to realize the devices used in this thesis work.

After the fabrication process, some customization procedures need to be adopted to improve quality of the surfaces. Electropolishing and electroetching are two valid candidates for this purpose: the procedures have been implemented to get hybrid flexible/stiff devices with smooth edges, avoiding the possibility to damage the recording sites or changing the electrical insulator properties.

In terms of packaging, correctly interfacing the device with the electrical setup for the recording operation could be challenging due to the fragility of the device itself. This operation needs to be customized in such a way that the mechanical stress for the device is minimized, without losing in signal quality, in terms of parasitics and yield of the packaging procedure. Adhesive flip chip bonding and Zero Insertion Force (ZIF) connectors have been used to obtain this result, by interfacing the probe back-end with customized flexible Printed Circuit Boards (PCBs).

Then, each device needs to be electrically characterized, to ensure good performance before the in-vivo implantation or to modify the fabrication process if major problems are encountered during the result analysis. Electrochemical Impedance Spectroscopy (EIS) is the technique adopted in this thesis work to analyze both the response of one single recording site and the crosstalk effects between two traces. The implemented setup uses a PCB board to switch between all the probe channels, resulting in an automatic routine that makes the process fast and increases reliability.

Another important aspect of implantable devices characterization is the estimation of the mean time to failure after the insertion in a biological tissue. The device aging has been artificially carried on and the probe electrical properties have been analyzed over time starting from different aging conditions.

Finally, the last step of the characterization is to test how each recording site responds to an electrical stimulus that emulates the neuron activity, before performing the in-vivo characterization directly on animals brain.

Keywords: Implantable neural probes, electroetching, electropolishing, packaging, electrical characterization, accelerated aging, in-vivo characterization.

Acknowledgements

Foremost, I would like to thank my parents for the support they have shown me during this experience, for the financial aid and for motivating me in times of difficulty.

I would like to thank my supervisor, prof. Danilo Demarchi because he proposed me to carry out this project abroad, providing me the contact I needed, helping and guiding me in the months before my departure and after my return.

I want to say thanks to prof. Maysam Chamanzar for allowing me to join his team, for giving me advices and following me along the way during the last six months. In particular, I appreciated how he made me feel part of the group despite the short period spent there, how he spurred me to give my best and how he guided me when I needed help.

This thesis work would not have been accomplished if not for the assistance of many people at Carnegie Mellon University. Of all, I want to thank Zabir for being the mentor and for guiding me among the several aspects of the project: he taught me everything I had to know about the neural probes, starting from microfabrication processes up to characterization level, advising me on the way forward and on the right decisions to make. I also want to thank Jay, for the valuable work in advising and helping me during the path.

Together with them, all the other people of the probe team, Hassan, Mats, Vishal, and the ones on the acousto-optic team, Matteo, Hengji, Yasin, for chats and productive meetings.

I also want to say thanks to my relatives, they are too many to list all of them by name, but they have my thankfulness for the support and the interested shown in my project and developments during my period abroad.

Finally I want to thank my friends, in Turin and Sutri, for laughter, advices and moments spent together during the university years.

Contents

Abstract	I
Acknowledgements	III
List of Figures	VIII
List of Tables	XII
List of Acronyms	XIV
1 Introduction to neuronal recording	1
1.1 The neuron	2
1.2 Neuronal response	4
1.3 Recording methodologies	6
1.3.1 Non-invasive BCI	7
1.3.2 Invasive BCI	12
1.4 Steeltrodes and polymer probes for in-vivo recording	15
2 Post-fabrication improvements	18
2.1 Polishing/etching process	19
2.1.1 Oxalic acid in DI water EP	21
2.1.2 Phosphoric acid and Sulphuric acid mixture EP	26
2.1.3 Two steps EP	29
2.1.4 Wet etching on steeltrodes	30
3 Packaging	32
3.1 Flip-chip bonding	32
3.1.1 Flip-chip joining using adhesives	34
3.2 ZIF connectors packaging	37
4 Electrical characterization	39
4.1 Impedance model	39
4.2 EIS characterization	42
4.2.1 Electrodes configuration	42
4.2.2 Potentiostat	43
4.2.3 Interfacing board	45
4.2.4 Measurement setup	47
4.2.5 Results and discussion	48
4.3 Crosschannel characterization	49
4.3.1 Crosstalk effect	49
4.3.2 Measurement setup	50
4.3.3 Results and discussion	52

5 Accelerated Lifetime Testing	54
5.1 Aging in unperturbed conditions	55
5.1.1 Results and discussion	55
5.2 Aging in perturbed conditions	57
5.2.1 Results and discussion	58
5.3 Statistical analysis on failures	60
6 Stimulation for in-vivo characterization	62
6.1 Synthetic stimulation	62
6.1.1 Measurement setup	64
6.1.2 Result and discussion	65
7 Conclusions	70
7.1 Future works	72
Bibliography	73

List of Figures

1.1	A woman uses a BMI to move a robotic arm and drink coffee [1]	1
1.2	The neuron [3]	2
1.3	Neuron membrane acts as a pump for ions inside and outside the cell. Polarization conditions: a) membrane polarized (or resting) b) membrane depolarized c) membrane hyperpolarized	3
1.4	Membrane potential: when the potential overcome the threshold the neuron is activated and an action potential is generated [6]	4
1.5	Most popular technologies for brain recording [7]	6
1.6	EEG recording system [8]	7
1.7	EEG signals [10]	8
1.8	MEG recording system on a child [11]	8
1.9	MRI equipment [12]	9
1.10	MRI brain mapping examples: a) fMRI b) dMRI [19, 20]	10
1.11	CAT acquisition technique [21]	10
1.12	PET acquisition technique [24]	11
1.13	ECoG acquisition technique [30]	12
1.14	Glass micropipette [33]	13
1.15	Metal microelectrode [34]	13
1.16	a) Utah array, b) Michigan array, c) Microwire, d) flexible probe [37, 38, 39, 40]	14
1.17	Fabrication process: a) steeltrode, b) flexible polymer probe [46]	16
1.18	Implemented steeltrode for neuronal recording	17
1.19	Implemented polymer probe for neuronal recording	17
2.1	Steeletrode after wafer release	18
2.2	EP process [50]	19
2.3	a) Fundamental voltage-current density electropolishing curve [51], b) Voltage-current characteristic of fabricated steeltrodes in phosphoric-sulphuric acid mixture	20
2.4	Probe sidewall for different polishing times: a) no polishing, b) 1 min, c) 1.5 min, d) more than 2 min	22
2.5	SEM of probe sidewall: a) before polishing, b) after 2 minutes of polishing	22
2.6	Deburring effect: a) burrs on the border of the stainless steel substrate, b) result after the polishing	23
2.7	Probe tip improvements: a) unpolished tip, b-c) polished tip, d) SEM of polished tip	23
2.8	AC waveform for EP [56]	24
2.9	AC EP results for two different samples: a) opaque spots on the sidewall (with an applied offset), b) interface between the polished and unpolished sections (with no offset) from the backside of the probe	25
2.10	AC+DC EP result a) probe sidewall before the process, b) sidewall after the process	26
2.11	Phosphoric acid + sulphuric acid EP: a) unpolished probe sidewall (large grain), b) polished probe sidewall (fine grain), c) unpolished probe sidewall (fine grain), d) polished probe (fine grain)	27

2.12 Phosphoric acid + sulphuric acid 3D scan profile: a) unpolished probe sidewall, b) polished probe sidewall	27
2.13 Bubbles after long time EP process	28
2.14 Two steps EP: a) unpolished probe sidewall, b) polished probe sidewall c) SEM of unpolished probe sidewall, d) SEM of polished probe sidewall	29
2.15 Two steps polishing 3D scan profile: a) unpolished probe sidewall, b) polished probe sidewall	30
2.16 EE on steelrode: a-b) hybrid probe after the process, c-d) particular of the interface between the flexible and rigid sections	31
3.1 Flip-chip bonding technique [61]	33
3.2 NCA flip-chip bonding technique [64]	34
3.3 ICF flip-chip bonding technique [65]	35
3.4 ACF flip-chip bonding technique [64]	35
3.5 Steeltrodes packaging using flip chip: a) before packaging, b) after packaging (quarter dollar shows the scale)	36
3.6 ZIF connector (Memcon)	37
3.7 Steeltrodes packaging using ZIF: a) before packaging, b) after packaging (quarter dollar shows the scale)	37
3.8 Polymer probes packaging procedure: a) Kapton tape to increase stiffness, b) final result (tweezers show the scale)	38
4.1 Equivalent circuit model of electrode-electrolyte interface	40
4.2 Electrical acquisition chain	40
4.3 Electrode examples: a) no plated, b) plated	41
4.4 Counter and reference electrodes used for measurements (<i>BASI Inc</i>)	43
4.5 Three electrodes EIS measurement configuration.[74]	43
4.6 Circuitual schematic of a potentiostat [75]	44
4.7 PGSTAT302N potentiostat (Metrohm AUTOLAB)	44
4.8 Schematic of the designed circuit	46
4.9 Interfacing board: a) PCB design, b) PCB after soldering	47
4.10 Measurement setup for EIS characterization	47
4.11 EIS characterization for a 30 channels steelrode	48
4.12 Crosstalk model of two recording electrodes with adjacent channels [70]	49
4.13 Crosstalk model between two channels	50
4.14 Combinations handling principle	51
4.15 Measurement setup for crosschannel characterization	52
4.16 Results of crosstalk characterization for a 30 channels probe	52
4.17 Analysis on metal failures in a 16 channels probe	53
5.1 ALT processes	54
5.2 Results for ALT under unperturbed conditions: a) intense insulator fail, b) metal fail, c) slight insulator fail, d) no fails	55
5.3 Results for ALT in perturbed conditions, $T = 60\text{ }^{\circ}\text{C}$: a) intense insulator fail, b) metal fail, c) slight insulator fail, d) no fails	58
5.4 Results for ALT in perturbed conditions, $T = 60\text{ }^{\circ}\text{C}$ and H_2O_2 in PBS: a-b)intense insulator fail, c) no fails	59
5.5 Statistical analysis on insulation failures	61
6.1 Stimulation electrode (<i>Microprobes for Life Science</i>)	62
6.2 Stimulating electrode approaching the recording site in: a) high density tip, b) high density shank, c) commercial probe (<i>Plexon</i>) (Camera images through PBS solution)	63
6.3 Synthetic characterization measurement setup	64

LIST OF FIGURES

6.4	Electrical components for synthetic stimulation: a) ZIF to Omnetics PCBs, b) Intan amplifier	64
6.5	Intan technologies software interface for the stimulation of a low density steeltrode	65
6.6	Baseline noise for a high density tip steeltrode	66
6.7	Baseline noise for a commercial high density probe (<i>Plexon</i>)	66
6.8	Stimulation results for a high density tip steeltrode: a) amplitude, b) SNR	67
6.9	Stimulation results for a high density shank steeltrode: a) amplitude, b) SNR	68
6.10	Synthetic stimulation to check the trace delamination	69

List of Tables

2.1	Most relevant experiments conducted in Oxalic acid by varying the voltage parameters and the EP time	25
2.2	Most relevant experiments conducted in AC-DC domains	25
2.3	Most relevant experiments conducted in Phosphoric and Sulphuric acid mixture by varying the voltage parameters and the EP time	28
2.4	Process parameters for two steps EP	29
4.1	Main components used for the design	46
5.1	Results for ALT under unperturbed conditions	56
5.2	Results for ALT under perturbed conditions ($T = 60\text{ }^{\circ}\text{C}$)	59
5.3	Results for ALT under perturbed conditions ($T = 60\text{ }^{\circ}\text{C}$ and H_2O_2 in PBS)	60

List of Acronyms

BMI	Brain Machine Interface
IoT	Internet of Things
BCI	Brain Computer Interface
ECoG	Electrocorticography
EEG	Electroencephalography
MEG	Magnetoencephalography
SQUID	Superconducting Quantum Interference Devices
SERF	Spin Exchange Relaxation-Free
MRI	Magnetic Resonance Imaging
fMRI	Functional Magnetic Resonance Imaging
dMRI	Diffusion Magnetic Resonance Imaging
PET	Positron Emission Tomography
SPECT	Single Photon Emission Computed
CAT	Computed Axial Tomography
EIT	Electrical Impedance Tomography
NIR	Near Infrared Tomography
SUA	Single Unit Activity
MUA	Multi Unit Activity
SNR	Signal to Noise Ratio
MEA	Multiple Electrode Array
MEMS	Microelectromechanical Systems
CVD	Chemical Vapor Deposition
PEG	Polyethylene Glycol
EP	Electropolishing
AC	Alternate current/voltage
DC	Direct current/voltage

DI	Deionized
SEM	Scanning Electron Microscope
EE	Electroetching
PCB	Printed Circuit Board
ZIF	Zero Insertion Force
NCA	Non Conductive Adhesive
ICF	Isotropic Conductive Film
ACF	Anisotropic Conductive Film
CPE	Constant Phase Element
EIS	Electrochemical Impedance Spectroscopy
PBS	Phosphate Buffered Saline
CE	Counter Electrode
RE	Reference Electrode
WE	Working Electrode
PC	Potential Control Amplifier
VF	Voltage Follower
CF	Current Follower
OCP	Open Circuit Potential
CMOS	Complementary Metal Oxide Semiconductor
DIO	Digital Input-Output
ASTM	American Society for Testing and Materials
RAA	Reactive Accelerated Aging
ROS	Reactive Oxygen Species

Chapter 1

Introduction to neuronal recording

Neuronal recording is the basis for the study of the human brain and acts as the connection between the human body and each electrical devices that can be controlled without exploiting the muscular system. It represents the basis to any Brain Machine Interface (BMI) used nowadays in biomedicine to help people mutilated or affected by neuromuscular diseases. As an example, the *Figure 1.1* shows the potential of such a technology in improving people's lives by helping a paralyzed woman to move a robotic arm.

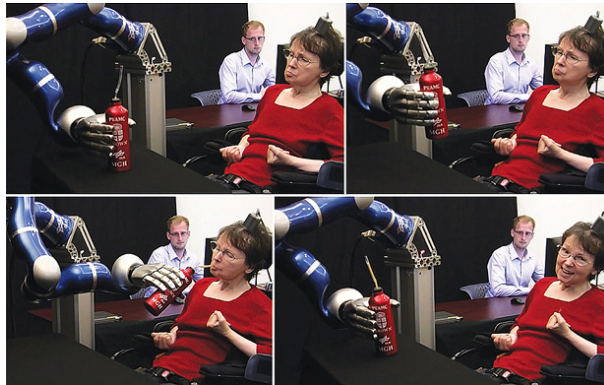


Figure 1.1: A woman uses a BMI to move a robotic arm and drink coffee [1]

At the same time, studying the brain through neuronal recording is a way to understand better brain diseases such as Alzheimer's or Parkinson's and find new methodologies for their treatment. Moreover, it could become a challenge to improve already existing technologies or some in development such as the Internet of Things (IoT), in which people might be able to interact with electrical objects using thought.

In a wide range of cases, these technologies exploit a direct contact between some bioelectronic devices and the human brain so that most of the research strengths are focused on making this interaction as less invasive as possible without losing in recording operation performance. Some important results have led to the discovery of new materials that do not cause rejection or that increase devices flexibility, resulting in a reduction of risks for brain tissue.

But some aspects of the research are still being studied. For example, the possibility of mixing neuroscience and optogenetics in order to combine optical stimulation and electrical recording to provide additional informations on particular ways of functioning of the brain.

1.1 The neuron

A neuron is the basic working unit of the brain that communicates with other cells via specialized connections called synapses. The average human brain contains around 86 billion neurons and, compared with all the cells of the body, the most important property is the capability of propagating signals quickly up to great distances [2]. This is possible thanks to the specific cell physiognomy showed in *Figure 1.2*.

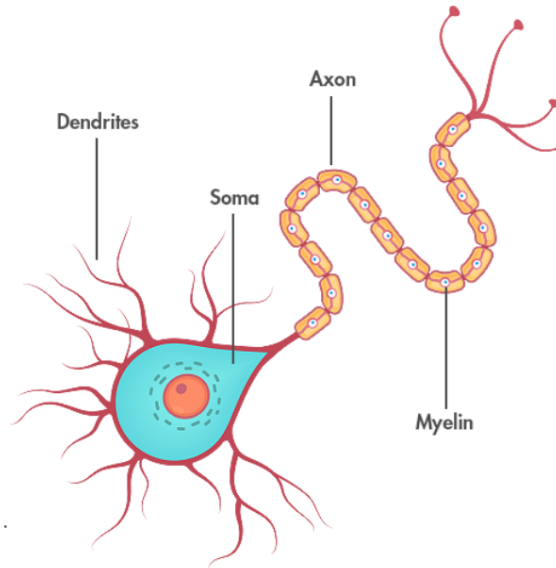


Figure 1.2: The neuron [3]

A useful analogy is to think of a neuron as a tree with three main parts [4]:

- **dendrites:** they are the branches of the tree, where a neuron receive inputs from other cells;
- **soma:** it is the trunk, where the nucleus is located and where most of the proteins are produced to be transported throughout the axon and dendrites;
- **axon:** it is the the root of the tree, used to send output signals towards other cells;

This kind of structure is extremely branched thanks to the synaptic connections that make a neuron able to receive multiple inputs from lots of other neurons. Moreover, neurons present physiological specializations such as membrane-spanning ion channels to exchange ions with the outside of the cell. The most frequent ions are potassium (K^+), sodium (Na^+), calcium (Ca^{2+}) and chloride (Cl^-) [5].

From an electro-chemical point of view, ions inside and outside the cell create different potentials. Generally, under resting conditions, inside the cell the potential is more negative, around -70 mV , with respect to the outside [4]. This condition is called polarization. Ions pumps in the membrane maintain concentrations to support resting conditions, in the specific case Na^+ is more concentrated outside the cell and K^+ inside it. Whenever the flux through the membrane changes, and so the concentrations, the value of that potential changes too: sometimes the potential (termed as "membrane potential") becomes less negative (so it increases) and other times more negative. In the first case, negative charges flow out of the cell, or positive come in, so there is a condition of depolarization. On the contrary, in the second case there is a condition of hyperpolarization because positive charges flow out or negative ones come in. The *Figure 1.3* shows these conditions.

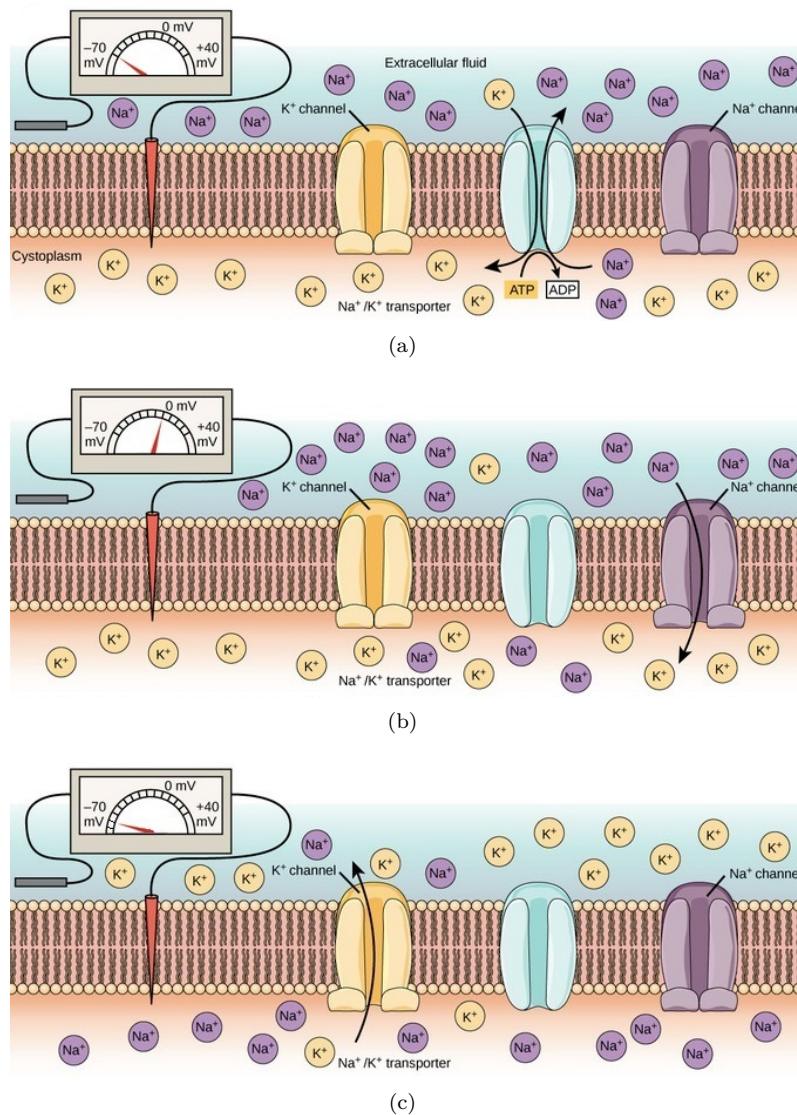


Figure 1.3: Neuron membrane acts as a pump for ions inside and outside the cell. Polarization conditions: a) membrane polarized (or resting) b) membrane depolarized c) membrane hyperpolarized

If the neuron reaches a certain threshold set to -50 mV , it becomes sufficiently depolarized to generate a signal called *action potential* or *spike*. The latter is the electrical signal that travels all along the axon and reaches all the adjacent neurons. In other words, it is the message that makes neurons able to communicate. During the period in which the spike moves through the cell, the neuron is considered activated and its activity takes the name of "neuronal firing".

At the junction between two neurons (i.e. synapse) the neuron that "fires" causes the release of other chemical neurotransmitters: they can either excite or inhibit the following neurons from firing their own action potentials [4].

In *Figure 1.4* is reported the whole membrane potential cycle.

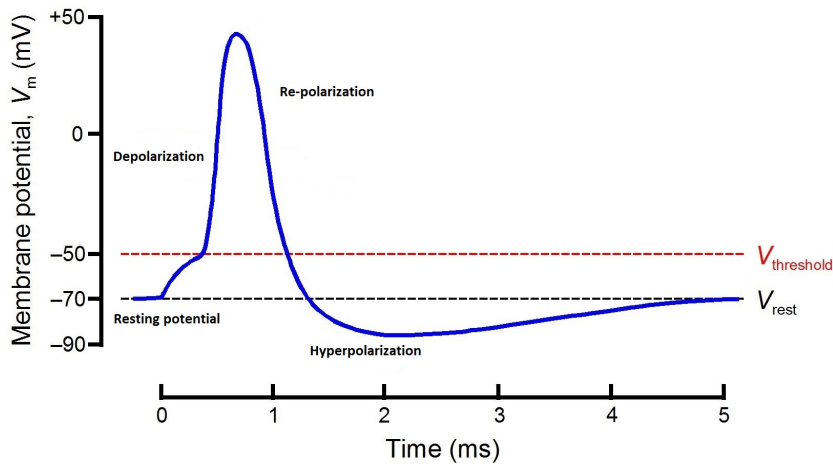


Figure 1.4: Membrane potential: when the potential overcome the threshold the neuron is activated and an action potential is generated [6]

As one can see, between the depolarization phase and the following hyperpolarization, there is an intermediate phase of re-polarization in which positive ions start going out of the cell making the potential more and more negative.

The process of evoked action potentials is continuous and make one spike be followed by another spike in time, causing the so called neuronal response.

1.2 Neuronal response

In general, depending on the brain activity intensity, a neuronal response can be seen as a sequence of spikes spaced in time. There are some physical constraints on the frequency that a sequence of spikes can achieve. These constraints can be summarized as "refractory periods". In fact, for after just few milliseconds an action potential has been fired, there is a first absolute refractory period in which, as the name suggests, no spikes are emitted. The second constraint is known as relative refractory period: it can last up to tens of milliseconds after a spike and in which it is almost impossible to see another spike follow the first one [5].

Although action potentials can have different duration, amplitude and shape, they can be treated as a sequence of the same copy in time. For this reason, by neglecting their brief duration which is around 1 ms, they can be represented as a pulse train [5]:

$$\rho(t) = \sum_{i=1}^n \delta(t - t_i) \quad (1.1)$$

where δ is the Dirac's function, $0 < t_i < T$ is the period of time in which the spikes are recorded and n is the number of the spikes in that period. As the notation suggests, at each instant of time i of the interval for one specific trial corresponds one spike and one only. In the expression (1.1), $\rho(t)$ takes the name of *neural response function*. Since the sequence of action potentials varies from trial to trial, typically probability or statistic are used to treat neuronal responses [5].

There are lot of figures of merit used in the neuro-recording field that help to handle different samples with similar features. The first one is the *spike-count rate*, obtained as the total number of action potentials in a trial divided by the duration of the trial [5]:

$$r = \frac{n}{T} = \frac{1}{T} \int_0^T \rho(\tau) d\tau \quad (1.2)$$

where $n = \int \rho(\tau) d\tau$ comes from the fact that the total number of spikes has to be computed as

the sum of each sample of the function ρ in the interval $[0, T]$.

The easiest way to compute spike-count rate is to average respect to one single trial, but this choice implies to get the worst temporal resolution for what concern variations during the course of the trial [5]. In other words, in this way the rate becomes time invariant and the information recorded is almost useless.

Another method to transform the rate in a time-dependent quantity, is to divide the trial in a finite number of intervals and compute the rate for each of them. Thus, the rate at time t will be the ratio between all the spikes occurred in the interval $[t, t + \Delta t]$ and Δt itself. Nevertheless, for small Δt needed for high temporal resolution, the result for the spike counting would be either 1 or 0, giving just these two results [5].

The solution is to the average over multiple trials in order to define a *time-dependent firing rate* as the average spikes number (over trials) in a certain interval divided by the duration of the interval. Basically, the numerator becomes the integral of the neural response function averaged on trials. By indicating with the angle brackets the average over trials, the *time-dependent firing rate* is expressed as [5]:

$$r(t) = \frac{1}{\Delta t} \int_t^{t+\Delta t} \langle \rho(\tau) \rangle d\tau \quad (1.3)$$

If Δt is small, in the best case scenario there will be one spike in the interval $[t, t + \Delta t]$. That means that $r(t)\Delta t$ is also the fraction of trials in which a spike manifested itself. At the same time, $r(t)\Delta t$ is the probability that a spike occurs during this interval. So the definition of *time dependent firing rate* can be formalized as: "it is the probability that a spike occurs during a small interval Δt around the time t " [5].

Starting from the point that the $\rho(t)$ can be averaged across trials to get the firing rate $r(t)$, it is possible to average the spike-count firing rate over trails obtaining a quantity defined *average firing rate* [5]:

$$\langle r \rangle = \frac{\langle n \rangle}{T} = \frac{1}{T} \int_0^T \langle \rho(\tau) \rangle d\tau = \frac{1}{T} \int_0^T r(t) dt \quad (1.4)$$

Depending on the kind of the recording activity that one would do, this quantity, as well as the spike-count rate, can be defined over any time period and not necessarily over the entire duration of a trial.

In general, these figures of merit are used to study the neuronal flux coming from different regions of the brain and to make a data analysis classification that can help to understand more about brain and its deseases. But, before this operation can happen, there is the need of record these signals from the brain.

1.3 Recording methodologies

The process of recording informations from the brain can happen in different ways. A first classification for Brain Computer Interfaces (BCI) is the following one:

- *non-invasive* techniques
- *invasive* techniques

Non-invasive BCI have been object of research primarily in the lasts years. These methodologies cause zero damages to the scalp or to the brain, but the recording operations are difficult because the distance between the neurons and the recording site is huge.

For this reason, a significant number of people in the neuroscience community has been focused on the study of invasive techniques. In this case the recording operation can be performed close to the neurons, inside the brain cortex or at dura mater level. In order to do that, it is important to reduce the risks of implantation such as reduction of the cell lifespan or permanent damages to the brain tissue. That can be done using different materials or designing implantable devices in a such a way that they are flexible and small at the same time.

The *Figure 1.5* shows the most popular methodologies in terms of spatial and temporal resolution. As it can be seen, at the cost of being invasive, with Penetrating Microelectrodes and Electrocor-ticography (ECoG) the highest spatial and temporal resolution is obtained.

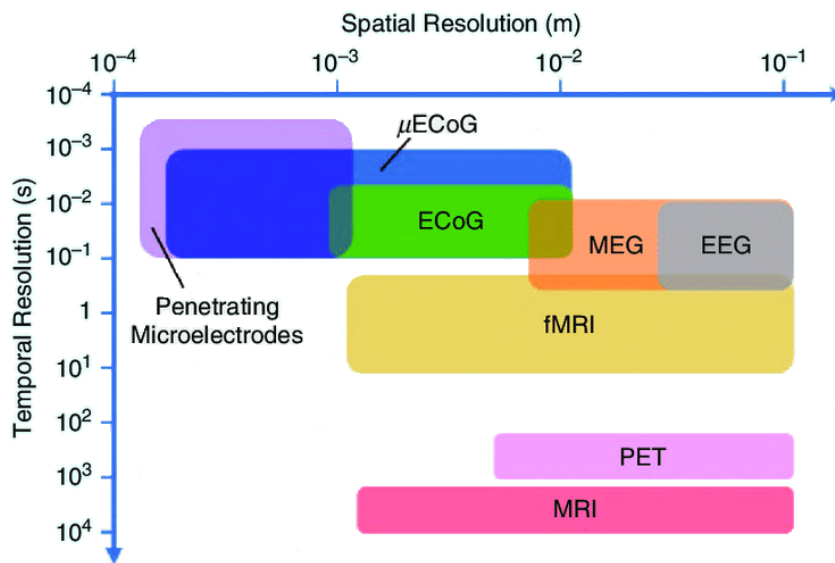


Figure 1.5: Most popular technologies for brain recording [?]

Here a review of these technologies in detail.

1.3.1 Non-invasive BCI

These technologies can perform recording operation remotely, without the need of surgery or anesthesia for the patient. On the other hand, the spatial resolution, that is the precision of the measurement with respect to the space, is low. That means that a recorded neuronal activity is the sum of multiple signals coming from different neurons, many of which are not interesting for the analysis because they come from different brain regions: they are present as noise.

Electroencephalography (EEG)

EEG is the recording operation of huge amount of neurons spikes from the outside of the scalp. The generated waveforms, coming from different regions of the brain, are related to the specific brain activities of those regions. For example, there are waveforms representative of cognition load, mind wondering, stimulation engagement and so on. To record this activity, some electrodes are applied on the patient's scalp as illustrated in *Figure 1.6*.

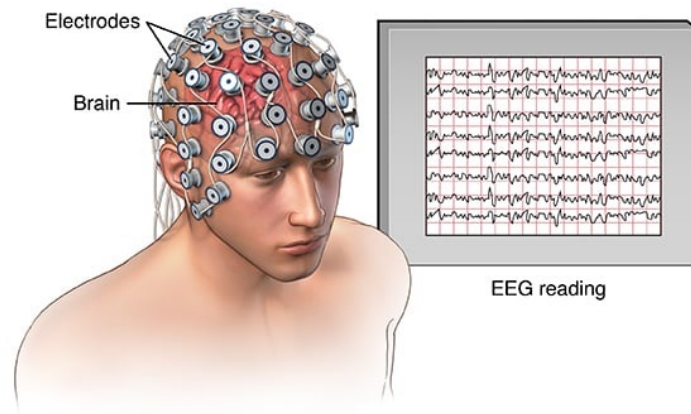


Figure 1.6: EEG recording system [8]

The biggest advantage of EEG is speed: neural activity can be recorded within fraction of a second after a stimulus occurred [9]. That means that the temporal resolution of this technique is pretty good. At the same time, the spatial resolution is lacking.

Typically, EEG signals are in the order of ten to hundred μV and they can be divided in five different categories by using frequency as discriminant [2]:

- delta waves [0.5 – 4] Hz
- theta waves [4 – 7] Hz
- alpha waves [7 – 13] Hz
- beta waves [13 – 30] Hz
- gamma waves [30 – 100] Hz

The *Figure 1.7* shows these waveforms.

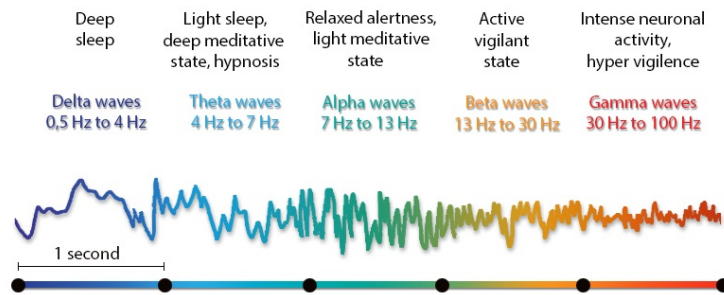


Figure 1.7: EEG signals [10]

EEG data are analyzed priorly to assess mental states, such as learning, resting or sleeping, and neuronal activities of neurological disorder patients.

Magnetoencephalography (MEG)

MEG technique is another non-invasive methodology. Starting from Maxwell's laws, the current flow causes a magnetic field around the wire in which current is flowing; in the specific case the wire is represented by neuron axon. The working principle is based on the recording of this magnetic response using high sensitive magnetic coils placed on the scalp. Superconducting quantum interference devices (SQUID) are nowadays the most common magnetic sensors used, while the spin exchange relaxation-free (SERF) magnetometer is under investigation for future machines. The magnetic field that SQUID can record is around $10 - 14 T$ [2].

While other kind of measurement require the complete absence of subject movement during recording, MEG measurement does not, so the patient can move his head within the MEG helmet: it represents the best method to treat pediatric patients. Figure 1.8 shows MEG technology used to record brain activity from a child.



Figure 1.8: MEG recording system on a child [11]

This technology has a lot of advantages in terms of high spatial and temporal resolution. Nevertheless, it is not widely used because of the cost and non-portability of the helmet with SQUID sensors [2].

Magnetic Resonance Imaging (MRI)

MRI is a pretty new technology born about 20 years ago to catch neuronal signals from brain activities non-invasively. The working principle is based on the resonance effect that blood flow and oxygenation level have into the orientation and resonance to the direction of an applied magnetic field [2].

To compensate the lack of spatial resolution there is the need to have a big magnetic field source: this implies having big equipment for MRI that is expensive and big in dimensions as *Figure 1.9* shows [2]:



Figure 1.9: MRI equipment [12]

Two kinds of MRI are commonly used for brain signal monitoring [2]:

- Functional Magnetic Resonance Imaging (fMRI)
- Diffusion Magnetic Resonance Imaging (dMRI)

fMRI is an indirect recording operation since it measures variations in blood flow when there is an increase in brain activity. In other word, it is a type of particular brain scan with the purpose to create a map of neural activity by imaging the variations in blood flow.

A limiting factor for fMRI is the low temporal resolution of the blood-oxygen level [13, 14]. Moreover, the measure is corrupted by noise from various sources, making statistical procedure to extract the signal required.

The results can be represented by using different colors on the map, in correspondance of different regions of the brain or by underlying different features on the specific studied region (for example to put in evidence malfunctions or diseases). Overall, the activity can be localized to within millimeters but, in terms of temporal resolution, no better than seconds. This is the biggest limit of this technology [15].

dMRI is usually used to study connectivity of various brain sections; it exploits the contrast in MRI images due to the diffusion of water molecules [2, 16, 17, 18]. So it maps the brain starting from the diffusion process of molecules in vivo and non-invasively.

The *Figure 1.10* shows two examples of brain mapping obtained with fMRI and dMRI.

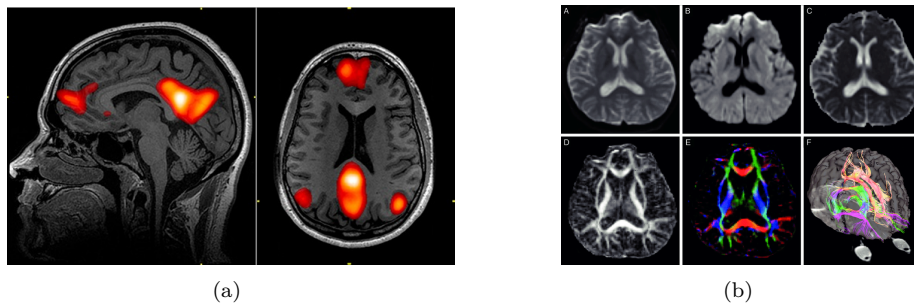


Figure 1.10: MRI brain mapping examples: a) fMRI b) dMRI [19, 20]

MRI is adopted for human brain activity monitoring where invasive methods are not necessary. Unfortunately, the setup requires the patient to be lying down inside the equipment, thus this technique is rarely used for real-life settings recording [2].

Computed Axial Tomography (CAT)

CAT (or CT) scan uses many combinations of X-rays measurements coming from different angles to produce tomographic images of a specific area, as shown in *Figure 1.11*.

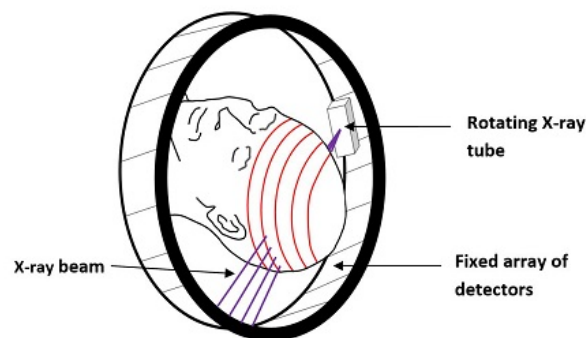


Figure 1.11: CAT acquisition technique [21]

X-ray pulses last only a fraction of a second, and it takes only a few seconds for the machine to record the spatial distribution of each sample. It is the most common form of tomography imaging technique used nowadays. With respect to MRI, it provides inferior information when one looks about headache to confirm a diagnosis of vascular diseases, cranial lesions or intracranial pressure disorders. CAT scans may be used when hemorrhage, stroke, or traumatic brain injury are suspected [22].

Positron Emission Tomography (PET)

This technique can be considered a non-invasive one because there is not a direct surgical operation, although it foresees the use of radioactive materials called radiotracers or radiopharmaceuticals, to evaluate brain functionality. The imaging operation is provided by a special camera (similar to the one used in MRI) and a computer. Particularly, the system is sensible to a gamma rays emitter, commonly fluorine-18, that is introduced into the body [23] so that the computer can reconstruct three dimensional images of tracer concentration.

In modern PET, three dimensional imaging is often obtained using X-ray scan executed on the patient during the same session [23].

In *Figure 1.12* is shown how the system works.

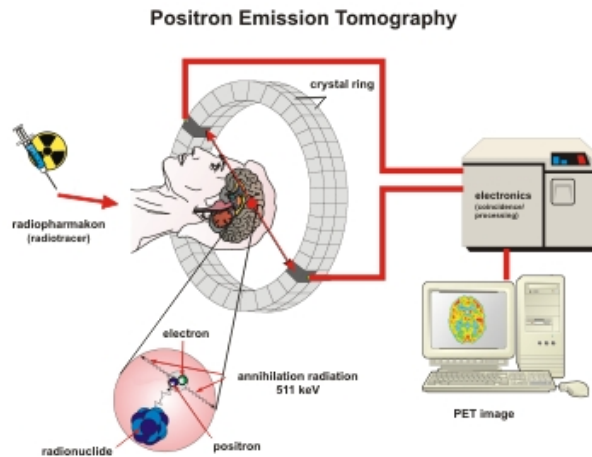


Figure 1.12: PET acquisition technique [24]

The resolution is of a few millimetres in space, comparable with the MRI's one. Even the temporal resolution is more or less the same (except for fMRI that has better performance). Due to the toxicity of radiotracers, this technique is generally used just in specific cases when MRI technology does not provide satisfactory results (for example to identify brain cancer).

With the same operating principle, Single Photon Emission Computed Tomography (SPECT) is similar to PET but it provides use of a radioisotope that does not release positrons.

Electrical Impedance Tomography (EIT)

EIT uses low-frequency sinusoidal signals injected through electrodes into the body. The system is quick to respond to changes in electrical conductivity, so by measuring the resulting electrical potential, it is possible to compute the resistivity of the region of the body subjected to the currents [25]. In other words, it behaves like an imaging technique on conductivity/resistivity. Even though EIT have been shown to work well in both geophysical and industrial settings, it has not yet gained a significant enthusiasm in the medical imaging community [25].

Among newer non invasive technologies to record brain activities, near infrared (NIR) sensing is promising [2, 26]. This technology utilizes the same working principle as fMRI, but aims to measure blood flow through the scalp and skull with NIR transmitter-receiver system.

1.3.2 Invasive BCI

Invasive BCI are those techniques used to record brain activity from the inside of the skull. Such implantable medical devices often contain active elements connected to one or more electrodes to record neural or to stimulate in a controlled way activities in brain [2, 27, 28]. By doing this, the spatial resolution considerably improves, but, at the same time, the risk of permanent damages to the tissue increases too.

Electrocorticography (ECoG)

One of the most famous invasive methodologies is the ECoG. Sometimes it is even called Intracranial EEG for the reason that it is performed with electrodes placed at subdural layer [29]. In other words, with ECoG technique just the skull is bypassed by electrodes without compromising the brain cortex, as *Figure 1.13* shows.

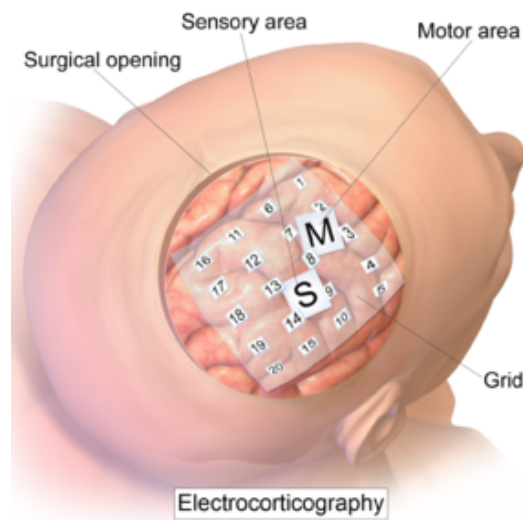


Figure 1.13: ECoG acquisition technique [30]

Usually, ECoG electrodes are Platinum/Iridium (Pt/Ir) strips that are designed for small-period use in humans [2]. Compared with non-invasive techniques, the electrodes of ECoG have the advantage of being placed over or under the dura mater, in proximity of the cortex and inside the skull, thereby the spatial resolution is bigger (at least than MEG and EEG) as well as temporal one that increases considerably.

This technology is generally used to record neuronal activity in patients with particular brain disease such as pre-surgical epilepsy: this allows to study ECoG results in human [31]. It can be considered as the last invasive methodology that does not penetrate the cortex, even though it penetrates the skull. However, since the implantation requires surgical procedures, there can be complication such as traumatic operation, brain damages or the possibility of infection [2].

Penetrating Microelectrodes

The highest spatial resolution of neuronal recording is achieved with implantable microelectrodes. Theoretically, if the electrode site is small enough, this kind of technique could allow to record neuronal activity from one single neuron. It is what is called single unit activity (SUA) in contraposition with multi unit activity (MUA) that is the recording operation from multiple neurons [2]. As a consequence, two different types of recording operations can be distinguished:

- **Single unit recording**

Glass micropipettes The tip of the pipette is very small, from $0.5 - 1.5 \mu\text{m}$. A Silver-Silver Chloride (Ag-AgCl) electrode is inserted from one side of the pipette (the bigger) as an electrical terminal and it is surrounded by an ionic solution to make conductivity. Ideally the concentration inside the electrode and surrounding fluid should be the same, thus a Potassium Chloride (KCl) solution is used [32].

The operating principle is based on the penetration of the cell membrane with minimal damage thanks to the small size of the tip. At this point a current starts to flow between the liquid at the junction and the inside of the pipette, establishing a closed circuit between the cell and Ag-AgCl electrode, allowing the measurement operation. There are some issues to consider when a glass micropipette has to be used. The biggest is the high capacitance that develops across the glass and the solution: it can result in attenuation of high frequency response [32].

Figure 1.14 shows a glass micropipette.

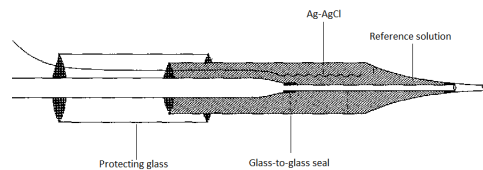


Figure 1.14: Glass micropipette [33]

Metal microelectrodes This kind of electrodes are built using different types of metals (typically Platinum or Tungsten) and they are more suitable for extracellular measurement. Metal electrodes are better even in some other cases because they show high Signal to Noise Ratio (SNR) thanks to the lower impedance at interest frequency. They also present better mechanical properties for penetration through brain tissue and, not less important, they are more easily manufactured into different tip shapes and sizes with respect to the glass ones. The only limitation is that the tips are very fragile [32].

In *Figure 1.15* is reported the structure of a metal microelectrode.

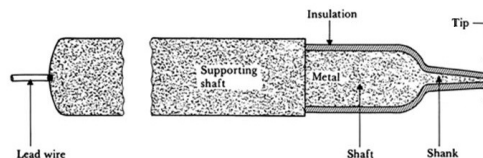


Figure 1.15: Metal microelectrode [34]

- **Multi unit recording**

Multiple Electrode Array (MEA) This is the name given to those systems used to record activity from more than one single neuron using multiple electrodes. There are three main categories of implantable MEA for in-vivo experiments: microwire, silicon-based, and flexible microelectrode arrays [35, 36]. Microwires are usually made of stainless steel or tungsten and they have been developed to perform sensing or stimulation [36, 2]. For what concern silicon-based electrodes, they exist in two different models: Michigan and Utah arrays. The differences between these two are mainly to be found in the positioning of the recording sites: if Michigan has electrodes all along the length of the shank, Utah allows electrodes only at the tip of the probe. Moreover, Utah arrays are manufactured with fixed dimensions while the Michigan ones are free from design constraints [36]. Lastly, flexible arrays, made with different polymer solutions (such as Parylene or polyimide), which focus on reducing brain damages due to excessive stiffness of the probe. In *Figure 1.16* some real examples are reported.

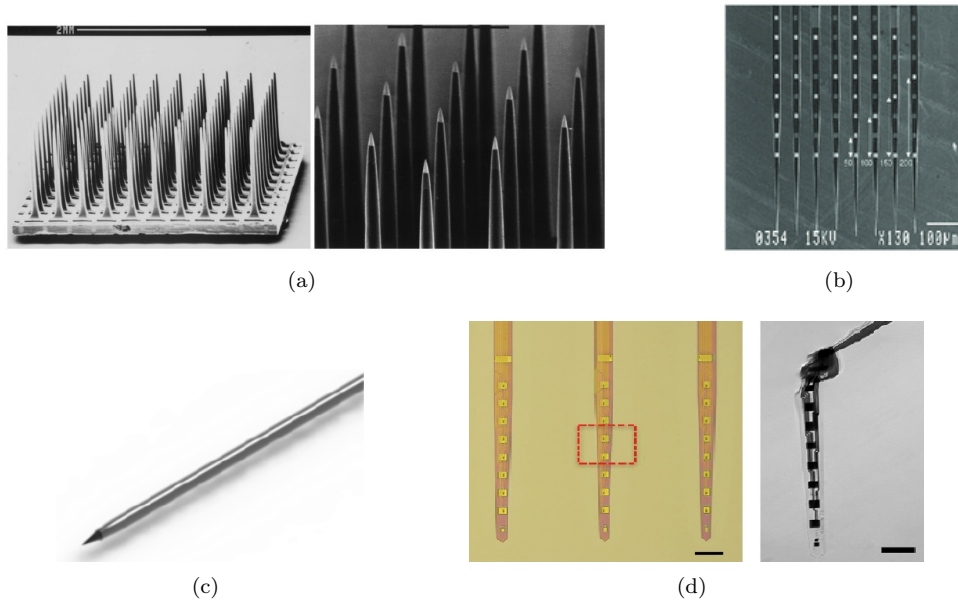


Figure 1.16: a) Utah array, b) Michigan array, c) Microwire, d) flexible probe [37, 38, 39, 40]

The implantable devices presented so far represent the state of the art of highly invasive techniques used to record neuronal activity with high spatial and temporal resolution. The history of multi-electrode cortical probe begins in 1966 at Stanford University where the electrode, an area of exposed metal, was surrounded by inorganic dielectrics as electrical insulation [2]. But it has been difficult to produce such electrodes until the microelectromechanical systems (MEMS) technology was developed along with nano and micro fabrication techniques [2]. Since then, much has changed and technology has today reached such experience as to be able to mix all these techniques to create implantable devices that can combine flexibility, strength and small dimensions at the same time. The following shows the result of this process in the fabrication of the implantable probes used for this thesis work.

1.4 Steeltrodes and polymer probes for in-vivo recording

Silicon micro and nano fabrication processes are very well developed, allowing to realize easily probes on this platform. But, at the same time, silicon suffers some problems whenever implanted in the brain cortex. First of all, mechanical limitations, such as brittleness and fragility, make implantation operations difficult. This makes this type of platform more suitable for implantation in rodents rather than more in human-like animals, such as monkeys: the small brain size allows to make shorter probes less susceptible of mechanical failures.

A second aspect is related to the stiffness of the silicon that causes more damages to the tissue because of the brain micromotions.

Assuming that a probe can be modeled as fixed at the base, or back-end, and pinned at the tip [39], the buckling force in the beam, that identifies the probe itself, can be computed using the Euler's formula [41]:

$$P_{cr} = \frac{\pi^2 E \omega t^3}{5.88 L^2} \quad (1.5)$$

where E is the elastic modulus, ω is the width of the beam, t the thickness and L its length.

It has been demonstrated that buckling force of 1 mN is the threshold to penetrate rat cortex without any insertion aids [42]. Threshold required to penetrate cortex through dura and pia mater is one order of magnitude bigger [43]. To respect these constraints, some new materials have been investigated with the focus on biocompatibility and flexural strength at the same time. Stainless steel offers these properties and, in addition, it exhibits an endurance limit, a long life cycle and inexpensiveness [44, 45]. However, microfabrication process in stainless steel is not developed as the silicon one, resulting in a mostly unexplored material from this point of view [46]. Another material with similar features, commonly used in biomedical devices, is Parylene C. Probes used in this thesis work takes advantage of the combinations of these two materials in two different microfabrication process configurations [46]:

- steeltrodes monolithically fabricated on stainless steel;
- polymer probes affixed to stainless steel shuttle post fabrication;

In the first case, taking advantages of the high throughput method for realizing planar probes, the device is completely microfabricated on a stainless steel substrate [46]. In order to do that, Silane A174 is used to increase the adhesion with the thin layer of Parylene C at the very beginning of the process [46].

In the second case, instead of using a stainless steel wafer, a classical silicon one is adopted. Moreover, there is no adhesion promoter meaning that, at the end of the process, the probe will be released from the substrate by itself.

Thanks to the extreme flexibility of this kind of the devices, one can potentially record neuronal activity for long time intervals without causing significant damage to the brain: the probe moves synchronized with brain micromotions limiting lacerations in the surrounding tissue. The issue is that flexible polymer probes do not have the mechanical strength required for brain penetration (even without considering dura mater). For this reason, at the end of the fabrication process, another step is needed to mount the probe with a stiff shuttle, like a 3D stainless steel one. The connection can be performed using bioresorbable adhesive materials such as Polyethylene Glycol (PEG) [39, 46]: after the implantation it dissolves into the brain allowing the shuttle removal and the releasing of the flexible probe.

Another way to handle this issue is to use coatings that increase stiffness of the probe for a certain period of time before the insertion. Common coatings used for this purpose are gelatine, silk, saccharose, table sugar and maltose [39].

In any case, using this methodology one needs to take care of the increase of flexible probes cross-section, thereby avoiding enlarging of the insertion section in the brain.

The fabrication process is pretty straightforward and it is the same for the two configurations. It is summarized here [46]:

- Parylene C deposition by Chemical Vapor Deposition (CVD);
- Platinum/Gold interconnects and electrodes deposition and patterning;
- Parylene C deposition (second layer);
- Chromium hardmask deposition and patterning;
- etching of electrodes opening and probe outlines;
- Chromium hardmask removal;
- laser cutting for probes release ¹.

Since the process is the same for both the configurations, it has been used the same mask design. The *Figure 1.17* shows the process flow for the two configurations [46].

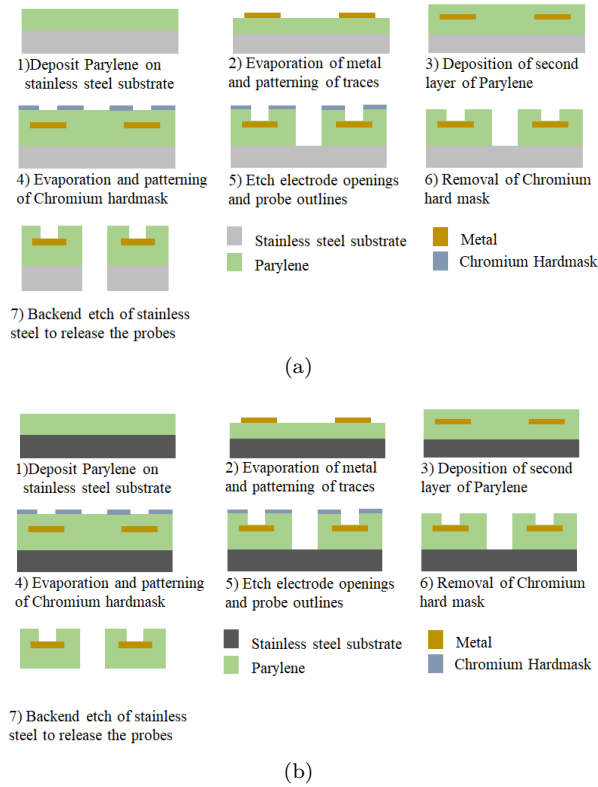


Figure 1.17: Fabrication process: a) steeltrode, b) flexible polymer probe [46]

The result of this process are probes consisting of 1 – 7 cm long shanks, [260 – 360] μm large, with electrodes in different arrangements [43]. As illustrated in *Figure 1.18*, each steeltrode has three different layer. On the bottom there is the stainless steel substrate that gives elasticity and strength at the same time. The second layer is the first Parylene C together with the interconnections and the electrodes for the neuronal recording. Finally, there is the second Parylene C working as insulator that covers the interconnections. Obviously the electrodes sites are left uncovered for the recording operation, even though some test probes, with Parylene C covering all the surface, have

¹This step is performed for the steeltrodes only.

been developed to test the goodness of the insulator. The picture shows details of the tip of the probe as well as the back-end for the electrical interfacing.

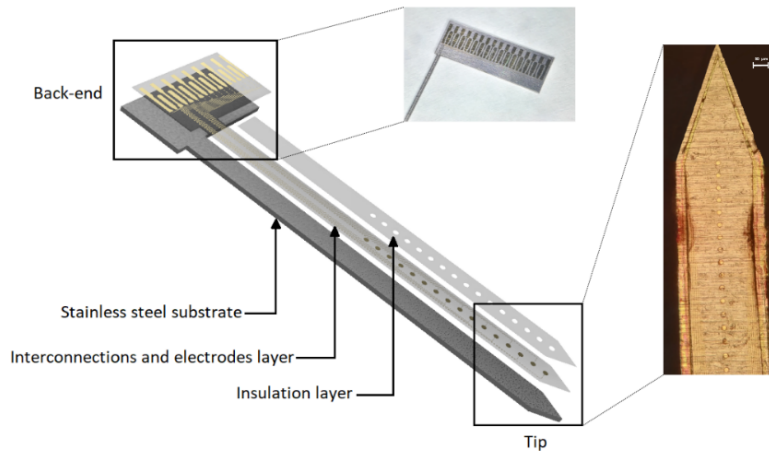


Figure 1.18: Implemented steeltrode for neuronal recording

As already mentioned, polymer probes do not have the substrate in stainless steel that make the whole structure more rigid. The result is a flexible two layers probe as shown in *Figure 1.19*.

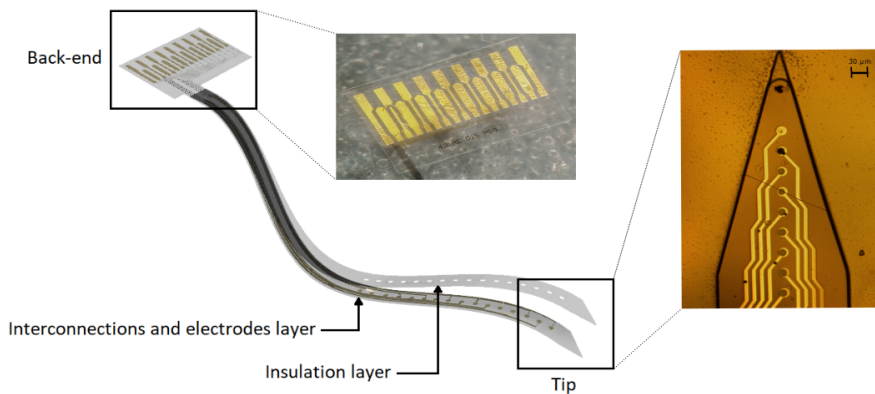


Figure 1.19: Implemented polymer probe for neuronal recording

Regardless of the probe type, but based on electrodes disposition, the probes can be classified into two other categories:

- high density tip;
- high density shank;

The first group includes those devices for which the electrodes are placed just at the tip of the probe, creating a high density of electrodes in that area. At the contrary, in the second case, the electrodes are disposed all along the probe, in such a way that the distance between two consecutive ones is bigger.

Even though many different probes have been implemented, this thesis work is mostly focused on packaging and characterization of the high density configurations with 16 and 30 channels.

Chapter 2

Post-fabrication improvements

After probes fabrication, several aspects need to be investigated in order to make the device free to be used in recording operations. As already mentioned, one of the materials used for the fabrication is stainless steel because it provides refined rigidity and robustness. Nonetheless, it risks turning into serious damage to neuronal tissue if not treated correctly. The main point is that the laser cutting around the perimeter of the probe leaves bumps and burrs along the edges that scratch significantly the tissue during the implantation and afterwards, due to the brain micromotions. In *Figure 2.1* is shown one steeltrode with wrinkly sidewalls after being released from the stainless steel wafer.

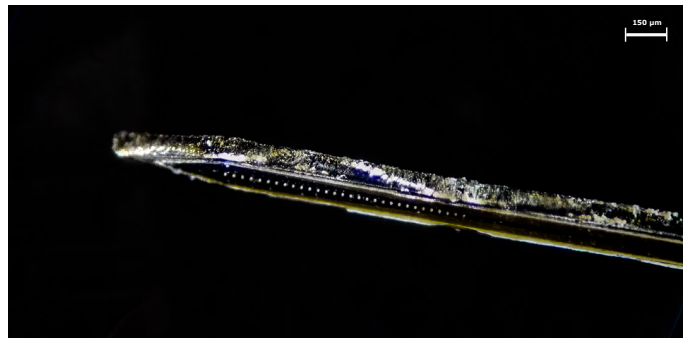


Figure 2.1: Steeltrode after wafer release

In addition to what already said, having a shank completely realized in stainless steel might represent a limit for long term neuronal recording. Indeed, when the electrodes are displaced just on the tip of the probe and the section inside the brain is small with respect to the section outside, the entire rigidity of the structure is no longer an advantage, but becomes a cause of strong mechanical stress. These two motivations make post-fabrication operations necessary to improve the physical quality of the probe.

The methodologies used in literature to refine biomedical devices are mostly in the field of electrochemical processing because of the small dimension and the fragility of those devices. For example, electropolishing (EP) is the most used technique to improve the quality of the stainless steel for endovascular stents as well as orthopedic or dental applications [47, 48]. In this thesis work this process has been adapted to the particular case of smaller devices such as implantable high density probes that require special care for the presence of insulating materials, recording sites and traces.

2.1 Polishing/etching process

For probe polishing has to be intended the process for which the roughness of the stainless steel surface is reduced after an electrochemical finish performed under certain conditions. The procedure foresees to use a voltage/current signal between two electrodes immersed in a temperature-controlled bath of acid solution. The sample (i.e. the probe) is the anode of the system, whereas the cathode is generally another metal-based electrode. When the current starts to flow between the two electrodes, the metal of the workpiece begins to dissolve into the electrolyte while at the anode an opposite reduction reaction occurs, producing hydrogen.

Even though the working principle of electropolishing has not been fully determined yet, it can be explained recurring to the differential dissolution that occurs when charges flow into the metal. What happens during this process is that an oxidation layer that covers the valleys of the surface is formed, protecting those regions [49]. At the contrary, the peaks of the surface, remain uncovered and, thanks to the high resistivity of those regions, they dissolve faster inside the solution. So, in the end, the peaks dissolves more quickly than the valleys: as a result the surface in the end is smoother. The *Figure 2.2* shows the experimental setup and the mechanism for which the EP process works.

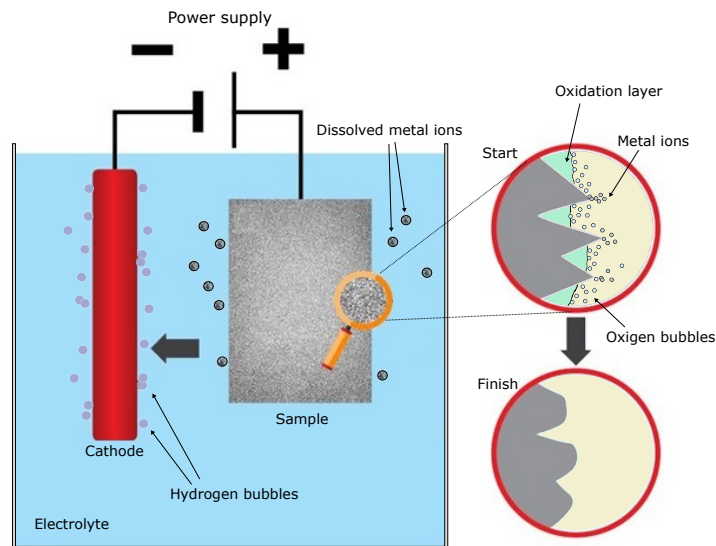


Figure 2.2: EP process [50]

The parameters that can be tuned to control the process are the following ones:

1. voltage/current parameters;
2. solution composition;
3. distance between the electrodes;
4. electrolyte temperature;
5. stirring speed;
6. time of the process;

For voltage/current parameters it is intended to decide whether to control the process by fixing the current or the voltage, as well as to define whether this must be alternate (AC) or continuous (DC). It has been chosen to impose the voltage or the current each time depending of the particular

type of the experiment and obtained results, in terms of process uniformity. Moreover, in order to decide which values to choose, a voltage-current characteristic has been plotted after some trials on real samples (the electrolyte for the experiment was a mixture of Phosphoric and Sulphuric acids). It is reported in *Figure 2.3* together with a fundamental voltage-current density curve for electropolishing [51]. The latter shows different regions for which the process can be conducted depending on the aimed result. In B-C region the dissolution of the material is unstable, in C-D there is the plateau that allows to conduct a more uniform polishing procedure and in D-E there is a high probability of getting pitting holes [52].

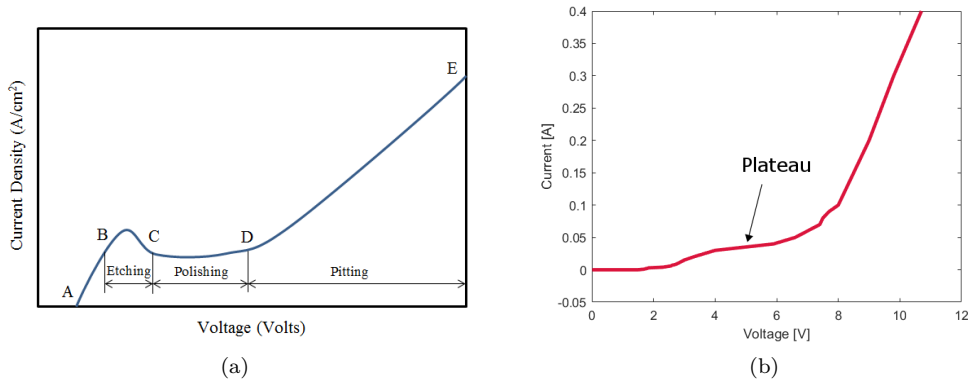


Figure 2.3: a) Fundamental voltage-current density electropolishing curve [51], b) Voltage-current characteristic of fabricated steelrodes in phosphoric-sulphuric acid mixture

As highlighted by the characteristic, the best voltage values for a good EP process are in the range 4 – 6 V because of the plateau.

A second important aspect is related to the choice of good chemicals for the electrolyte solution. At the state of the art, many research projects suggest to use the following:

- Oxalic acid in deionized (DI) water;
- Phosphoric acid and Sulphuric acid mixture;

The second one is actually the most widely adopted solution to perform EP on stainless steel because the high viscosity helps the formation of the oxidation film around the specimen. However, this combination of acids is particularly aggressive and might damage the Parylene C above the stainless steel. For this reason Oxalic acid, which is less aggressive, has been used as well. As it will be explained better further in the discussion, a multi-step EP process with both the two solutions has been performed too.

All other parameters are secondary factors that can be varied from trial to trial to improve the process. Thus, the distance between the electrodes and the stirring speed of the solution are generally combined with the ability to maintain a good oxidation layer on the probe surface and to quickly remove the dissolved metal ions, while the temperature of the solution and the time are mainly related to the speed of the process. In particular, moving among different trials, it was proved that the time of the experiment is the most important parameter to get a smooth surface without damaging the device.

In order to provide a quantitative analysis of the surface roughness before and after the process, *rms* parameter is used. It is the root mean square average of the height deviations from the main line, recorded within the evaluation length; it is expressed as follow [53]:

$$rms = \sqrt{\frac{1}{n} \sum_{i=1}^n y_i^2} \quad (2.1)$$

where n is the number of points equally spaced along the trace and y_i is, for each of the i^{th} data point, the distance along the y axis with respect to the mean value [53]. This value can be evaluated for each sample using an optical profilometer that uses light interference to measure the deviance of each peak or valley on the surface.

As mentioned in the introduction to this chapter, another goal is to reduce the mechanical stress to whom brain tissue is subjected when a steelrode is implanted for long term recording operations. One possibility is to create hybrid flexible-rigid probes that can float inside the brain after the insertion. The hybrid structure is realized using electroetching process for the removal of the stainless steel below the Parylene C in just one section of the shank. The electroetching process is basically the same electropolishing process conducted for a longer interval of time so that the metal is not only polished, but completely removed. For this reason, the main difference between the two consists of a different process time, which becomes again the most important parameter to get the wanted result.

2.1.1 Oxalic acid in DI water EP

Oxalic acid ($H_2C_2O_4$) is an organic compound that appears as a white crystalline solid soluble in water with a moderate aggression strength. His use for electrochemical processing of mechanical specimens of stainless steel is well known since many years [54]. On the contrary, the localized use for small biomedical devices it is quite new and promising. Its strengths are related to the fact that, not falling into the category of super dangerous chemical reagents, it does not require the use of an acid desk, it is safe to be used in a laboratory environment and it does not present too critical corrosion features that can damage the probes.

The concentration chosen for the EP experiments is of 3% by weight in DI water, so that a total amount of 500 mL of solution requires 15 g of compound [55]. The acid is dissolved in the water using a rotating hot plate in order to control the temperature and the stirring speed of the solution. For all the carried out experiments, the temperature of the solution has been kept fixed around 37 °C to avoid non-linear variations of the polishing procedure, while the stirring speed of the solution was set at 300 rpm to maintain a good compromise between recirculation and level maintenance into the beaker (and then avoid spills).

The cathode electrode used is a stainless steel one, but platinum or copper can be used as well. For what concern the voltage/current parameters, the experiments have been conducted in these domains:

- DC polishing;
- AC polishing;
- two steps process: AC+DC polishing;

DC polishing

In the DC domain it has been noticed that the first polished samples showed better results with an imposed current. Although the V-I characteristic for Phosphoric acid and Sulphuric acid mixture exhibits that the plateau occurs for very small current values, the procedure for Oxalic acid has been carried out for bigger currents (0.2 A) to engrave a first and quick finishing improvement to the impurities of the stainless steel surface.

Then the experiment has been conducted over time and the edge of the steelrode was observed under microscope. The *Figure 2.4* reports one probe sidewall for different polishing times.

As can be seen in *2.4(a)*, the side of the probe at the beginning presents rather obvious irregularities in the form of roughness peaks and valleys not convents to an implantable device. Moreover, the surface also appears oxidized and the metal melted in some points due to the high temperatures reached during the laser cutting procedure: the scratching effect could be dangerous for the surrounding brain cells. The EP process improves the roughness over time as can be qualitatively

observed in 2.4(b), 2.4(c) and 2.4(d).

If the process lasts too much the stainless steel substrate starts to decrease in size on the edges. That implies to leave the Parylene C floating on the edges, with the risk that some channels break during the insertion. Hence this condition has to be avoided. After several experiments, it has been found that the perfect interval of time to get a good result without reducing the section of the probe too much is 2 – 6 minutes, depending on initial size of the probe that can vary between 260 μm and 360 μm . Most of the time 3 minutes is a good compromise.

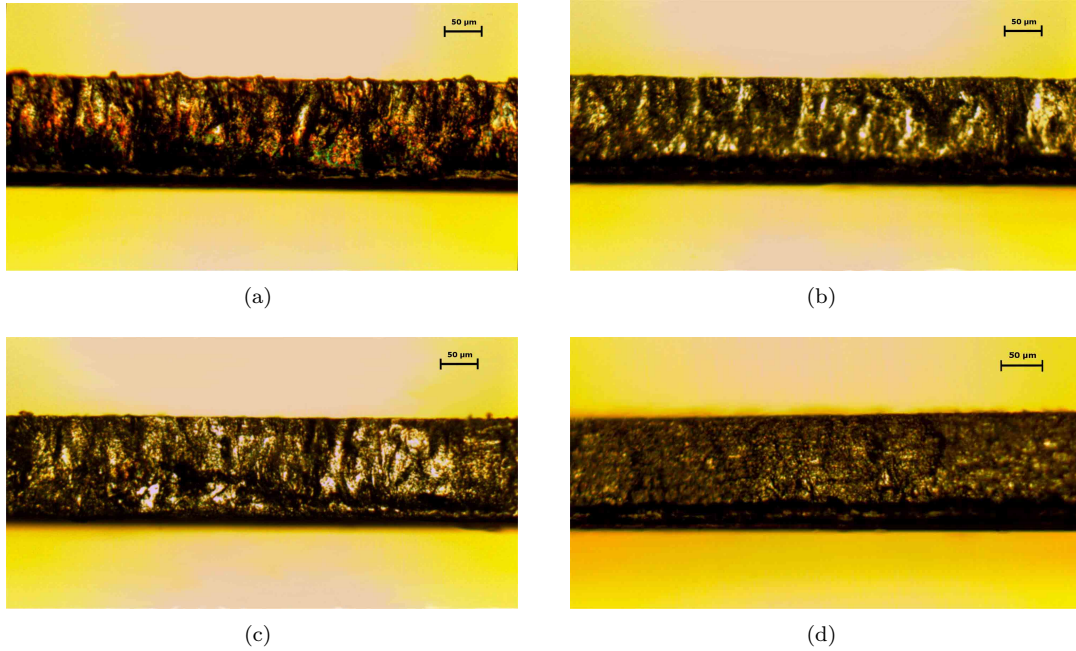


Figure 2.4: Probe sidewall for different polishing times: a) no polishing, b) 1 min, c) 1.5 min, d) more than 2 min

In order to get a more defined and detailed image of the stainless steel roughness, a Scanning Electron Microscope (SEM) can be used. In *Figure 2.5* are reported the sidewall scans before the polishing procedure and the obtained result after the polishing.

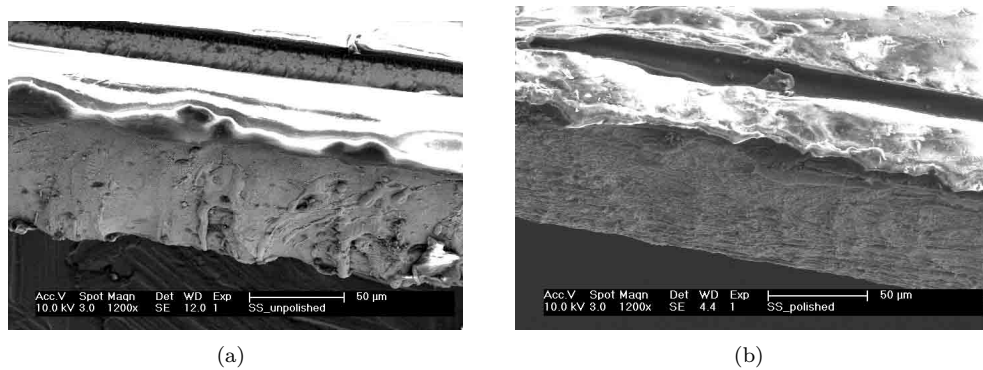


Figure 2.5: SEM of probe sidewall: a) before polishing, b) after 2 minutes of polishing

As can be noticed, the big peaks of the unpolished section are removed after the polishing together with the bumps on the bottom corner (on the top the Parylene covers the stainless steel so the

results are less evident). However, some smaller but denser roughness contributes are introduced after the process. In a certain way it can be said that this process substitutes low frequency and high amplitude roughness with high frequency and low amplitude roughness. This represents a good result in itself because it results in a much smoother surface that causes less damages to the tissue. Anyhow, the quantitative analysis of roughness parameters will show substantially no-improvements because peaks are still present and their smaller amplitude will be averaged over a smaller mean value.

Another characteristic of this procedure is the capability of being an optimal deburring process. As can be seen from *Figure 2.6*, the border protusions indicated with the white arrows are completely gone after the EP, even with a low-time process. That happens because the burrs extend far beyond the stainless steel surface compared to the normal roughness peaks and, as a consequence, far beyond the oxidation layer. Thus, the effect of polishing is faster.

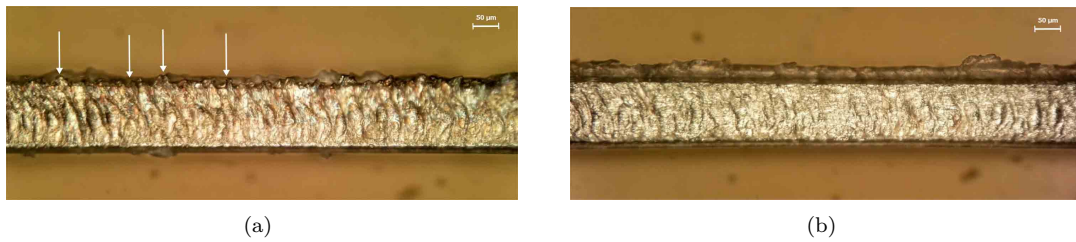


Figure 2.6: Deburring effect: a) burrs on the border of the stainless steel substrate, b) result after the polishing

Finally, DC polishing has an effect even on the shape of the probe tip. As mentioned above, if the process is long enough to ensure a good roughness improvement it can also model the square corners until turning them into a curved shape. Hence the sharp tip becomes rounded as shown in the different pictures of *Figure 2.7*.

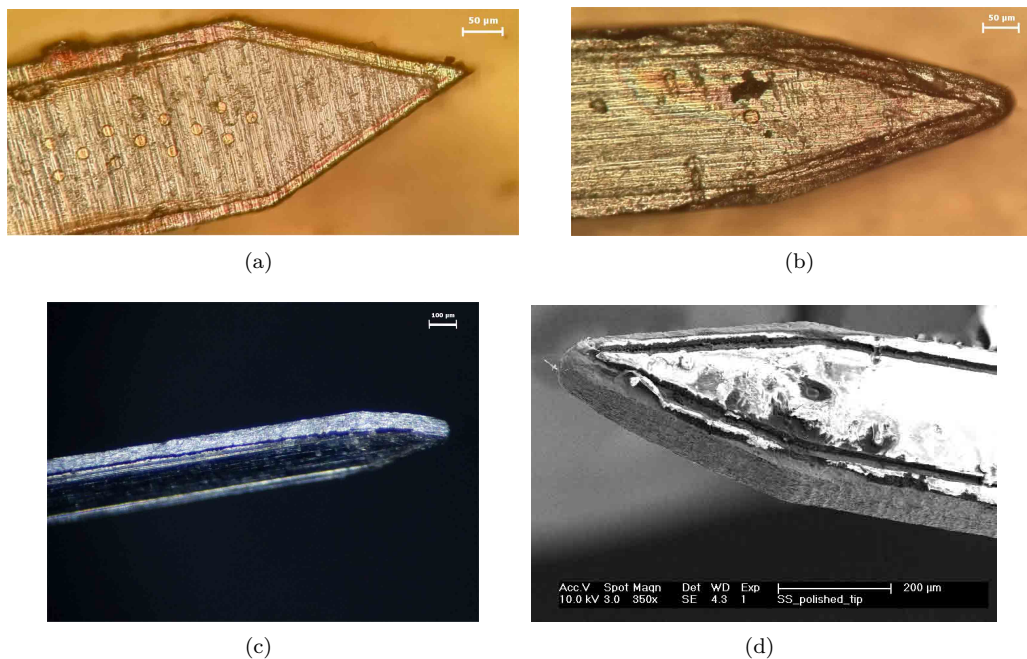


Figure 2.7: Probe tip improvements: a) unpolished tip, b-c) polished tip, d) SEM of polished tip

It has been calculated that the radius of curvature of the probe passes from a few micrometres to more than $30 \mu\text{m}$ after an EP of 4 minutes. Obviously, the limit of this procedure is that, at some point, the stainless steel will be completely removed if the polishing lasts too much, therefore the procedure still has a constraint in the processing time.

AC polishing

In the same way, some experiments have been conducted in AC domain for different intervals of time. The big difference with respect to the DC is that here more parameters can be tuned in addition to the ones already mentioned: frequency and duty cycle of the applied signal are the most important ones. Furthermore, it can be chosen to impose a certain offset in such a way that the signal is completely positive or both positive and negative.

The main point is that stainless steel, as well as titanium or nickel, are very strong passivating metals for which the probability to get a pitting surface is very high in continued EP. This is the reason why high viscosity electrolyte solution is always preferable in these cases. However, some research works have proved that an AC pulse-pulse signal can be applied to obtain good results even in aqueous environments [56]. The process improves the quality of the polished surface using the pulse/pulse technique presented in *Figure 2.8*.

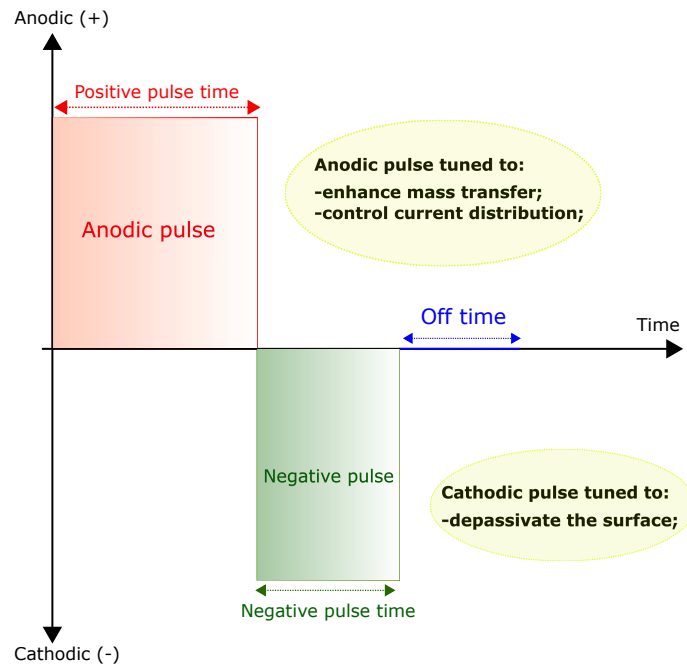


Figure 2.8: AC waveform for EP [56]

As from the figure, the positive pulse enhances mass transport and controls the polishing process on the roughness peaks. On the contrary, the negative one has the task to depassivate the surface and thereby making useless the need of a viscous solution. During this phase the oxide film is removed and a new one will form as soon as the next positive pulse arrives. Moreover, an off time may be useful to get solution replacement in the proximity of the surface.

The *Table 2.1* reports the most relevant experiments conducted.

Amplitude [V_{pp}]	Frequency [Hz]	Offset [V]	Duty Cycle [%]	Time [min]
6	[1 – 100]	0	30	2
6	[1 – 100]	3	50	6
4	[1 – 100]	0	30	2
4	[1 – 100]	2	60	6

Table 2.1: Most relevant experiments conducted in Oxalic acid by varying the voltage parameters and the EP time

Although different tests have been carried out with different polishing times and different AC signal parameters, the desired results have not been obtained on Oxalic acid. The *Figure 2.9* reports the probe sidewall for two different conditions (with or without offset). For summary reasons, not all the results are shown.

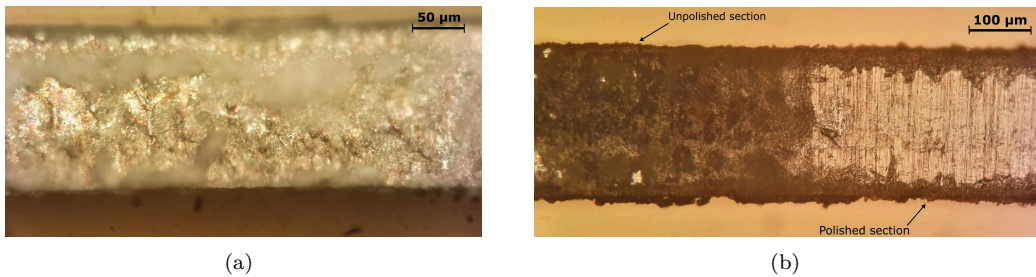


Figure 2.9: AC EP results for two different samples: a) opaque spots on the sidewall (with an applied offset), b) interface between the polished and unpolished sections (with no offset) from the backside of the probe

As can be seen, in both cases the surface is not smooth enough and, in addition, the roughness seems increased after the polishing process, in particular in the case 2.9(b) (in which no offset means both positive and negative pulses). That could be an effect of the Oxalic acid itself, which is probably not the best kind of compound for this process. In fact, as the research work suggests, sodium chloride-sodium nitrate electrolyte is preferable for stainless steel polishing [56].

AC+DC polishing

As a third experiment, it has been chosen to carry on some trials on mixed AC-DC environment. Since it has been proved that AC provides the worst result, the process is developed following this order:

1. AC polishing;
2. DC polishing;

The current/voltage parameters used are those that allowed to obtain the best results in the previous tests. They are resumed in *Table 2.2*.

	Amplitude	Frequency [Hz]	Offset [V]	Duty Cycle [%]	Time [min]
AC	$6 V_{pp}$	1	3	30	2
	$4 V_{pp}$	1	2	60	6
DC	$0.3 A$	—	—	—	2
	$0.2 A$	—	—	—	3

Table 2.2: Most relevant experiments conducted in AC-DC domains

The AC polishing process has been conducted only for positive voltage signals, seen and considered that those for zero offset, and hence positive and negative pulses, did not result in improvements of surface roughness.

As a result, once again the sidewall of the probes have been analyzed before and after the process, as illustrated in *Figure 2.10*.

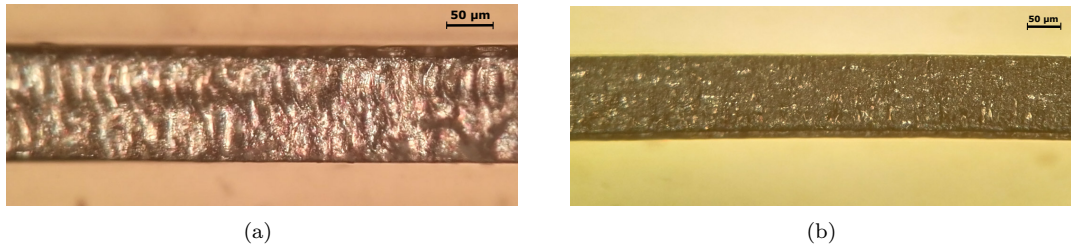


Figure 2.10: AC+DC EP result a) probe sidewall before the process, b) sidewall after the process

In this case the sidewalls appear smoother. All the low frequency peaks are gone as well as the burrs on the edges. At the same time, a high frequency roughness component is still present, similarly to what was observed in DC polishing. Hence, since the results for these two are very similar, it can be said that DC polishing is better because it allows to obtain the same result with a shorter process time, reducing the probability of damages to the probe interconnections or insulator.

2.1.2 Phosphoric acid and Sulphuric acid mixture EP

As from literature on EP of biomedical devices, Phosphoric acid (H_3PO_4) and Sulphuric acid (H_2SO_4) are two of the most used compounds for stainless steel processing [49, 57, 58]. Their main features are related to the slow and uniform dissolution that they are able to guarantee, as well as the limitation of oxidation or corrosion effects [57]. Unluckily, the extremely aggressive behavior of these acids can affect the probe functionality in some cases. Anyhow, during all the experiments carried out, none of the probes used showed qualitative differences compared to before processing.

The solution was made using 75% of Phosphoric acid and 25% of Sulphuric acid by weight. No additive heat has been used during the process to increase the rate of the polishing, so everything has been carried out at room temperature. The distance between the electrodes is the same of the previous configuration, 1 cm, as well as the stirring speed of the solution, fixed at 300 rpm. Finally, for the voltage/current parameters it has been chosen to run the experiments only in the two following conditions, since it has been observed that the AC+DC trial provides similar results of DC polishing:

- DC polishing;
- AC polishing;

DC polishing

The same current parameters used in the processes on Oxalic acid have been used in this configuration. Thus, a 0.2 – 0.3 A DC current has been imposed using a sourcemeter. The process has been repeated for many samples changing the processing time for each of them. After many tests it was observed that the polishing rate is much slower compared to the Oxalic acid one. For example, under 20 minutes of processing just some irregularities on the surface are removed, whereas the majority of them remains unpolished. For this reason, the process needs to be carried on for at least 25 – 30 minutes. The *Figure 2.11* reports two samples of 30 minutes processing in the unpolished/polished versions. As can be seen the grain of the irregularities on the probe

sidewall is different for the two devices, large for the first one and finer for the second one. As already mentioned, the starting condition of the surface depends on the quality of the stainless steel wafer (that can be different for two probes if they come from different wafers) and on quality of the laser cutting process (that varies depending on many machining factors).

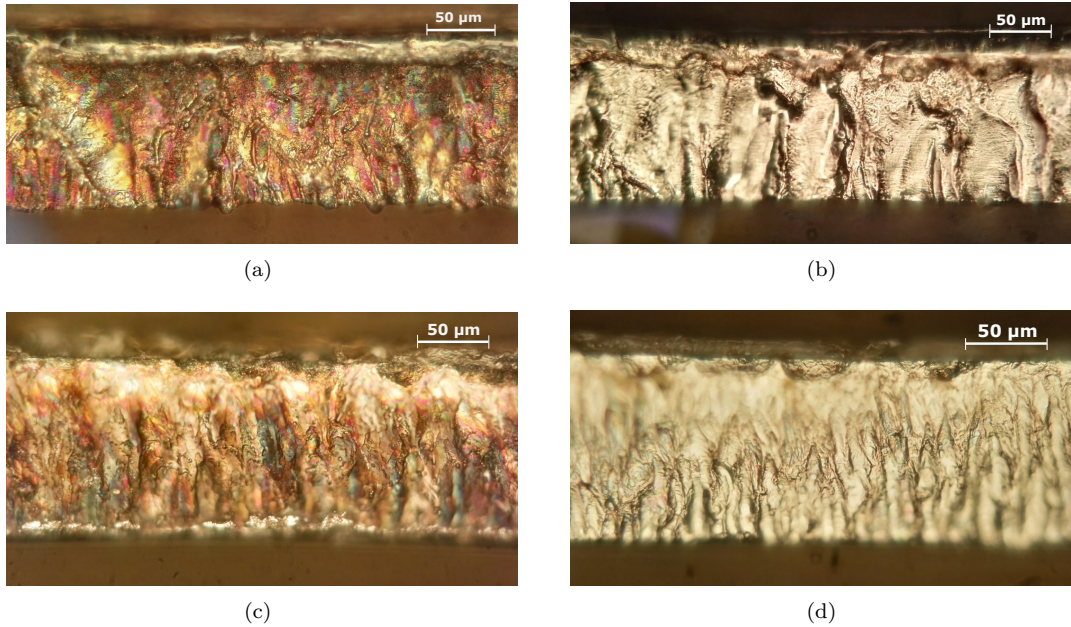


Figure 2.11: Phosphoric acid + sulphuric acid EP: a) unpolished probe sidewall (large grain), b) polished probe sidewall (fine grain), c) unpolished probe sidewall (fine grain), d) polished probe (fine grain)

Even though the process is exploited for a long time, no significant variations are highlighted in terms of low frequency roughness. Indeed, all the big peaks are present even after the process. On the contrary, the probe is polished in high frequency domain, as one can see from the the increased brightness on the surface in correspondence to the valleys.

These preliminary and only qualitative analysis are confirmed by the roughness measurements performed with an optical profilometer (Zygo). The *Figure 2.12* reports the 3D scans of the surface for the unpolished and polished large grain probe.

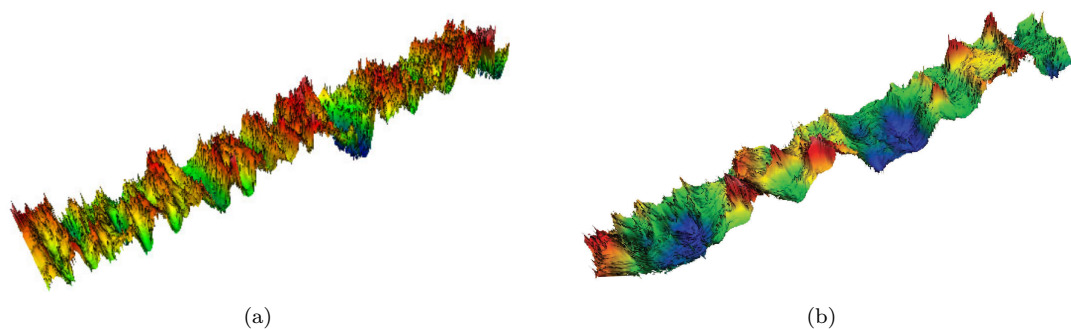


Figure 2.12: Phosphoric acid + sulphuric acid 3D scan profile: a) unpolished probe sidewall, b) polished probe sidewall

One can notice from the pictures how the high frequency peaks are mostly gone, while the low frequency ones (so the wavy shape of the surface itself) is still present. The *rms* analysis gives a value of $0.68 \mu m$ for the polished section compared to $0.8 \mu m$ for the unpolished one, with an improvement of around 14%.

An interesting consequence of this experiment is shown in *Figure 2.13* that reports a zoom image of the polished probe sidewall.

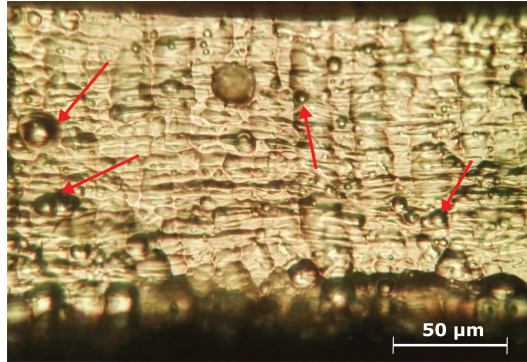


Figure 2.13: Bubbles after long time EP process

Some concave bubbles, indicated by the red arrows, form all along the polished surface after the process. The reason behind this undesirable effect could be related either to a too high current signal amplitude, as suggested by literature works [59], or it could be a problem related to a too long EP process. This effect is clearly the so called pitting holes effect that should appear only for very high voltages; therefore, in order to demonstrate that this was an amplitude-related consequence, it has been chosen to decrease the current in order to have very low voltages (lower than the one required to get the plateau region): the result shows that bubbles are still present. On the contrary, for small EP time a smaller number of bubbles manifests, even if at those conditions the polishing process is not good enough.

AC polishing

The AC polishing has been conducted on the same voltage conditions of the Oxalic acid case with different polishing times; they are reported in *Table 2.3*.

Amplitude [V_{pp}]	Frequency [Hz]	Offset [V]	Duty Cycle [%]	Time [min]
6	[1 – 100]	0	30	30
6	[1 – 100]	3	50	30
4	[1 – 100]	0	30	30
4	[1 – 100]	2	60	30

Table 2.3: Most relevant experiments conducted in Phosphoric and Sulphuric acid mixture by varying the voltage parameters and the EP time

The result are pretty much the same of the previous configuration so, for summary reasons, they are not shown again. The only difference with respect to the DC polishing is that more bubbles have been created during this process for higher voltage amplitudes. That means that, once again, DC polishing is the best choice for our purposes.

2.1.3 Two steps EP

The final experiment that it has been decided to perform is the two steps EP. As from the previous sections, it has been found that the DC polishing is the best choice for both Oxalic acid and Phosphoric/Sulphuric acids mixture. In particular it has been observed that the first one has better performance in low frequency roughness removal, whereas the second one in high frequency roughness improvements. For this reasons, the two of them can be used one after the other to achieve smoother surfaces, with this order:

1. Oxalic acid EP to remove low frequency roughness components;
2. Phosphoric acid + Sulphuric acid mixture to remove high frequency roughness components.

The parameters for the processes are reported in the *Table 2.4* below:

	Amplitude [A]	Time [min]
$H_2C_2O_4$	0.2 A	4 – 5
	0.3 A	2 – 3
$H_3PO_4 + H_2SO_4$	0.2 A	30
	0.3 A	25

Table 2.4: Process parameters for two steps EP

Many probes substrates have been polished with this technique and the obtained results are similar for all of them. In *Figure 2.14* is reported one case. As for the other experiments, the probe sidewall is shown before and after the polishing procedure, including SEM pictures.

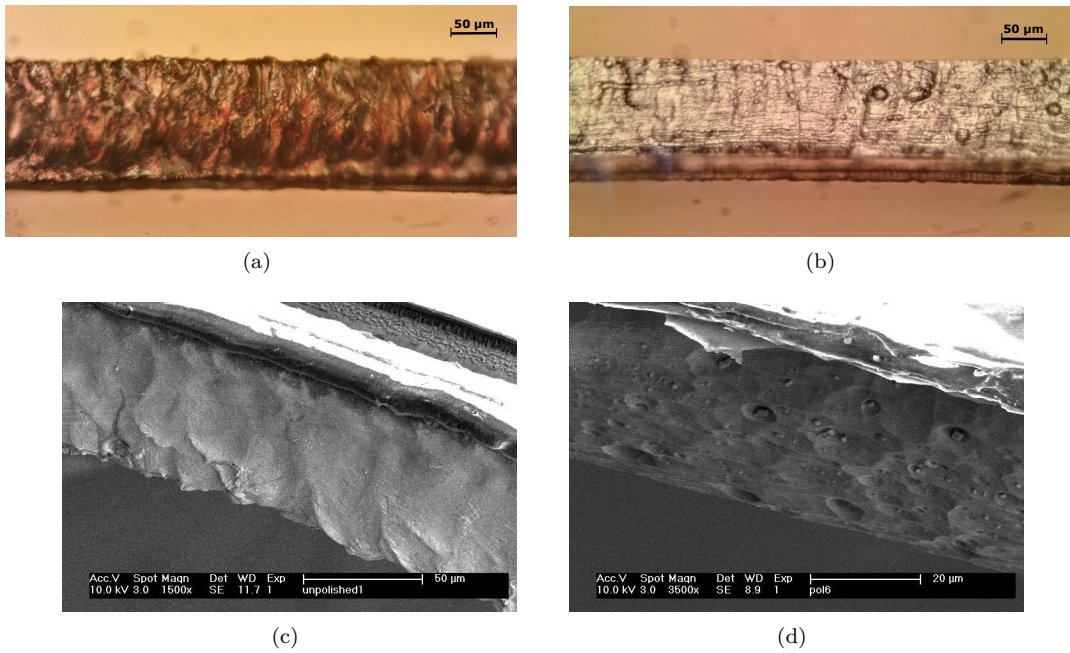


Figure 2.14: *Two steps EP: a) unpolished probe sidewall, b) polished probe sidewall c) SEM of unpolished probe sidewall, d) SEM of polished probe sidewall*

As can be seen, the stainless steel appears smoother after the process both for what concern high frequency and low frequency roughness contributes. This is particular evident by looking at the SEM picture in *2.14(d)*. However, as already mentioned, some bubbles are introduced during the

second step polishing that must be performed to improve high frequency roughness. This does not represent a big issue because these bubbles are mostly concave, so they cannot scratch too much the brain tissue. Anyhow, the procedure needs some optimizations to avoid the bubbles formation and provide a completely flat surface.

The profilometer analysis gives the 3D surface scan pictures reported in *Figure 2.15*.

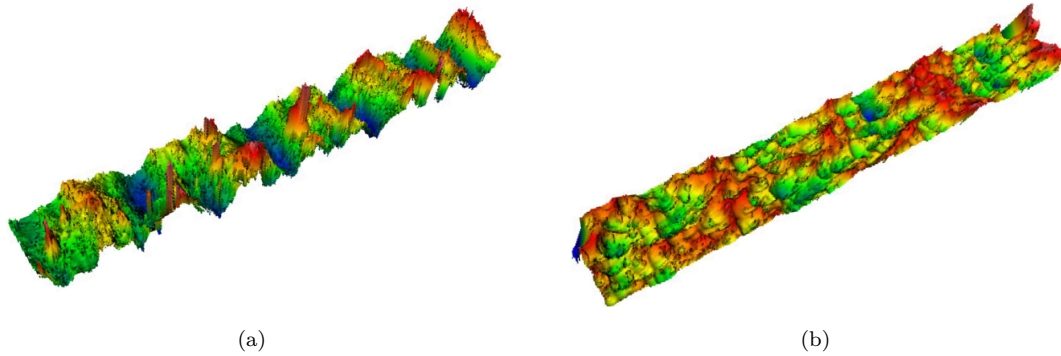


Figure 2.15: Two steps polishing 3D scan profile: a) unpolished probe sidewall, b) polished probe sidewall

As one can see the considerations done are valid: the roughness is reduced for both high and low frequency contributes even though some valleys are introduced because of the bubbles phenomenon. Quantitatively, it has been measured an improvement of *rms* around 45%.

2.1.4 Wet etching on steeltrodes

The last step of post-fabrication processing is related to the realization of hybrid rigid-flexible probes for in-vivo implantation to improve probes non-invasiveness.

As already mentioned, the biggest problem of such stiff devices is the fact that they are not free to move synchronized with the brain micromotions. As a result, the surrounding tissue can be truly damaged during long term neuronal recording.

The same technique introduced to make smooth surfaces can be adopted here to remove a stainless steel section and release the Parylene above the substrate, like in a flexible probe. In this way, the probe can be easily implanted without the use of external shuttles because the tip is still rigid enough and, at the same time, it can float inside the brain without the constraints of a completely stiff design. Since with this procedure one aims to remove completely the metal below the polymer, the technique is called Electroetching (EE) and it is different with respect to EP only because the processing time is bigger. Indeed, since the substrate has to be removed completely, the process needs to be carried on until the two polished edges on the sides join each other in the middle of the shank: the difficulties of this procedure are related to the capability of maintaining uniformity so that the etching starts from the bottom and then reaches the top. Only in this case it is ensured always an electrical connection between the cathode and the anode so that the process can go on. On the contrary, if, for some reasons, the connection is lost on the top before the metal on the bottom is completely etched, the process stops by itself and the result is not achieved. In order to maintain this uniformity it has been chosen to use a micromanipulator along the z axis to slowly move down the probe in the electrolyte solution, 2 – 3 mm for each step of the process. Moreover, there is the need to protect the bottom section of the probe (i.e. the tip) in which the stainless steel substrate must remain intact. For this purpose crystal bond has been adopted. Once the process is concluded the latter can be removed in Acetone.

The electrolyte solution used for this process is composed by 3% Oxalic acid in DI water by weight, since the aggressivity of this chemical composition is small compared to other chemicals. The process has been carried out in DC domain with a current of 0.2 A to keep the etching process slow.

The *Figure 2.16* reports the obtained result.

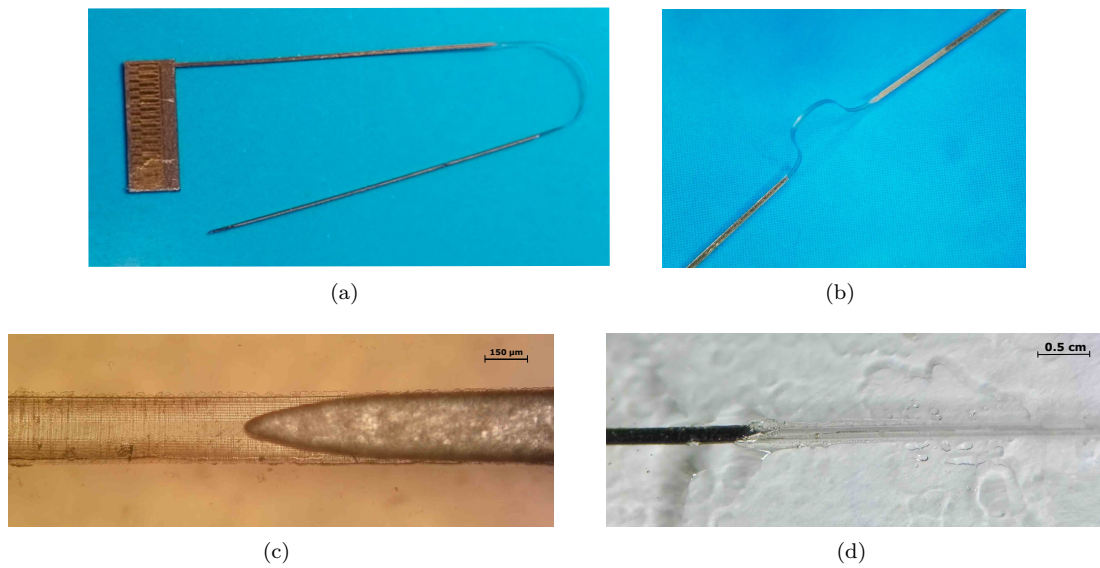


Figure 2.16: *EE on steelrode: a-b) hybrid probe after the process, c-d) particular of the interface between the flexible and rigid sections*

As shown in *2.16(a)* and *2.16(b)*, the released section can be obtained gaining in flexibility without damaging the rest of the probe. Moreover, by using the micromanipulator, that section can be extended up to some centimeters, depending on the specific probe application. The interface between the stiff region and the flexible polymer is reported in the *2.16(c)* and *2.16(d)*: as can be observed, no residues of stainless steel remain under the Parylene so that no other damages to the Parylene or to metal traces are caused during implantation.

Chapter 3

Packaging

Packaging is the key operation required to interface the probe with an electrical setup that allows to collect recorded data. At the same time, it is the design and production of an enclosure for the probe back-end which has to protect from mechanical stress and other environment variables. Designed flexible Printed Circuit Boards (PCB) have been used as a back-end extension to interface the probe with the electrical equipment. They aim to physically isolate the fragile probe back-end, thus reducing mechanical stress and damage probability. At the same time, the electrical connection is established so that the recording operation or the electrical characterization can be performed easily.

The connection between the probe and the flexible PCB can be obtained through:

- *Flip-chip bonding*;
- *Zero Insertion Force (ZIF) connectors*;

Among packaging techniques, flip-chip bonding is one of the most known methodologies. It represents a valid alternative to wire bonding because it allows to reduce back-end dimensions, resulting in robust layouts without introducing critical issues such as fragility of the interconnections or tricky procedures. However, depending on the particular device features, it is not always the fastest technique that can be adopted: it can make the device packaging procedure in series too long.

For this reason, a custom packaging technique using ZIF connectors has been developed and used as well.

3.1 Flip-chip bonding

Wire bonding is the most used technique for chip level interconnects, but it introduces some critical issues when it has to be adopted for medical devices applications, such as fragility and long time procedures for each device. It foresees the use of a thin metal wire, generally in gold or aluminum, that connects the chip pads to the substrate. For this reason, the result is a peripheral interconnection, which means, in the specific case of implantable probes, increasing the area of the electrical back-end. Another problem of wire bonding is the introduction of high electrical parasitics, resulting in poor electrical performance, that is the most important aspect to take care of in case of small electrodes for neuronal recording.

Flip-chip bonding, on the contrary, does not present these issues and, furthermore, has advantages over other packaging methods in terms of reliability, flexibility and cost. Anyhow, the major advantage of this technique remains the possibility to use the whole chip surface when interconnecting, following an approach called "area array bonding" [60]. A common property of this bonding is that the chip (i.e. the probe back-end) is flipped facing down to the substrate (i.e. the flexible PCB) and the connection between the two of them is made using bumps of electrically conducting material. In order, these are the main process steps for a conventional flip-chip bonding procedure:

1. bumps placing on the chip surface;
2. chip flipping and alignment procedure;
3. bonding condition application.

In *Figure 3.1* this process flow is reported .

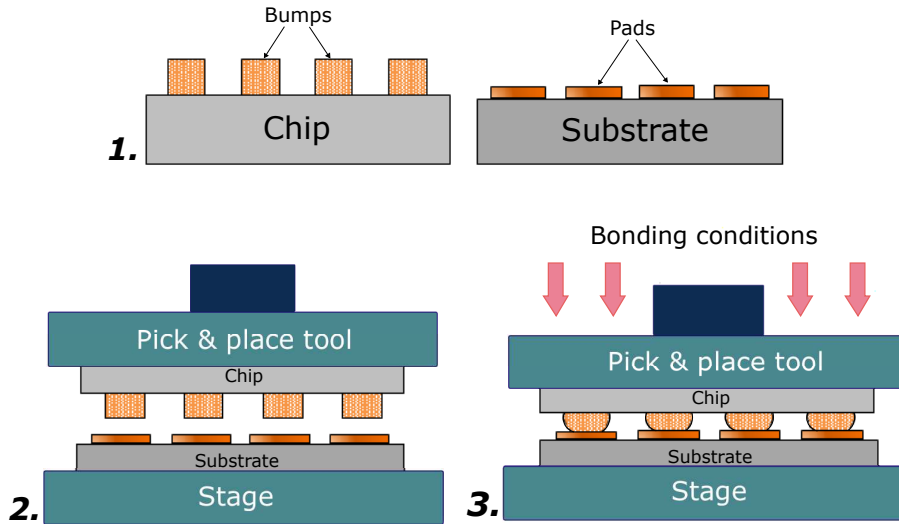


Figure 3.1: Flip-chip bonding technique [61]

Flip-chip assemblies are commonly classified by the type of bumping, method of attachment and processes used [62]. A first classification can be made in terms of bonding conditions [63]:

- **Flip-chip process by solder reflow** As the name suggest, in this process the bumps are soldered directly on one of the two surfaces, generally the one that will be facing down. Sometimes, for small die, solder can be deposited using electroplating technique as well as solder ink jet or solid solder deposition [63]. After the alignment, reflow of the bumps allows to create the joints. Since the exposed connections are most of the times very fragile, underfill material is forced to fill the empty space between the two surfaces. In the end, this material is cured with heat. Since joint fixing operations is most of the time impossible after the underfill process, the testing operation must be performed before it [63].
- **Flip-chip joining by thermocompression** In thermocompression bonding process, the connection between bumps and pads is performed by using force and heat. The process requires that gold bumps are placed on one of the two surfaces. Thus, after the alignment, a uniformly pressure is applied at a certain temperature (the latter is generally applied with a gradient). Since the process requires high bonding force and temperature, the process is limited to robust substrates such as metals or silicon [63].
- **Flip-chip thermosonic joining** In order to speed up the thermocompression process, ultrasonic power can be applied. The energy is transferred from the tool to the bonding area through the back surface of the chip. Thus, the energy introduced, slowly deforms the bumps and help the join process. Since the latter is speeded up with the ultrasounds, there is no need to keep the temperature as high as the previous case, making this process more suitable for low temperature applications. On the other hand, silicon or similar materials can crack under the application of excessive ultrasounds [63].

All the previous described techniques are valide candidates to be used in a packaging process for implantable medical devices. At the same time, there is the need to find a procedure that can help to make the packaging procedure in series faster and with a high yield.

Given this assumption, placing solder bumps on the pads of the back-end, regardless of whether it is done manually or by adding one or more steps to the fabrication process, it is something that takes time and can damage the probe. For this reason, conductive adhesives can be used as a viable alternative.

3.1.1 Flip-chip joining using adhesives

The basic idea is to glue together the two surfaces using an adhesive that establishes a physical connection and an electrical interconnection at the same time.

Adhesively bonded flip-chip has the advantage to combine cost efficiency with the properties of thin structures. Among the adhesives advantages, ease of processing, low curing temperatures and no need to use underfill materials after the process are the most relevant [63]. There are three different types of adhesives that can be used. The following to present them.

Non conductive Adhesive (NCA)

It is an adhesive made in polymer having no conductive particles, so it is often used in combination with stud bumps or other substrate metallizations. In this way, when heat is applied, it dries and establishes the mechanical contact between the bumps and the corresponding pads under compression, allowing the electrical connection [64]. The *Figure 3.2* shows flip-chip bonding technique using NCA.

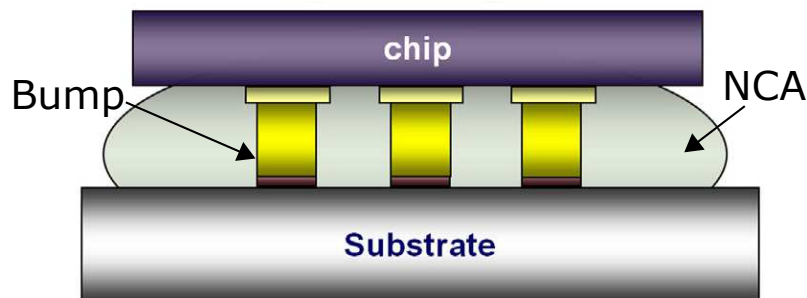


Figure 3.2: NCA flip-chip bonding technique [64]

Isotropic Conductive Film (ICF)

ICF are polymer mixtures filled with conducting particles that assures conductivity [63]. Commonly, the conductive particles are silver or nickel [60]. The particular feature of this adhesive is that it is isotropic, meaning that the electrical connection can be established in all the directions. Before to apply the adhesive, it is generally necessary to create gold bumps on the die padsto provide a good electrical contact with the polymer particles [60].

The *Figure 3.3* shows flip-chip bonding technique using ICF.

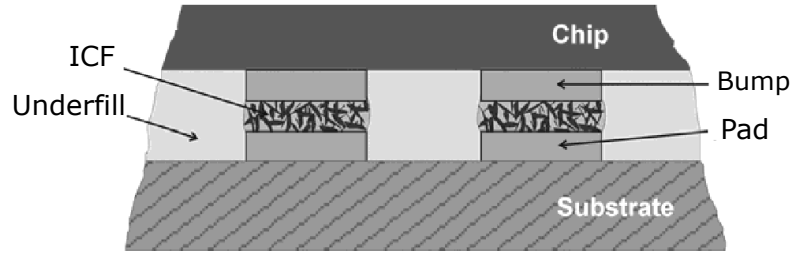


Figure 3.3: ICF flip-chip bonding technique [65]

Anisotropic Conductive Film (ACF)

ACF are films consisting of adhesive polymers and conductive particles dispersed in the adhesive itself, similarly to ICF. The particles can be made of Au, Ag, Ni, or Au/Ni metal balls or even polymer coated with metal. The typical diameter of particles is from 3 to 10 μm [64]. Before bonding, the electrical conductivity is ensured in all directions, whereas, after bonding, the adhesive becomes electrically conductive only along z-direction: that is the reason why it is called anisotropic. Because of its advantages of low-temperature processing, ACF bonding technology has been widely used for lot of applications, especially those requiring fine pitches. The *Figure 3.4* reports ACF flip-chip bonding technology.

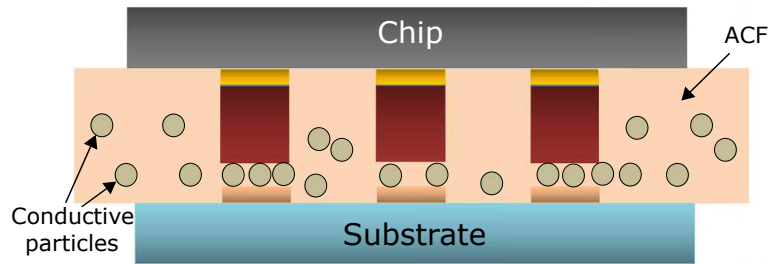


Figure 3.4: ACF flip-chip bonding technique [64]

Because of its versatility, easiness and, thanks to the fact that it does not require any kind of bump, ACF technology represents, among the ones described, the best choice to package implantable neural probes.

As already mentioned, each probe has to be connected with a flexible PCB that will be used as an interface for the electrical characterization system. Each PCB consist of a replica of the probe back-end, with electrical pads from one side interconnected to pads on the other side via metal interconnections. The reason behind the choice of having flexible PCB is related to the fact that in this way the back-end is less exposed to mechanical stress. Moreover, this structure allows to quickly interface the probe with the electrical setup as explained more in detail in *Chapter 4*.

The packaging procedure is straightforward and can be synthesized in the following steps:

1. ACF deposition and preheating;
2. probe/flexible PCB placement in bonder device;
3. alignment operations;
4. bonding process;

A small portion of ACF is cutted from the tape and the thin protection layer is removed. Then it is carefully applied along one side of the PCB covering the electrical pads (a small portion remain

uncovered to allow alignment operation). A preheating process of few seconds at $35\text{ }^{\circ}\text{C}$ is needed to glue the ACF and making the connection stable. Thus, the two samples can be placed inside the flip-chip bonder tool (*Laurier M9 flip-chip die bonder*). The PCB is flipped and the pads are aligned using a high precision camera. Once the two of them are completely aligned, the camera is moved all the way out and a mass of 4500 g is applied as to establish a pressure. Since stainless steel is a conductive material, a high temperature can damage the Parylene C that cover the top layer of the probe. For this reason, the temperature has been kept under a safety threshold of $150\text{ }^{\circ}\text{C}$. The process is carried on for 2 minutes; afterwards, the tool, together with the packaged probe, needs to be cooled for few minutes.

A correctly packaged 16 channels probe is shown in *Figure 3.5*, before and after the process.

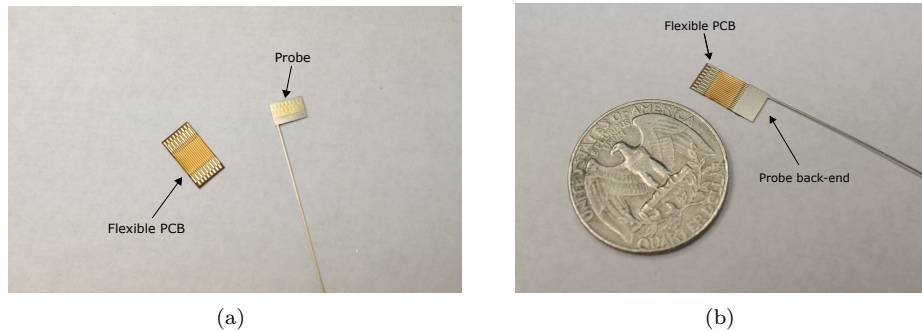


Figure 3.5: Steeltrodes packaging using flip chip: a) before packaging, b) after packaging (quarter dollar shows the scale)

As can be seen from the picture, this process allows to obtain very small back-end configurations, in which the size along the x direction does not increase at all. On the other hand, flexible polymer probes cannot be packaged with this procedure because of the extreme flexibility of the back-end that does not permit to align correctly the electrical pads. Therefore, another packaging method has been implemented; it is going to be used even with steeltrodes to further improve the speed of the process.

3.2 ZIF connectors packaging

As already mentioned, another possibility to easy package implantable neural probes is represented by ZIF connectors. Each of these requires very little force for insertion, explaining the reason of the name. Before the device insertion, a movable lever on the side of the socket is moved all the way up, pushing all the contacts apart so that the insertion does not damage the pads. The lever is then moved back so that the contacts grip the pins of the device. Due to this required mechanical mechanism these kind of devices are more expensive than standard integrated circuit sockets, justifying the expenses just for very high precision applications. Moreover, they tend to have a large board area due to the space occupied by the lever mechanism: this implies that the flexible PCB has to be designed to cover this space. In the *Figure 3.6* a ZIF connector is shown.

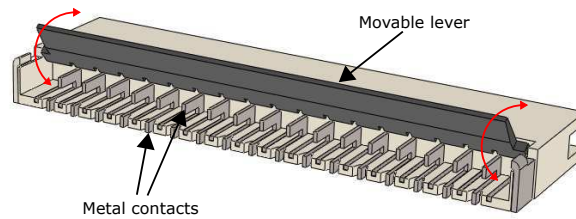


Figure 3.6: ZIF connector (*Memcon*)

The ZIF is soldered to the flexible PCB using reflow technique. It is a process in which a mixture of solder and other materials, called solder paste, is used to temporarily glue electrical components to their contact pads. After the placement the entire structure is heated into an oven so that the solder paste first reflows into a molten state and then solidifies, creating permanent solder joints. Once the ZIF is correctly soldered over the PCB, the probe can be inserted into the connector establishing the electrical contacts. The pre-fixed dimensions of the ZIF, which are a standard, have been used in mask design to get back-end that perfectly fit into the connector. In this way, no further mechanical stress is added to the probe during the packaging operation. Although the probe can be easily removed from the ZIF if requested, the electrical pads can seriously be damaged during the operation. For this reason, each packaging process has to be intended as not reversible. The *Figure 3.7* reports examples of steeltrodes packaging, before and after the process..

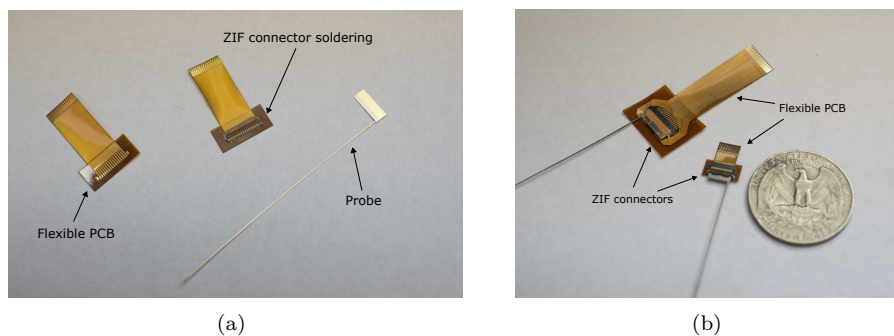


Figure 3.7: Steeltrodes packaging using ZIF: a) before packaging, b) after packaging (quarter dollar shows the scale)

Packaging is challenging for polymer probes. Due to the extreme flexibility of the back-end they cannot be bonded with flip chip technique in the same way as they cannot be easily interfaced with the ZIF. The latter, in fact, requires to have a rigid surface with high planarity to manage the insertion.

The polymer does not provide these properties, but they can be obtained using Kapton tape. The implemented procedure exploits the sticky surface of the tape to glue the probe back-end on it. Thus, the tape in excess can be cutted away and the probe carefully inserted into the ZIF. The operation of gluing the tape with the probe back-end can be managed using a paintbrush and Isopropanol to flatten the probe during the process. The result of this process is reported in *Figure 3.8*

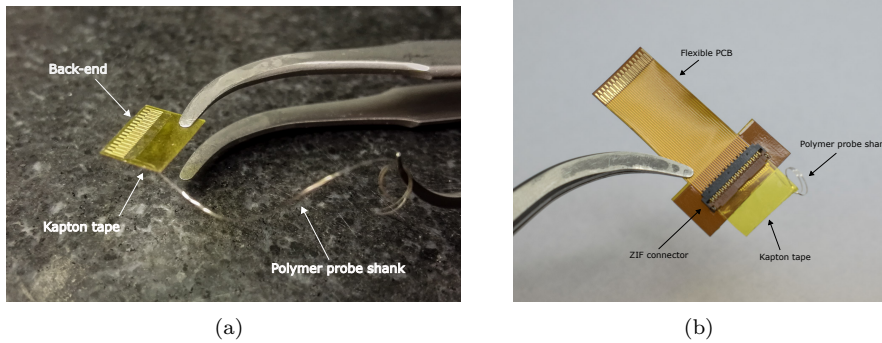


Figure 3.8: *Polymer probes packaging procedure: a) Kapton tape to increase stiffness, b) final result (tweezers show the scale)*

Once the described processes have been carried out, the electrical properties of the probe must be evaluated. The goal is to verify if the probe has a good number of working channels and, at the same time, if the packaging operation has been performed correctly. The following chapter describes more in detail the adopted procedure.

Chapter 4

Electrical characterization

Once the probe has been released from the wafer and packaged, it is ideally ready to be used for recording operation. This can happen under the assumption that the fabrication process has worked properly and electrodes are able to record from neurons correctly. But, since lithography is subject to various kinds of malfunctions, there is the need to test experimentally the realized probes before *in vivo* implantation.

At the same time, the process could have been performed perfectly without introducing any kind of problem, but the electrical features of the electrodes could not be the targeted ones. For example, a low electrode-brain tissue impedance interface is critical when a high spatial resolution has to be achieved. In order to verify all these aspects, post-packaging electrical characterization of the probe is required.

4.1 Impedance model

Impedance characterization of the electrodes is of fundamental importance in order to get important informations about the functionality of the implemented device. By an electrochemical point of view, brain tissue can be approximated with an electrolyte solution in direct contact with the recording electrode. For this reason, from now on, in this thesis work it will be referred to the impedance of the electrode as the electrode-electrolyte impedance at the interface.

There are several reasons to want this quantity as low as possible. The first reason is strictly connected to the fact that a high impedance would result in high thermal noise that there is the need to minimize.

A second aspect is related to the quality of signal that one wants to get. From the recording point of view, the extracellular signals to be recorded are low, on the order of microvolts per neuron. The neuronal signals will be lost in the noise, if the electrode impedance is not low enough [66]. A clarification on this aspect is possible by introducing a model able to describe the electrode-electrolyte impedance interface.

The first model was presented in 1899 by Warburg that supposed that the interface could be described by a polarization resistance in series with a polarization capacitor [67]. The use of a constant phase angle impedance it was subsequently introduced after that experimental findings revealed that the capacitance is frequency-dependent [68].

Randles proposed a third version in which the interface capacitance was shunted by a reaction impedance; the parallel was in series with the solution resistance [69]. In this version, the capacitance is represented by a classical double layer capacitor that does not approximate well the non-ideal behavior at the interface.

The model used in this thesis work is an adaptation of the theoretical ones mentioned above: it consists of a constant phase element (CPE) impedance shunted by a charge transfer resistance, together in series with the solution resistance [70].

The *Figure 4.1* shows the circuit.

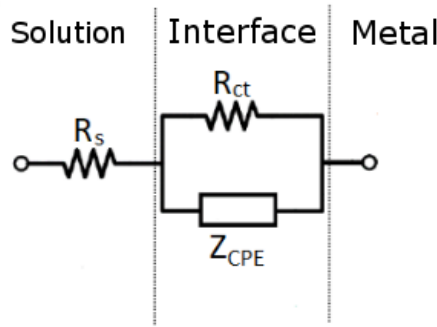


Figure 4.1: Equivalent circuit model of electrode-electrolyte interface

The impedance of the CPE is described by the empirical relation [71]:

$$Z_{CPE}(\omega) = \frac{1}{Y_0 (j\omega)^\alpha} \quad (4.1)$$

where $\omega = 2\pi f$ and Y_0 and α are fitted parameters ($0 \leq \alpha \leq 1$). As can be noticed, if $\alpha = 1$, Z_{CPE} describes an ideal capacitor, whereas if $\alpha = 0$ it describes a pure resistor with resistance $1/Y_0$. Starting from this model, the complete chain of electrical systems can be built as shown in *Figure 4.2*. The source is obviously represented by the neuron that fires. Thus, the generated signal is the input which will be recorded from the electrode and, therefore, will arrive at an amplification system before the acquisition.

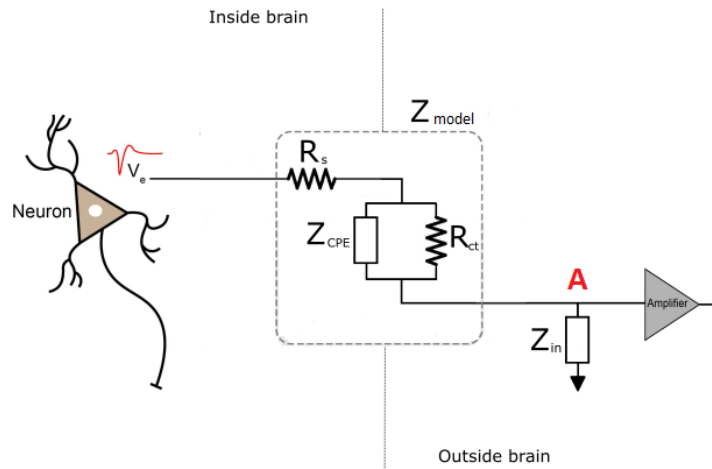


Figure 4.2: Electrical acquisition chain

As shown in the schematic, the amplifier system has its own input impedance that is in the order of tens of $M\Omega$. The input impedance is in a divider configuration with the whole impedance of electrode-electrolyte interface described by the model. This implies that, if the impedance at the interface is too high (comparable with the input impedance of the amplifier), due to the partition the voltage at the input A would become too low for the amplification system. In other words, the already low signal coming from the neuron will arrive even smaller to the acquisition system, making difficult the post-acquisition analysis.

Therefore, there is the need to keep the impedance at the interface as much as low as possible. However, between high spatial resolution and low impedance, a trade-off is established. In fact, to

obtain a high spatial resolution, it is necessary to decrease the electrode area, so as to measure signals from a small number of electrodes. Since the area is inversely proportional to the impedance, whenever the area is reduced the impedance increases, resulting in conflict.

One solution to reduce conflictuality, is to improve the roughness of the interface by performing electroplating. Due to the rough surface, the overall exposed area is big enough to maintain impedance low even though the electrode diameter remains the same. Electroplating is accomplished with poly (3,4-ethylenedioxythiophene) polystyrene sulfonate (PEDOT:PSS polymer). The *Figure 4.3* reports a microscope image of plated electrodes in a fabricated steeltrode.

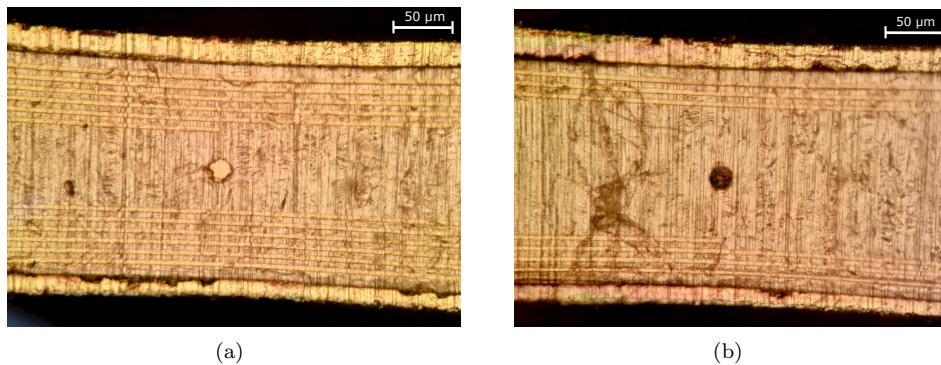


Figure 4.3: *Electrode examples: a) no plated, b) plated*

Plated electrode area can be distinguished by the non-plated one thanks to the color that becomes darker after the plating procedure. Only working electrodes will be plated during the procedure because an electrical interconnection has to be established between the cathode and the anode in the solution bath [72]. As can easily be understood from the fact that the roughness of the electrode has to be increased, electroplating is the opposite of electropolishing process presented in *Chapter 2*.

To quantitatively characterize the impedance at the electrode-electrolyte interface, Electrochemical Impedance Spectroscopy (EIS) has been used.

4.2 EIS characterization

In EIS technique a small sinusoidal signal is used to test the impedance characteristics of a cell over a more or less large frequencies range. The result is the impedance spectrum for the electrochemical cell plotted with Bode diagrams. In other words, this technique allows to study the capacitive, inductive, and diffusion processes taking place in the electrochemical cell [73].

Depending on the fact that the applied signal is a voltage or a current, there are two different configurations that can be adopted:

- potentiostatic mode;
- galvanostatic mode.

In the first one, a sinusoidal AC potential is applied and the resultant current is measured as a frequency-dependent parameter. The ratio between the applied potential $E(\omega, t)$ and the current $I(\omega, t)$ is the impedance $Z(\omega, t)$. For the galvanostatic mode a current is applied and a voltage evaluated. Generally results provided by the two techniques are the same. However, if the device under test suffers of some variations in time, the computed values of impedance may differ.

EIS measurements are more often performed in potentiostatic mode than under galvanostatic mode. The reason is mostly convention, but there are even reasons related to the materials. For example, coatings and corrosion-resistant materials have a higher impedance, so that the application of a 10 mV sinewave results in a nA (or smaller) response. At the contrary, for low impedance devices, such as batteries or large supercapacitors, the application of the same sinewave produces amperes of current-flow, possibly damaging the device itself. For devices with intermediate impedance (like smaller batteries, smaller supercapacitors, and sensors), either potentiostatic or galvanostatic modes may be used [73].

For this reasons, potentiostatic method has been adopted during this thesis work to characterize electrically all kind of implantable neural probes succesfully fabricated and packaged.

In order to perform the measurement, some aspects have to be taken into account. First of all, there is the need to define in which measuring environment the experiments will be carried out, by specifying which has to be the starting setup and how data will be collected once the measurement is completed. Then, it has to be defined how to make the measurement process automatic gaining in reliability and speed (lots of electrodes in each probe means lot of time to perform each characterization). Finally, and this is linked to the previous considerations, how to interface the whole system measurement with the computer for data post-analysis.

4.2.1 Electrodes configuration

EIS measurement provides the use of different types of electrodes in a solution bath that works as electrolyte solution. In the case of implantable neural probes, the electrolyte is a solution that replicates electrochemical properties of the brain. For this purpose 1xPBS (Phosphate Buffered Saline) can be used. The preparation is very simple because it just consists in the dilution in DI water of purchasable PBS solution.

The most common configuration to perform EIS characterization is three electrodes mode. As the name suggests, three different electrodes are used:

- *Working Electrode* (WE);
- *Reference Electrode* (RE);
- *Counter Electrode* (CE).

The WE is the electrode where the potential is controlled and where the current is measured; it is the probe electrode under test. The potential is measured with respect to a reference represented by the RE. The latter should have a constant electrochemical potential as long as no current flows

through it. This electrode is in Silver/Silver Chloride (Ag/AgCl). Finally, the CE, or Auxiliary Electrode, is a conductor (Platinum Pt) that completes the cell circuit, making a current flow possible. For this thesis work, *BASI Inc* electrodes have been used, respectively MW-1032 and MF-2052 models, as shown in *Figure 4.4*.

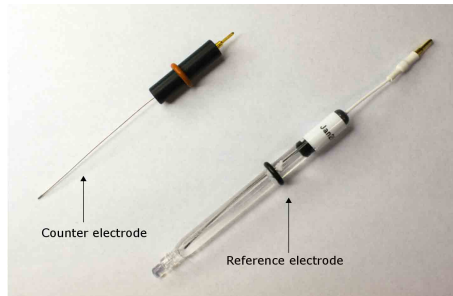


Figure 4.4: Counter and reference electrodes used for measurements (*BASI Inc*)

Another configuration that can be adopted provides the use of just two electrodes, WE and CE, without the reference. The difference is related to the fact that RE is used to determine the potential across the electrochemical interface accurately because it establishes a reference in the solution in which the system works. A two electrodes system is used just to control the potential across the electrochemical interface between WE and CE. That means that, whenever the measurement is performed in two electrodes mode, even the electrochemical impedances of the measurement electrodes are included in the measurement. In other words, the three electrodes configuration allows to get a more precise measurement because it confines the measure just at the electrode-electrolyte interface.

Hence, three electrodes configuration will be used for EIS characterization unless differently specified.

In *Figure 4.5* is reported three electrodes configuration schematic.

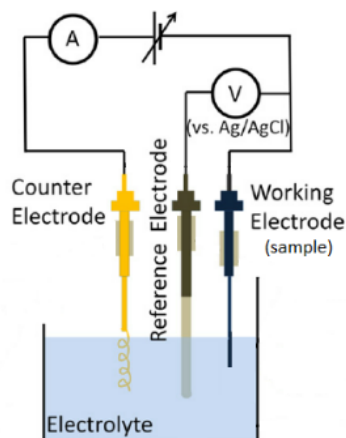


Figure 4.5: Three electrodes EIS measurement configuration.[74]

4.2.2 Potentiostat

In order to control a three electrodes cell and run electrochemical experiments, a *potentiostat* is required. The task of this electronic component is to control the voltage difference between WE and RE by adjusting the value in relation to the current measured on the CE.

Bipotentiostat and polypotentiostat are two other configurations capable of controlling different

applied potential as an offset as a preliminary step before the measurement. As already mentioned, this is possible in three electrodes configuration, by measuring the impedance just at the electrode-electrolyte interface without including other electrochemical impedance contributes.

The potentiostat with the NOVA control software represent the interface between the physical measurement setup and the computer, allowing to record the final data for the following analysis.

4.2.3 Interfacing board

As already said, each probe consists of a certain number of channels terminated by recording electrodes. For the EIS configuration presented so far, each of those electrodes has to work as a WE for the potentiostat, so it needs to be electrically interfaced with it. For this purpose a specific PCB has been designed.

The interface has to switch between one channel and the following one, allowing the characterization of all of them. Of course this procedure can even be manually carried out, but the cost in terms of time, reliability and mechanical stress for the probe back-end would be high. For this reason, an electrical circuit needs to be adopted, by paying attention to keep impedance parasitics as much as low as possible to avoid fake results.

From an electrical point of view, a so defined circuit it is a demultiplexer, because it has to take a single input (the WE) and transfer it to each of its outputs in subsequent times. So, theoretically, a classic digital demultiplexer can be adopted. The main issue of this solution is represented by the technology adopted. Indeed, complementary metal-oxide semiconductor (CMOS) technology that is used to implement this kind of devices, introduces parasitics resistances even in the case of switched-off transistors. This mainly happens because whenever an open circuit is established, there is not a physical interruption of the trace, so a small charges flow is still present. This implies that this type of device cannot be used to do the requested operation of demultiplexing, because those resistances are going to be in parallel with the electrodes of the probe.

In replacement, electromechanical relays have been adopted. Their advantage is in the fact that it is possible to obtain a closed circuit when required by the electrical control of a mechanical switch, with infinite impedance until then.

Since the number of channels per probe can vary between 4 and 32, it is necessary to use 32 different relays to be able to use the board in the worst case scenario. Inevitably, this makes the PCB larger, as each relay takes up a lot of space on the board compared to a digital component. CMOS demultiplexers have still been used as drivers for the relays, controlling the switch rate of each of them. The AUTOLAB potentiostat provides some digital output through a Digital Input-Output port (DIO) which have been used as control signals for the demultiplexers.

Finally, the design procedure focused on choosing the correct connectors to interface the probe back-end with the board. As mentioned in *Chapter 3*, the flexible PCBs used for packaging, have been explicitly designed to fit the back-end of each probe with the ZIF connector. So the latter was included in the design along with a standard pin connector. Since OMNETICS is another widely used standard, it has been chosen to include it as a third connector.

In *Figure 4.8* is reported the schematic of the designed circuit.

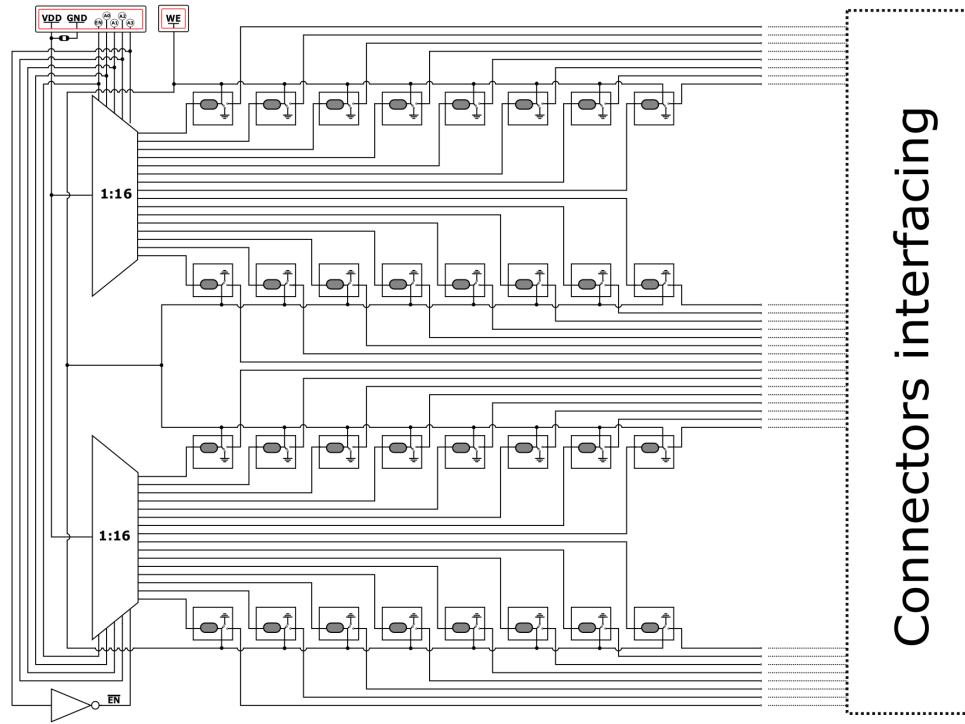


Figure 4.8: Schematic of the designed circuit

As can be seen, the enable for the two demultiplexers is provided by the AUTOLAB system, through the DIO port, as another digital output. It directly controls one of the two demuxes, while the second one receives the denied version from a digital inverter. This ensures that the first demux works for the first 16 relays, while the second one for the remained 16. A decoupling capacitor of $10 \mu F$ has been included in the design between the supply voltage and the ground. Each of the three connectors on the bottom is interchangeably and, depending on the back-end of the probe, each of them can be used for interfacing.

As already mentioned, the WE must be the output of each relay, whenever it has to be specifically activated. Then the supply voltage is provided to that specific relay according to the control signal coming from AUTOLAB, by correctly switching the demux. Therefore, the voltage signal controlled by the potentiostat on the WE is directly applied to the specific electrode of the probe, leaving all the others in open circuit conditions.

The designed PCB is a two layers configuration with two ground planes, one per face. In order to minimize as much as possible the board physical dimensions, it has been chosen to place 16 relays per side, using surface-mount terminal instead of through-hole terminal version.

The *Table 4.1* reports parts of main components used in this project.

Component	Producer	Name
Relay	Omron	G6L-1F
Mux/Demux	Analog Devices	ADG1606
Inverter	Texas Instruments	SN74AHC1G04
Capacitor	Samsung Electro-Mechanics	CL05A106MP5NUNC

Table 4.1: Main components used for the design

The components have been soldered using the reflow soldering technique.

The Figure 4.9 reports the PCB schematic and the complete board after soldering; red lines represent the top layer, blue ones the bottom layer. They are interconnected via vias.

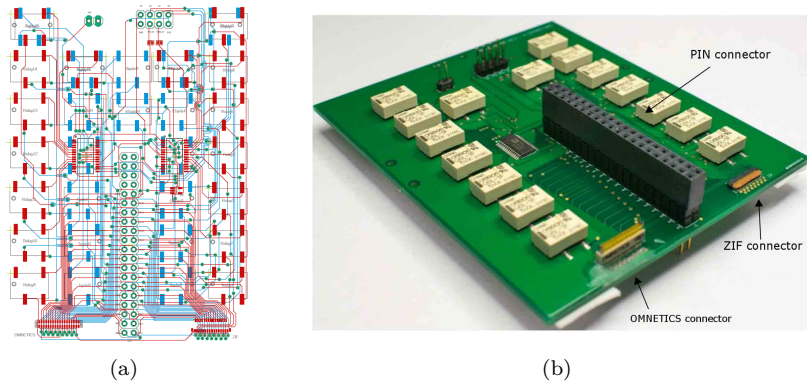


Figure 4.9: Interfacing board: a) PCB design, b) PCB after soldering

After the realization, the board has been tested to prove its functionality. Initially it has been tested under electrical point of view, to verify if the connections had been routed correctly or if there had been damages during the soldering procedure. Furthermore, the board has been used to perform some dummy measurements with probes whose operating mode was known. No issues have been reported.

4.2.4 Measurement setup

The whole measurement setup for EIS characterization is the one reported in Figure 4.10.



Figure 4.10: Measurement setup for EIS characterization

The measurements have been done in a Faraday cage to avoid the possibility that electromagnetic noise could corrupt the analysis. As soon as the electrolyte bath with the three electrodes and the PCB board have been placed, the measurement can be started by using a computer as an interface with the potentiostat. The software that allows the communication between the two of them is provided by NOVA producer. It allows to set all the measurement parameters together with the possibility to change the control signals through the DIO port. As previously mentioned, these digital controls are used in the interfacing PCB to switch between the channels.

Within the parameters that can be set in NOVA, there is the possibility to impose the OCP control, the sinewave characteristics and the range of frequencies for which the impedance must be evaluated. For this thesis work, a $50mV$ root-mean-square sinusoidal signal at OCP has been used. The range of frequency varies depending on the type of measurement that has to be carried out. Most of the time it was chosen to study the trend of impedance in the range $[10^2 \ 10^4]Hz$. The reason behind this choice is related to the fact that neurons are generally not capable of firing at more than $1000 Hz$, so that range is of particular interest.

During the measurement operation, data are collected in separate files, so they can be easily plotted and analyzed.

4.2.5 Results and discussion

Impedance values are reported in terms of Bode diagrams, showing the trend of module and phase over the chosen range of frequencies. The *Figure 4.11* reports an EIS characterization for a 30 channels steeltrode.

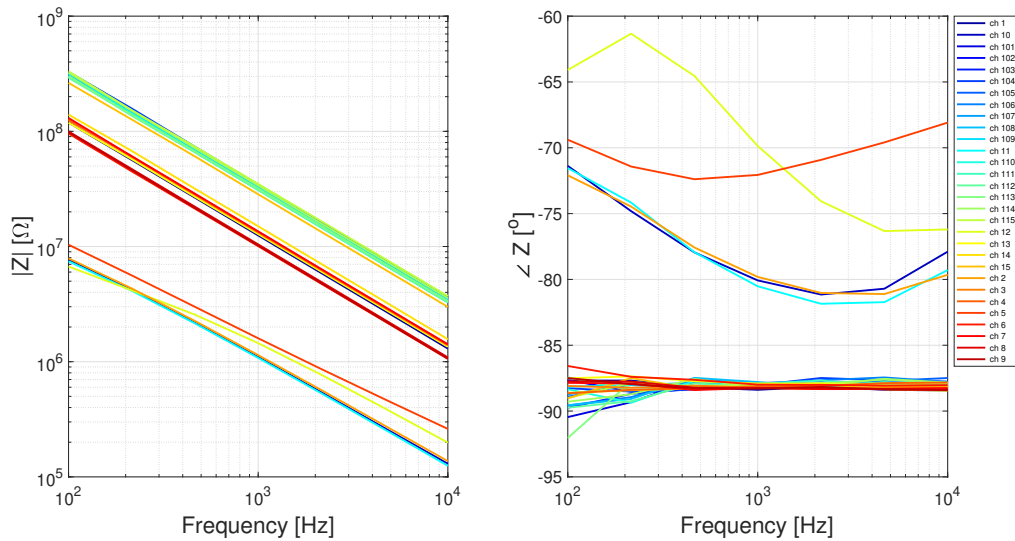


Figure 4.11: EIS characterization for a 30 channels steeltrode

In order to understand these results one needs to think about the metal trace of the channel as an equivalent impedance. When the trace is working, it behaves like a wire, making the electrical signal able to propagate. In this case the impedance measured at the interface will assume a value depending on the area of the exposed electrode. It has been verified that, for $15 \mu\text{m}$ diameter electrodes, the impedance at 1 kHz is in the range $[1 \text{ } 2.5] \text{ M}\Omega$. Hence, in the picture, those channels in this window values are working channels. On the contrary, a not working one presents somewhere along the trace an metal break that makes it an open circuit: the behavior of such structure is pretty capacitive. Indeed, the insulator at the breaking point works as the dielectric of the capacitor, with the two wire pieces on the sides working as the metal plates. As a result, the module of this structure will be higher than the previous one.

For what concern the phase, similar considerations can be done. As can be noticed from the graph, the phase for not working channels is close to -90° : this is how a capacitor works in phase. On the contrary, for working channels, the trend is to have a phase "less negative" than the previous one, around -70° . This is reasonable because the channel is a conductive wire, so the resistive component brings the phase towards positive values (a resistor in phase has a contribute equal to 0° over frequency). Anyhow, since some big capacitive effects are still present because of the parasitics of the wire, it is almost impossible to reach 0° .

This kind of analysis aims to give a benchmark on functionality of microfabricated probes in terms of number of working channels, quality of the processes and yield of the packaging procedures. It is focused on the response of a single channel because it measures the impedance at the interface for just one single electrode. At the same time, could be interesting understand which is the response of combinations of channels with respect to particular interference effects such as crosstalk. This kind of analysis is addressed in the next section.

4.3 Crosschannel characterization

As previously shown, each probe consists of a shank in which several electrodes are placed and interconnected with the back-end through many conductive channels. While the electrodes are exposed to record neuronal activity, the channels are insulated under a layer of Parylene C, in a such a way that it does not interact with the environment. Since the channels pitch is small, in the order of tens of μm , the crosstalk effect could be severe. The effect of crosstalk can be analyzed taking into account that the model for the electrode-electrolyte interface, described in *Section 4.1*, is still valid. Moreover, it is important to understand how the effect of crosstalk can vary depending on the conditions of the insulation above the traces.

4.3.1 Crosstalk effect

Current density accumulation in a wire can cause a change in current density in adjacent wires through capacitive charging with the two wires acting as the capacitor. The described effect is called crosstalk and the channel that causes the coupling is called "aggressor" compared to the channel that suffers the aggression, called "victim".

By defining with V_{out2} the output of the victim and with V_{in1} the input of the aggressor (where the signal source is imposed) the crosstalk is defined as [70]:

$$Crosstalk[dB] = \frac{V_{out2}}{V_{in1}} = -20 \log \left(2 + \frac{Z_{cc}}{Z_{elec}} + \frac{Z_{cc}}{Z_{sh}/Z_L} \right) \quad (4.2)$$

where Z_{elec} is the electrode impedance, Z_{cc} is the coupling impedance, Z_{sh} is the shunting impedance, and Z_L is the load impedance. In the specific case of electrodes for neuronal recording, Z_{elec} is represented by the impedance model of the electrode-electrolyte interface introduced in *Section 4.1*. The shunt impedance is the one across the insulation layer from the center of the metal trace to the electrolyte bath conductor. Since it physically represents the interconnect parasitic coupling to ground, it is sometimes called shunt impedance to ground. Then Z_L , that represents the amplifier input load impedance. Finally, the coupling impedance Z_{cc} that mostly models the interconnect parasitic coupling capacitance: each channel behaves as one plate of the capacitor and the insulator in the middle is the dielectric.

The circuitual schematic of crosstalk model between two channels is reported in *Figure 4.12*.

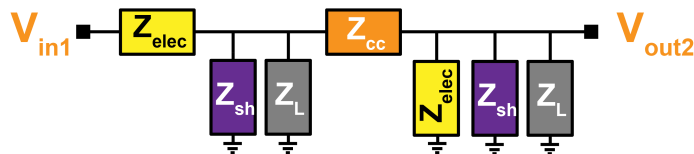


Figure 4.12: Crosstalk model of two recording electrodes with adjacent channels [70]

Equivalent circuit models developed implantable biomedical devices show that crosstalk effect affects the amplifier impedance above the electrode impedance (composed by the resistance of the electrolyte solution as well as resistance and capacitance of the electrode). As a result, the recorded signals can be attenuated by crosstalk effect, resulting in false signal in adjacent electrodes during recording or in unwanted accumulation of charge density between adjacent electrodes during stimulation [76]. Since the probes are going to be implanted in brain to record in-vivo neuronal activity, there is the need to characterize the response of the channel to the crosstalk. This means to evaluate the impedance between the channels in order to understand if the fabrications process or the geometry of the probe has to be modified (for example by increasing the channels pitch). Imposing one electrical signal to one electrode and measuring the response on the adjacent ones

is tricky due to the small dimensions of the probe. It would mean obtaining only a qualitative analysis of the crosstalk whereas it is more important to get values of the impedance between the traces. In order to do that, EIS similar setup can be adopted as described in *Section 4.15*. Since no amplifier system is used in EIS configuration, the previously described model can be simplified by removing the load impedance Z_L and expliciting the resistive and capacitive components in probe design. The *Figure 4.13* shows the model.

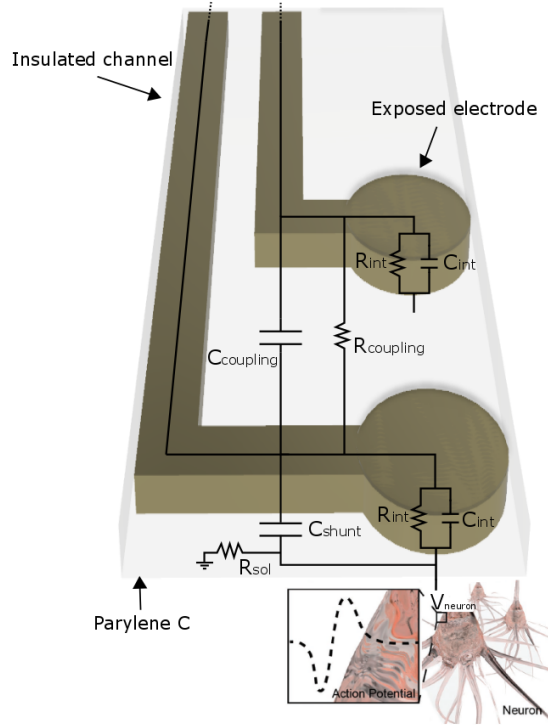


Figure 4.13: Crosstalk model between two channels

As can be noticed, for each recording electrode, the model of electrode-electrolyte impedance interface is exploited. The solution resistances are incorporated in one single resistance R_{sol} as well as the shunt capacitances in C_{shunt} . The resistive effects of the shunted impedances are negligible for the purpose of this analysis so they are not shown. For what concern the coupling impedance, it is mostly capacitive but there is even a resistive component that becomes relevant when insulation fails or shorts between channels are present.

4.3.2 Measurement setup

Starting from EIS measurement setup and introducing some changes, crosschannel response can be evaluated. So far, EIS characterization has been performed for single channel using three electrodes configuration. The multiplexer PCB board was used as the interface between the WE provided by the AUTOLAB potentiostat and the channels of the probe. Now the measurement has to be conducted between two channels at a time covering all the possible combinations of channels. The evaluated value is going to be the sum of the two electrode-electrolyte impedances at the interface, together with the coupling components between them.

In order to do that, PCB task must change from "choosing a specific channel" to "choosing a specific combination of channels". Actually, this does not require a modification in the board design. In fact, instead of complicating the design of the board, the same design can be adopted for a second PCB board to be used in tandem with the first one. The connection between the two can be made through male/female pin connectors; hence the first one can choose for a channel of the probe,

whereas the second one for another channel, resulting in a combination of channels at a time. The switching operation for the two boards can be managed using different digital control signals from the DIO port (25 pins are provided). An easy way to proceed is to start keeping one channel fixed on the first board and switching between all the others on the second board. Then, the first board can move towards the second channel and the second board again can switch between all the others, and so on. In this way, the procedure is automatically handled and, although the time required to cover all the combinations could be huge (depending on the number of channels on the probe), reliability is guaranteed and the risk of error avoided. The *Figure 4.14* shows the operating principle for a 16 channels probe. Each column represents the channels of the probe for each cycle of measurement; the activated channels are in green while the red ones represents disabled channels. The impedance measurement is carried out between the activated channels in each cycle. For summary reasons, not all the combinations are reported.

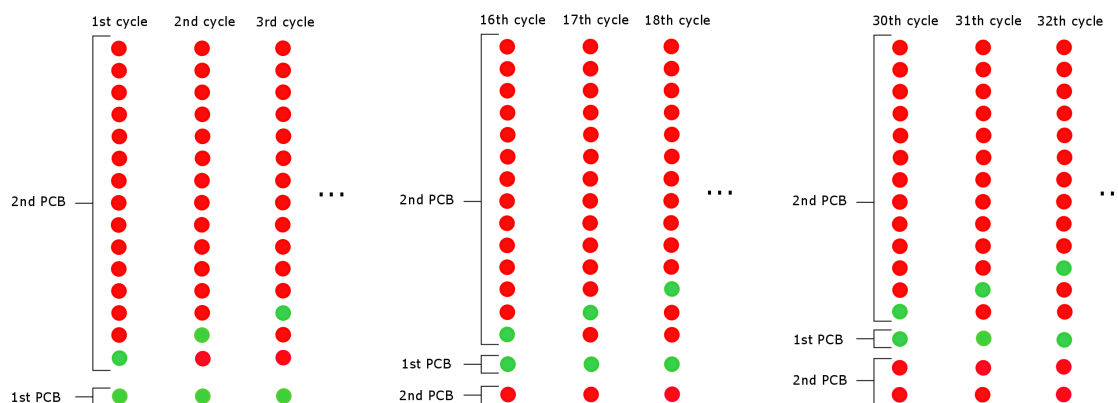


Figure 4.14: Combinations handling principle

All the routines for the switching operation, in terms of digital control signals to the demultiplexer of the board, have been generated automatically by C programming language scripts and then imported in NOVA.

A clarification needs to be done in terms of electrodes used for the setup. As previously described, the interfacing board for EIS characterization provides the connection between one probe electrode and the WE of the potentiostat. In other words, that specific electrode works as the WE of the system. This assumption is still valid in crosschannel characterization. The difference here is that there is a second board that cannot provide another WE, which is single for the potentiostat system. Since the second channel task is to close the circuit allowing the impedance measurement in the discontinuity section, in practice it works as the counter of the potentiostat; so the second board has to be connected to CE.

In this setup, it has been chosen to use a two electrodes configuration, without using the RE. In fact, the effect of the electrochemical impedances of the electrodes, corrected by the RE, has a very low impact on the overall value of the impedance measured, which is bigger than the case of the single electrode characterization. In this way, the setup is strongly simplified, with the probe connected to the two-boards configuration and alone immersed inside PBS, with one electrode working as the WE and another one as the CE of the potentiostat at each measurement cycle. This is illustrated in *Figure 4.15*.

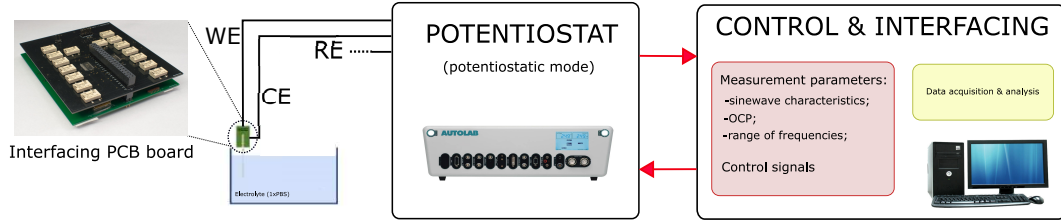


Figure 4.15: Measurement setup for crosschannel characterization

4.3.3 Results and discussion

The previously described setup has been used to perform impedance measurements in the specified range of frequencies. Since the impedance of each combination is interesting at the neuron firing frequency, the response at 1 kHz has been extrapolated. Then the data can be arranged in a matrix configuration in which the channel number is reported both on the two axis. Thus, each point on the matrix represents the wanted combination between the channel on the x and the one on the y. The *Figure 4.16* reports the results of one characterization on a 30 channels probe.

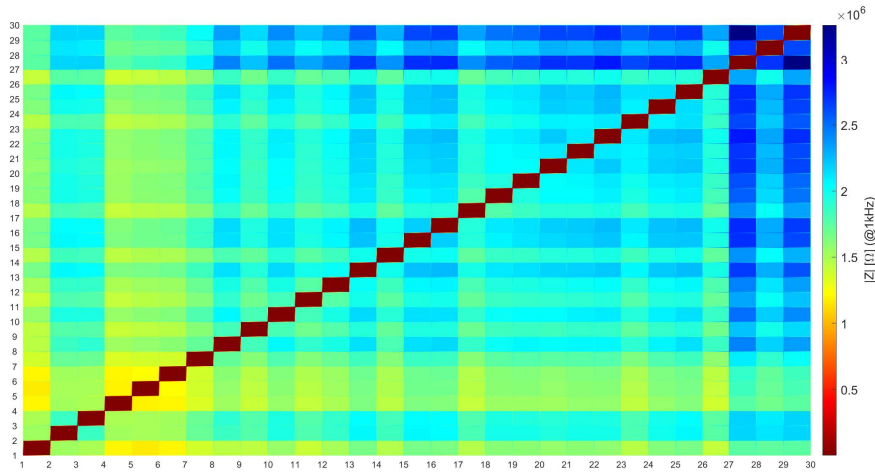


Figure 4.16: Results of crosstalk characterization for a 30 channels probe

The matrix is mirrored along the main diagonal because the combination of channels repeats two times. As the solution can take a while to infiltrate in Parylene C cracks, the effects of bad insulation do not occur immediately after immersing the probe in the solution. For this reason the probe is left dived for a while before starting the measurement.

The diagonal of the matrix corresponds to all the combination of one channel with itself, in a sort of dummy measurement that verifies that each channels is actually interfaced with the two PCB boards. As expected, the impedance values for those combinations are close to $0\ \Omega$ because each trace is in short circuit configuration with itself. The other combinations suggest more considerations regarding the metal/insulator deposition quality. The values with high impedance are the combinations in which the crosstalk effect is less evident, meaning that the insulation is working properly. At the contrary, for lower values, the crosstalk effect is more consistent and problematic. That can happen for several reason but the main cause is related to the infiltrations of water/solution between the cracks of the insulator. That means that the coupling impedance between the channels assumes a particularly resistive behavior, resulting in parallel contributions

to the impedances at the electrodes interface. Since the values of these parasitics are generally low, they cause a drop on the impedance. The quality of the insulator deposition is one of the most challenging during the fabrication process: the correct functioning of the probe, as well as its ability to last over time, depends on its success. This aspect will be further developed in *Chapter 5*.

In addition, there can be short circuits between channels due to complications during the metal deposition: for example during the evaporation process or the traces patterning. Crosstalk characterization provides more precise informations than EIS characterization in this sense. *Figure 4.17* shows another crosschannel measurement for a 16 channels probe.

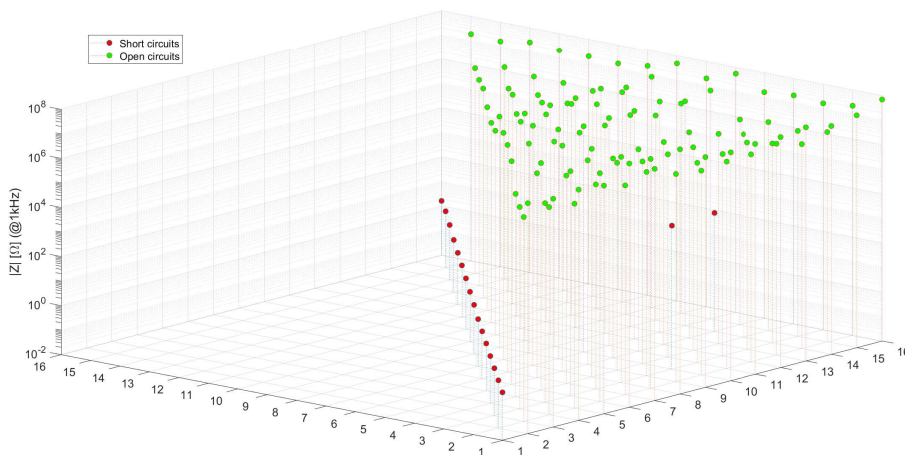


Figure 4.17: Analysis on metal failures in a 16 channels probe

In this case data have been arranged in a 3D plot, so it is simpler to identify all the short circuits (in red). As for the *Figure 4.16*, fake shorts can be recognized on the main diagonal, and, in addition, two others occur in different positions. The impedance values for those are higher than the ideal case along the diagonal. This happens because most of the time the junction that creates the short is not so evident. At the contrary, the unwanted link between two traces is often very thin, far from having the electrical properties of the short circuit itself. This results in higher impedance values even though, in practice, a short is present. Anyhow, it can be assumed with some confidence that all impedance values below hundreds of $k\Omega$ are metal failures which compromise the functionality of the affected channels.

The crosstalk analysis, together with the classical EIS characterization, allows to get important informations on the quality of the fabrication process and, as a consequence, on the fabricated devices. Among the well working devices, it may be interesting to quantify durability over time to understand if this technology can be adopted for long terms recording. This aspect is studied in the next chapter.

Chapter 5

Accelerated Lifetime Testing

In order to understand which is the response of the electrodes to a long term recording operation, Accelerated Lifetime Testing (ALT) needs to be performed. This kind of operation is something that is generally carried out on samples for each kind of device that has to be commercialized or used for not-research-confined applications. The idea is to replicate a process in which the device is subjected to certain conditions in excess with respect to its normal service parameters. By analyzing the results in terms of device response, meaning failures and damages, a prediction about the service life can be made. The process can happen under unperturbed conditions, meaning that the process is not speeded on, or, viceversa, under perturbed conditions. As shown in *Figure 5.1*, temperature and solution bath composition are the most important parameters that can be controlled to increase the process of degradation and hence assessing durability.

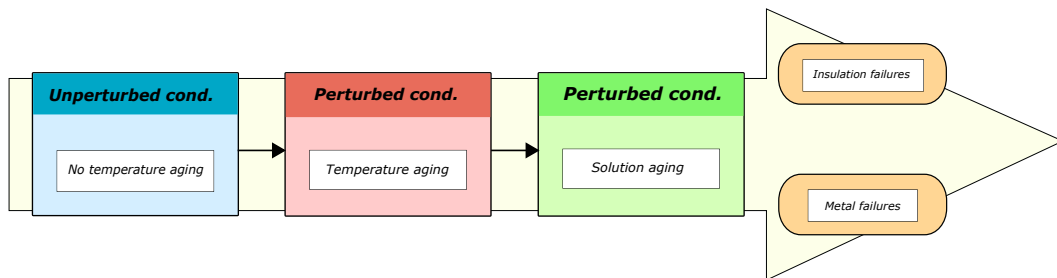


Figure 5.1: ALT processes

In addition to durability, ALT can be used to explore more in detail the problems that affect implantable probes, such as metal and insulation failures.

Indeed, these two are the most important fails that can be observed over time whenever an ALT is conducted. They affect the correct functionality of the probe from different point of views. In the first case, the recording operation is not possible anymore because the electrical connection between the electrode and the back-end is interrupted.

In the second case, the metal trace remains uncovered in such a way that the recording operation is still possible, but the spatial resolution of the probe is lost because, due to the shank length, a single channel can record neuronal activity from different brain regions.

Given the criticality of these aspects, ALT in different environment conditions has been conducted and a statistical analysis on probe failures has been integrated in the discussion.

5.1 Aging in unperturbed conditions

As already discussed, materials that are going to be implanted into the human body should not deteriorate too fast during their period of use. Since the main problems are represented by bad insulation, a first step should be to study how the probe reacts whenever left into the solution for a long period of time with no external perturbations. In other words, the goal of the experiment is to see how much time is required to get significant changes in the impedance behavior without artificial acceleration of the process (*i.e.* increasing the temperature).

The way in which the experiment is conducted is pretty straightforward. The probe, a 32 channels steeltrode, is left inside PBS solution at room temperature performing EIS characterization at prefixed time intervals. For the specific experiment it has been chosen to repeat the measurement each hour. To guarantee consistency, each measurement has been done twice and results compared.

5.1.1 Results and discussion

The results for the device under test are reported in *Figure 5.2*. EIS characterization data have been reported in terms of Bode diagrams. Each diagram is relative to one single channel of the probe. For summary reasons, just channels corresponding to cases of interest are shown.

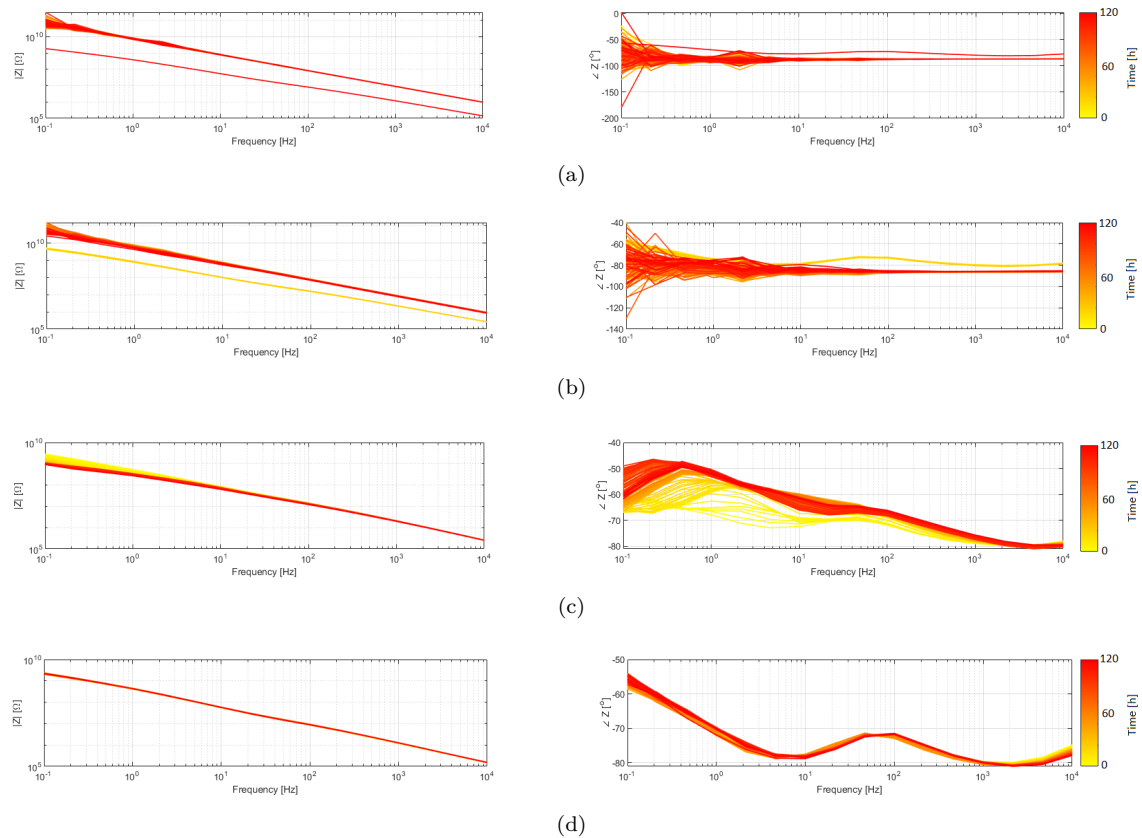


Figure 5.2: Results for ALT under unperturbed conditions: a) intense insulator fail, b) metal fail, c) slight insulator fail, d) no fails

As can be noticed, the channel 5.2(a) has a drop of the impedance around 100 hours after the start of the experiment. In 5.2(b) the trend is the opposite direction, with an increasing of the impedance after around 40 hours.

In the first case, the impedance drop is caused by the insulator delamination. It consist of the

failure of the Parylene that starts to fracture in several layers. This implies the loss the electrical insulation between the metal trace and the environment, causing a false exposed electrode (i.e. the trace itself). Since the exposed area of the channel is now larger, the impedance will decrease. It can be caused by many factors, first of all the presence of thin faults on the surface which are more prone to aqueous infiltrations. Once the water has entered inside, it is easier to see large portions of insulator rise from the metal, leaving the trace uncovered.

The second case of failure affects the metal below the surface which can break because of the saline contributions in the PBS solution. As a consequence, the channel, that was a working one, becomes a not working one because the electrical connection is lost.

Between these two extreme cases, there is a wide range of possibilities for which the impedance module can vary depending on the depth of infiltration. Generally the pre-delamination effect is more evident for working channels at low frequencies, following an exponential decrease. This can be observed for channel in 5.2(d). The drop of the impedance module is followed by the increasing of the phase, meaning that the infiltrations make the impedance more resistive.

At the same time, some channels are more robust and do not present changes in impedance such as to justify faults. It is the case of the channel 5.2(c).

Table 5.1 shows how the fails are distributed over time.

Time [h]	Insulator fails [%]	Metal fails [%]	No-damaged channels [%]
20	0	0	100
40	0	3	97
60	0	3	97
80	0	3	97
100	3	3	94
120	6	3	91

Table 5.1: Results for ALT under unperturbed conditions

Overall, the total number of faults is small compared to the number of the probe channels. That means that the quality of the metal and the insulator is good enough to last a long time in unperturbed conditions. On the other hand, observing a sufficient number of failures to get a more detailed analysis in these conditions could take very long time; the process can be accelerated by disturbing the experiment conditions.

5.2 Aging in perturbed conditions

As mentioned, the conditions can be varied in order to get an acceleration of the degradation process. Essentially two are the factors that can be modified:

- *temperature* of the solution bath;
- *composition* of the solution bath;

The temperature variation allows to test the evolution of the impedance over effective times longer than the testing period at room temperature.

In order to simulate the aging process, so-called "accelerated aging", a common approach to determine the degradation rate is to consider the Arrhenius equation. It provides the dependence of the rate constant of a chemical reaction on the absolute temperature and other constants of the reaction [77, 78]:

$$k = Ae^{\frac{-E_a}{RT}} \quad (5.1)$$

where T is the absolute temperature, A is the pre-exponential factor (constant for each chemical reaction), E_a is the activation energy for the reaction (constant as well for not so big temperature variations) and R is the universal gas constant. This relation showcases how the degradation process is speeded on exponentially (in terms of rate k) when the temperature T is increased.

In terms of aging rate factor f recent studies have shown that this value can be expressed as [77]:

$$f = 2^{\Delta T/10} \quad (5.2)$$

where $T = T - T_{ref}$ is the difference between the imposed temperature at which the effects of aging must be determined and the reference. For a material that is to be implanted into the human body, T_{ref} is the body temperature of $37^\circ C$. Since American Society for Testing and Materials (ASTM) recommends that aging temperature has to be kept below $60^\circ C$ to avoid non-linear variations in the rate of reaction [78], it has been chosen to set the aging temperature to this value. This means that the factor of aging will be around 5. In other words, theoretically, 1 hour of use at room temperature corresponds to 5 hours of use at the $60^\circ C$ in absence of other perturbations. On the other hand, this is just a qualitative estimation that can be made a priori, but that cannot take into account the specific features of the probe under test, in terms of previous damages or mechanical stress that can influence the final result.

The second factor that can be modified to assess the mean time to failure of the probe is the composition of the solution bath. Neural implants studies have shown how Reactive Accelerated Aging (RAA) in harsh aging environment can be obtained using Hydrogen Peroxide (H_2O_2) [79, 80]. In recent studies, H_2O_2 has been used in RAA soak tests as a source of Reactive Oxygen Species (ROS) to simulate the aggressive environment created by immune cells in response to chronic implants [79, 80]. In a biological context, ROS are the result of the metabolism of oxygen and have important roles in cell signaling and homeostasis. However, during environmental stress, ROS levels can dramatically increase [81]. This is the effect called "oxidative stress" because the production of ROS is strongly influenced by stress factor responses. The issue is that heated PBS solution does not reproduce this effect that naturally occurs when, for example, the probe is implanted inside the brain. Through hydrogen peroxide this effect can be simulated even in not *in-vivo* environment.

The required concentration of solvent in solution is from 10 to 20 *mM* in PBS; for this thesis work 15 *mM* has been used.

Taking into account that the process has to be fast enough to cover the whole device life time cycle, together with the solution modifications a constant temperature of $60^\circ C$ has been maintained. As a result, one can expect the fastest aging process in the last configuration.

The heating process was conducted using an analog Heatblock (VWR). A digital thermocouple (OMEGA) was adopted to constantly measure the temperature of the solution and avoid over-heating peaks. Moreover, to reduce risks of evaporation, the tank for the probe heating was sealed

using Parafilm.

Then EIS characterization has been performed at different time intervals using the measurement setup described in *Section 4.2.4*. The chosen range of frequencies is $[10^{-1} 10^4]Hz$.

5.2.1 Results and discussion

Results at 60 °C in PBS

ALT results for PBS at 60 °C are reported in *Figure 5.3*. As for the case of unperturbed conditions, just the most relevant results are reported. Compared to the previous case, EIS characterization has been conducted over a smaller period of time because fails occurred earlier. On the other hand, since an accurate prediction of the decay rate was not possible, it was chosen to perform measurements with a certain frequency, which was then modified according to the obtained results. In other words, the intervals between one measurement and the following one were initially short and subsequently they have been increased to deal with the initial slow aging rate.

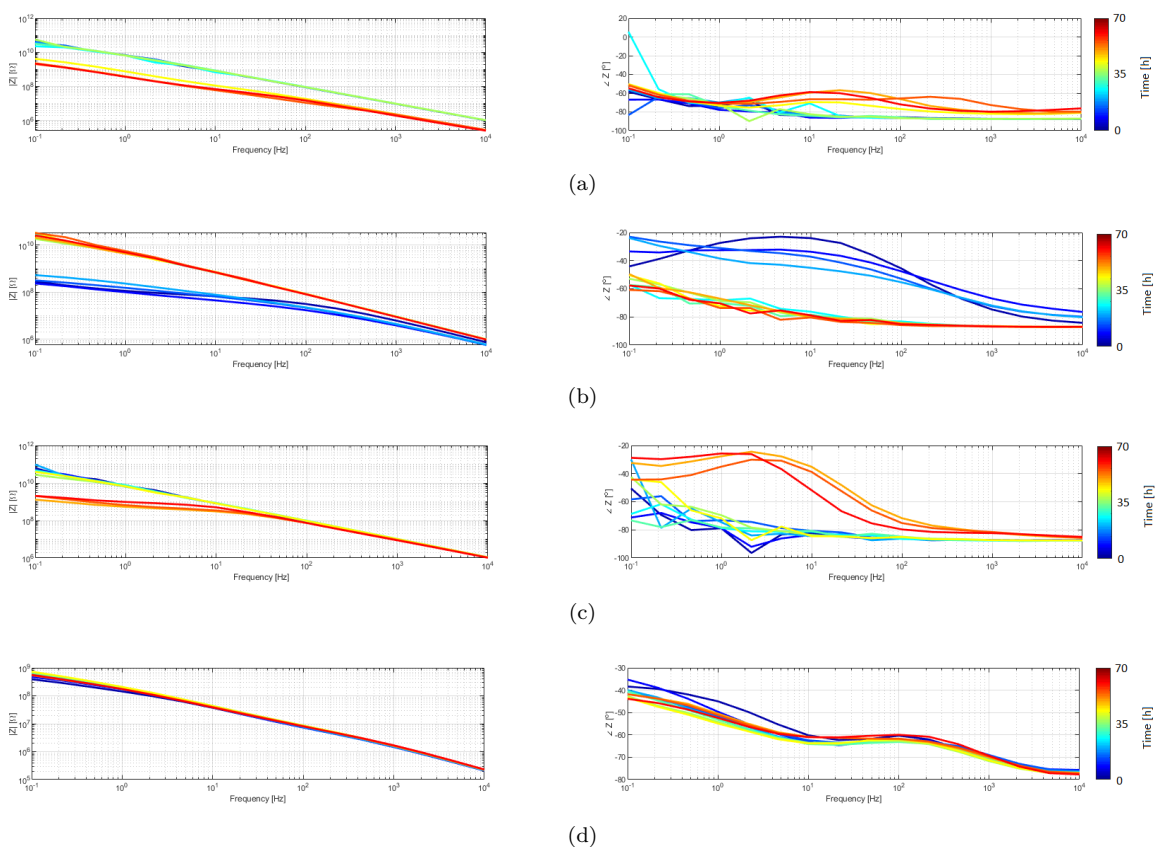


Figure 5.3: Results for ALT in perturbed conditions, $T = 60\text{ }^{\circ}C$: a) intense insulator fail, b) metal fail, c) slight insulator fail, d) no fails

As can be seen, the four reported cases are similar to those discussed for the previous configuration. The difference is that the delamination effects are now being observed after about 40 hours since the start of the experiment, whereas metal fails takes less than 20 hours. That means that the process has been accelerated by over 50% in both cases.

Furthermore, while in the other case just few channels presented fails, the percentage of broken/delaminated traces is now much higher. *Table 5.2* reports all the values in terms of percentage over time.

Time [h]	Insulator fails [%]	Metal fails [%]	No-damaged channels [%]
10	0	0	100
20	0	6	94
30	0	6	94
40	6	6	88
50	19	9	72
60	22	9	69
70	22	9	69

Table 5.2: Results for ALT under perturbed conditions ($T = 60\text{ }^{\circ}\text{C}$)

By looking at the obtained results, it is easier to quantify how much faster the effect of infiltration under the Parylene occurs thank to the temperature for each characterization step.

Results at $60\text{ }^{\circ}\text{C}$ with H_2O_2 in PBS

Finally, results for ALT at $60\text{ }^{\circ}\text{C}$ in hybrid hydrogen peroxide/PBS solution are reported in *Figure 5.4*. For this experience a 16 channels low density probe has been used.

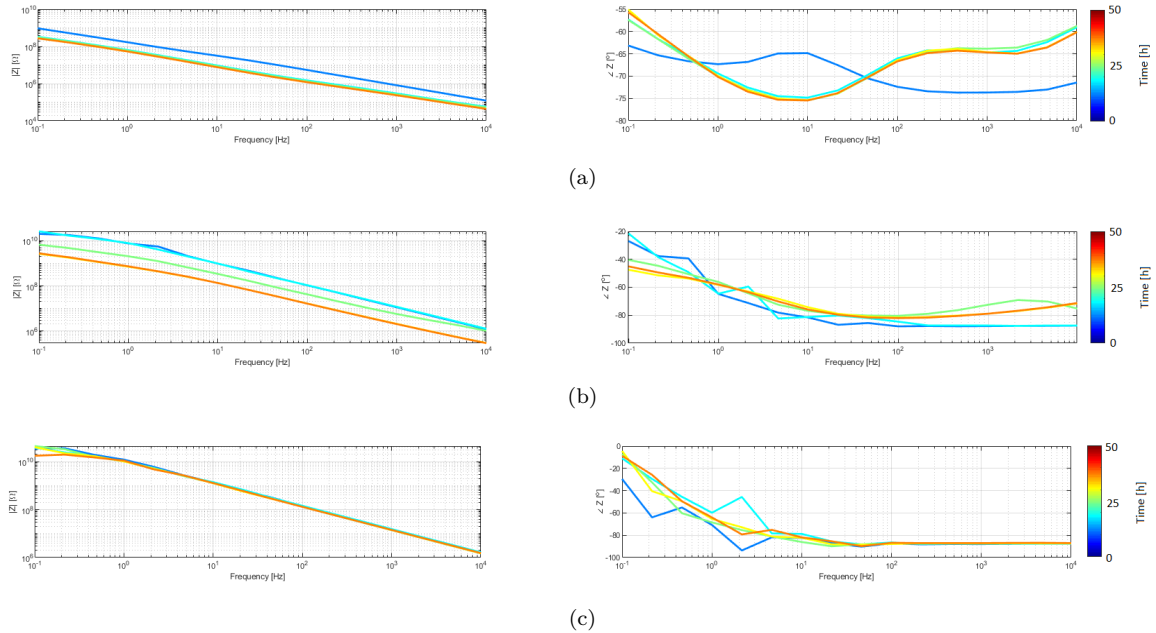


Figure 5.4: Results for ALT in perturbed conditions, $T = 60\text{ }^{\circ}\text{C}$ and H_2O_2 in PBS: a-b) intense insulator fail, c) no fails

In this experience no damages to the metal have been observed. At the contrary, lots of channels start to delaminate quickly at low frequency (5.4(c)), or they are completely delaminated in the all frequency range after just 20 hours (5.4(a),5.4(b)). In other words, this process is more than 50% faster than the previous one and 80% faster then the one with no perturbed conditions. A more detailed analysis can be made by looking at the data reported in *Table 5.3* (completely delaminated channels are reported under the voice "Insulator fails").

Time [h]	Insulator fails [%]	Metal fails [%]	No-damaged channels [%]
10	0	0	0
20	37	0	63
30	44	0	56
40	56	0	44
50	56	0	44

Table 5.3: Results for ALT under perturbed conditions ($T = 60\text{ }^{\circ}\text{C}$ and H_2O_2 in PBS)

5.3 Statistical analysis on failures

Each experiment has a dependence with the sample under test starting conditions. For example, during the fabrication process, there may be different conditions depending on the wafer region, resulting in particular features in some probes compared to others. In terms of analysis, this means that, in order to get a qualitatively understanding of the results, it is necessary to conduct more and more experiments in search of consistency between the data.

In the specific case of ALT, this operation takes a long time and, to be as accurate as possible, lots of experiments must be carried out with different samples coming from different wafers and fabrication processes. The goal of this section is to collect the results obtained so far and make them available for future upgrades.

As already mentioned, the value of the impedance at interesting frequencies (i.e. 1 kHz) is in the range $[1\text{ }2.5]\text{ M}\Omega$ for the implemented technology. This is true for electrodes diameter of $15\text{ }\mu\text{m}$ which is the most common arrangement for the probes used in this thesis work.

On the other hand, electrodes diameter can be bigger, $25\text{ }\mu\text{m}$, for some probes that do not have constraints in terms of pitch length between one trace and the next one (electrodes along the shank). For these probes, the value of impedance module at 1 kHz is lower because the overall exposed area is larger. So in these cases one can get hundreds of $k\Omega$, close to the $1\text{ M}\Omega$.

Although the fabrication process is going improved over time, insulator fails are the most common issue that occurs at each new probe generation, therefore it needs to be identified quickly at each preliminary analysis.

Previous analysis on ALT has shown how the impedance drop is related to the effect of delamination that occurs in damaged probes. In those cases the probe was artificially damaged so the result was expected but, in general, recognizing good working channels from delamination effect is challenging. One way to do that is to make a statistical investigation on most common impedance values for insulation failures in such a way that, by just performing EIS characterization, is it possible to understand if there are delaminations on the current probe generation or not.

For what concern metal failures, the statistic is not needed. The reason is related to the fact that EIS characterization already allows to know in advance informations about functionality of each specific channel. If the impedance is too high the metal is broken and there is not the need to distinguish this value from something else.

The graph in *Figure 5.5* reports the first collected data for the analysis on insulation failures for the two analyzed probe categories. The values have been extrapolated from ALT characterization analysis at 1 kHz .

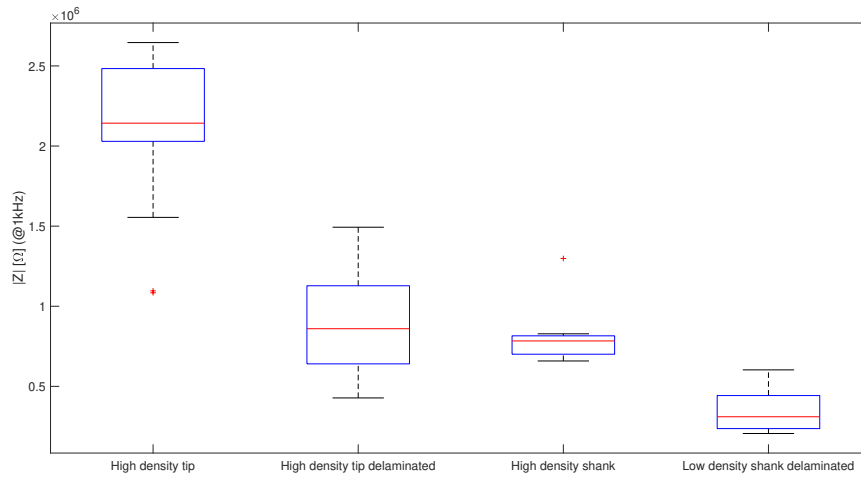


Figure 5.5: Statistical analysis on insulation failures

As can be seen, the values for delaminated probes in small electrodes configuration are confined in a range around $900\text{ k}\Omega$. So it is pretty discernable from good channels values in that configuration. The same happens for big electrodes configuration in which the range of delamination is close to $300\text{ k}\Omega$, far from the value of $900\text{ k}\Omega$ required to have a working recording site.

Anyhow, this analysis remains a statistic, so there is no warranty that ensures the correct identification of a specific insulation issue. In this sense it is not intended to be the definitive version on which to characterize the next generation of probes, but rather the starting point for a more in-depth study of the problem.

Chapter 6

Stimulation for in-vivo characterization

The last step of the characterization process is the simulation to prepare the in-vivo recording. The goal is to reproduce the in-vivo environment to verify what supposed with EIS characterization: in other words this characterization is a more precise analysis to check working channels functionality. Since the goal of the experiment is to reproduce neuronal stimulus in an artificial environment, the procedure is called "synthetic stimulation".

6.1 Synthetic stimulation

As already said in the introduction of the current chapter, this characterization allows to simulate the condition in which a working channel of the probe has to record electrical activity coming from the outside. In order to do that, neuronal activity inside the brain it is reproduced using a stimulus electrode immersed in PBS solution. The electrode is a very thin needle interfaced with a function generator: in this way the signal parameters can be chosen to be more realistic as possible or, on the contrary, to accomodate different needs depending on the type of experiment. The *Figure 6.1* shows the microneedle (*MicroProbes for Life Science*, WE series) used as a stimulus.

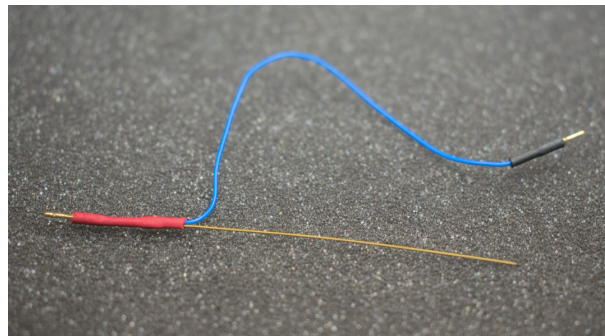


Figure 6.1: Stimulation electrode (*Microprobes for Life Science*)

The stimulus can be moved to be brought closer to the probe electrodes. The camera pictures in *Figure 6.2* show this in three different situations: in the first case a high density tip probe, in the second one a high density shank one and, finally, a high density commercial probe (*Plexon*). Commercial probes have been characterized as well, providing a benchmark for evaluating the obtained results.

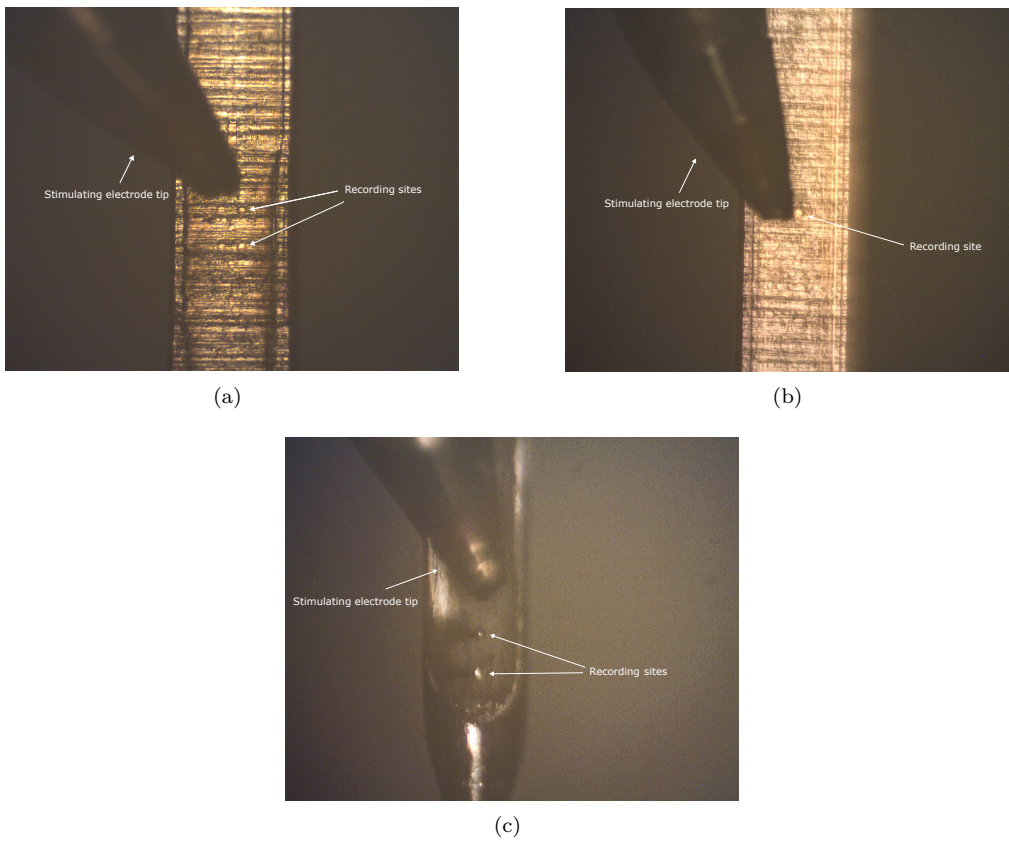


Figure 6.2: Stimulating electrode approaching the recording site in: a) high density tip, b) high density shank, c) commercial probe (Plexon) (Camera images through PBS solution)

As can be guessed, the stimulation operation can be difficult in high density tips (6.2(a) 6.2(c)) because the electrode cannot be moved with high precision along the probe. All the recording sites are close each other, meaning that, whenever the stimulus is approaching, it is difficult to stimulate only one of them at a time. In terms of response the amplitude of the recorded stimulus will be as low as the tip is further away from the electrode, resulting in a gaussian response. This concept is explained in the next sections.

The whole measurement setup is shown more in detail in the next section.

6.1.1 Measurement setup

The complete schematic of the stimulation system is reported in *Figure 6.3*.

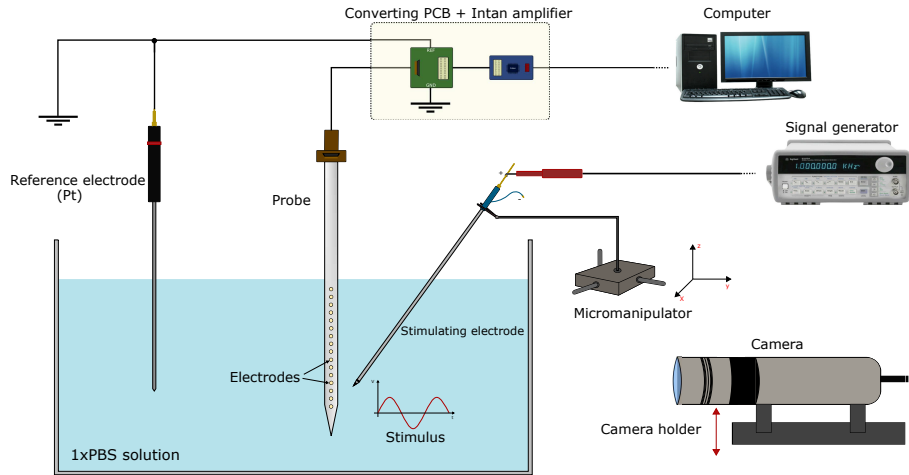


Figure 6.3: Synthetic characterization measurement setup

Since the probe is very thin, the stimulus has to be moved very slowly along the probe. In order to do that, a micromanipulator has been used. A camera (*Thorlabs*) allows to scan the probe surface and carefully approach the stimulus to the recording site. The probe is interfaced with an Intan amplifier through Omnetics connector, using a ZIF-Omnetics converter PCB. The *Figure 6.4* reports the implemented converter PCB and the Intan amplifier used for the measurement.

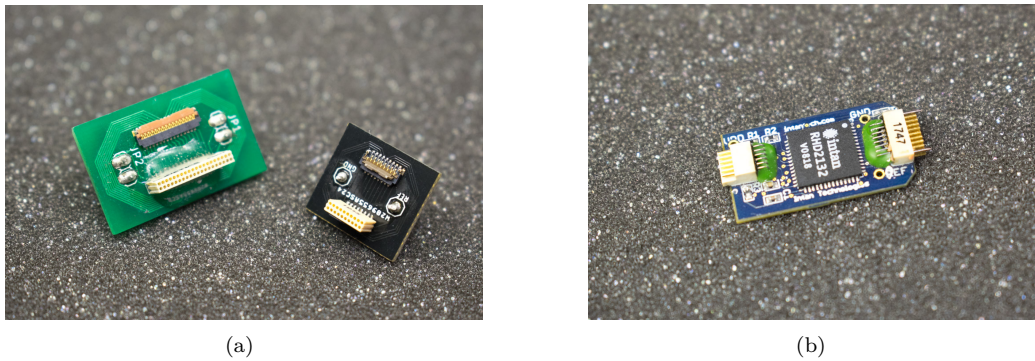


Figure 6.4: Electrical components for synthetic stimulation: a) ZIF to Omnetics PCBs, b) Intan amplifier

Due to the fact that the Intan amplifier system exploits different references for the ground and the signal reference, two different pins have been included in the PCB. However, some experimental results have shown that the level of noise reduces in the case in which the two are shorted together. For this reason, the same Platinum electrode used for the EIS characterization has been used to establish a reference in PBS solution and, then, it has been shorted with the ground of the system. On the contrary, the negative reference of signal generator has been left floating: in this way it is easier to stimulate the recording site just on the proximity of the stimulating electrode tip. That happens because there are two exposed metal sections on the stimulating electrode, one on the tip and a thin ring slightly above. Overall, these two poles make the electrode working like an antenna when the two of them are connected. The electromagnetic field in the middle of the two

poles is less intense, so when the probe is stimulated all the electrodes in the vicinity of that point have lower response. At the contrary, electrodes closer to the two poles have bigger response. This does not represent a big issue in low density configurations, but could make the analysis of the response a little bit more complicated for high density probes. By leaving the negative reference of the signal generator floating, the ring pole does not propagate an electromagnetic field, so the stimulation can happen just on the tip of the probe.

6.1.2 Result and discussion

The signal chosen for the stimulation is a sinewave of 70 mV_{pp} in amplitude with a frequency of 800 Hz . Intan technology interface software has been used to record the amplified signal from the Intan amplifier and save the data. The *Figure 6.5* reports its interface during a stimulation for low density steeltrode.

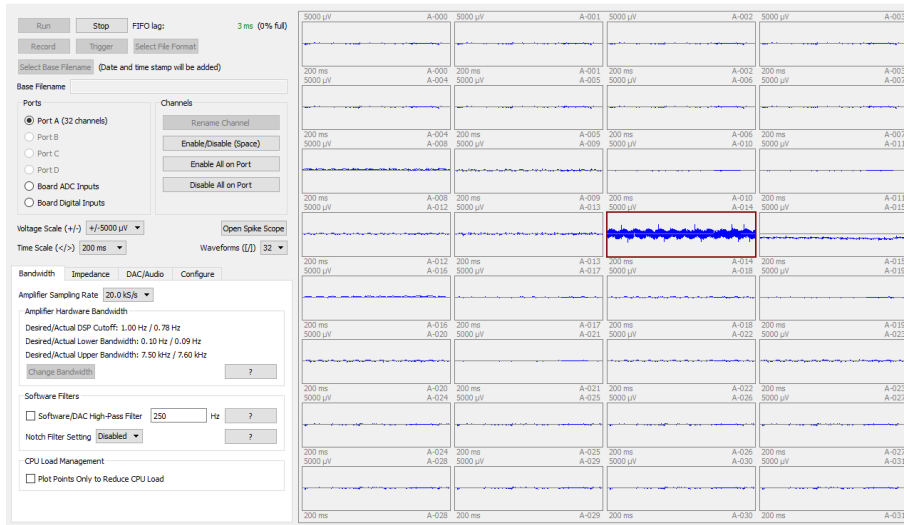


Figure 6.5: Intan technologies software interface for the stimulation of a low density steeltrode

The channel circled in red is the stimulated electrode which responds correctly to the stimulation. As can be noticed, some other channels present a slight response to the stimulation. That happens because, even if the stimulus is far from the recording site, it travels through the solution. In a real brain environment this behavior simulates the response of other neuronal signals coming from different regions of the brain, resulting in a noisy background. The latter can be recorded in a worst case scenario where the stimulus electrode is placed close to the probe in the middle of the shank so as to be a noise source for most of the working channels. Thus, the baseline noise can be measured and used to compute the SNR.

In *Figure 6.6* is reported the result of this measurement for a 32 channels probe.

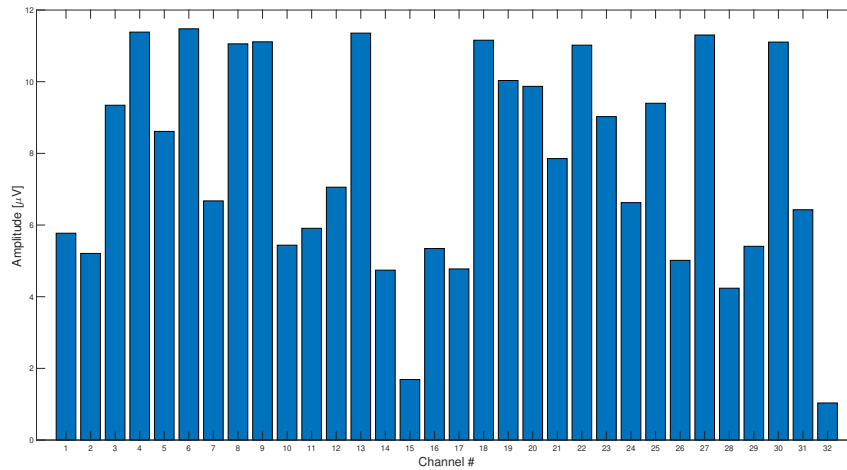


Figure 6.6: Baseline noise for a high density tip steeltrode

One can notice that not all the channels are responding to the noise in the same way. For example, channels 1 or 2 has very low response whereas channel 15 measures just $2 \mu V$. This is due to the fact that those channels are not working, so the measured noise is only the one introduced by the electrical equipment. On the contrary, commercial probe does not have not working channels so the response is uniform for all the channels as can be seen in the *Figure 6.7*.

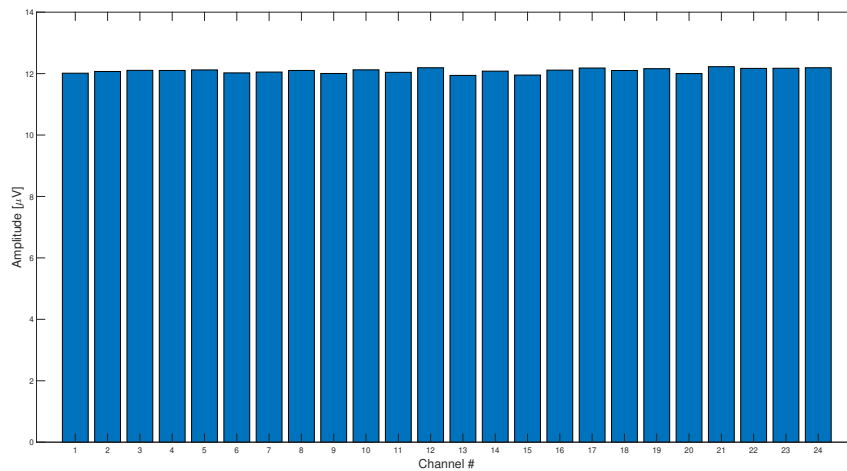
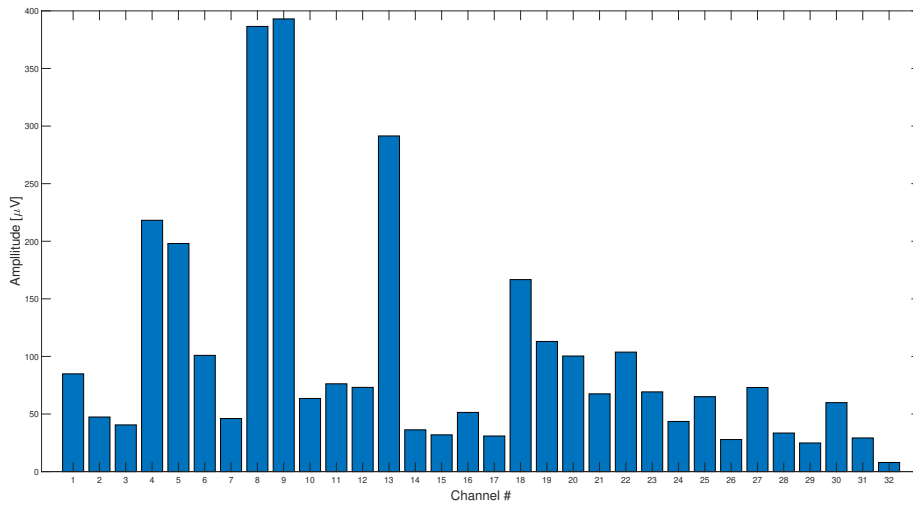


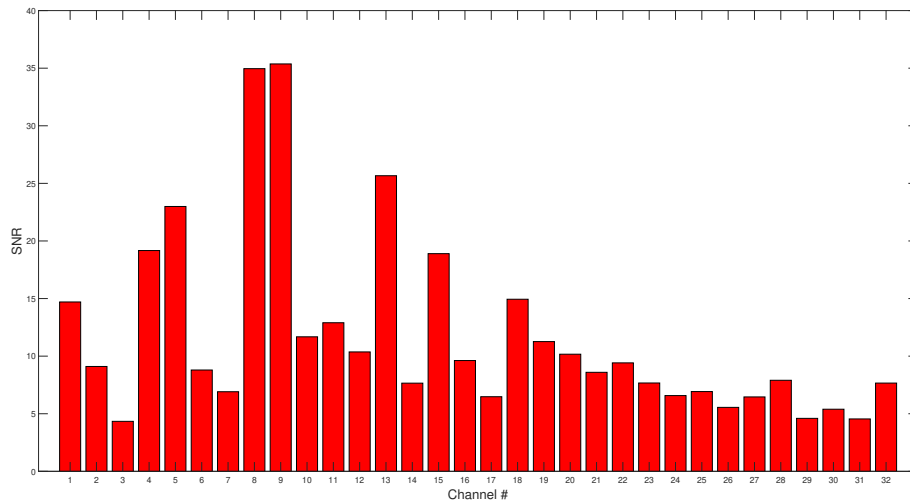
Figure 6.7: Baseline noise for a commercial high density probe (Plexon)

Anyhow, for the working channels the level of measured noise is in the range $10 - 12 \mu V$ in all the cases.

The response of the single channel can be measured in the same way, by moving the stimulus closer to the recording site. In the *Figure 6.8* is reported the result in terms of amplitude and SNR for the case of high density steeltrode. The SNR is calculated using the noise values previously measured for each channel.



(a)

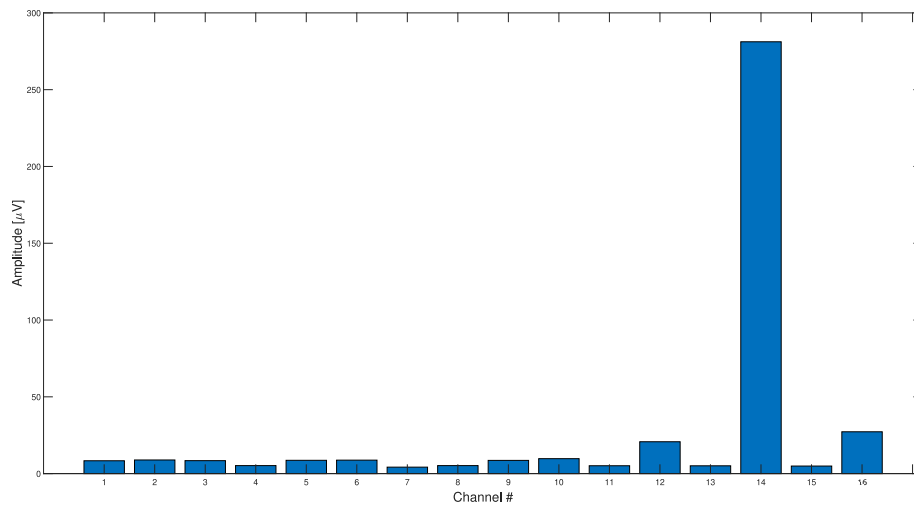


(b)

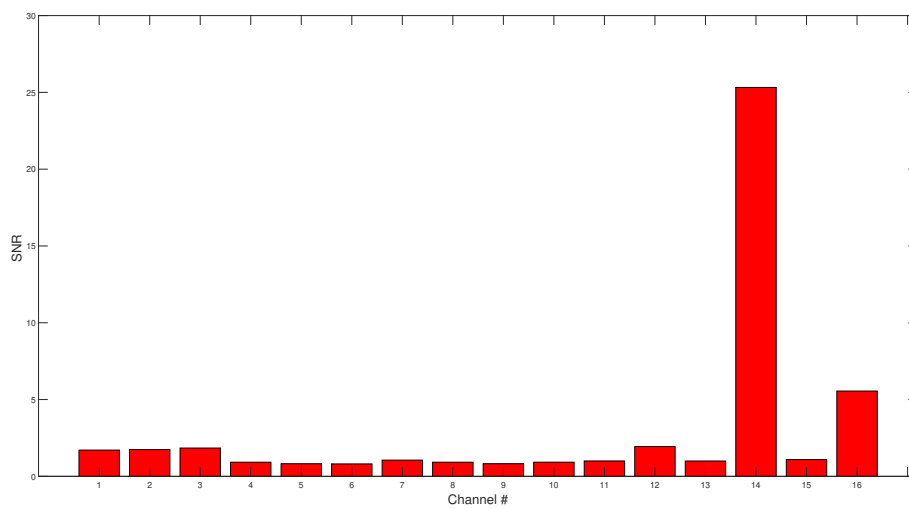
Figure 6.8: Stimulation results for a high density tip steeltrode: a) amplitude, b) SNR

The measured amplitudes put in evidence how the response has a peak corresponding to the stimulated channel, and then decreases by moving away from along the adjacent electrodes. In other words it can be modeled with a gaussian. As for the baseline noise, the not working channels do not respond to the stimulus, so they leave holes in the model.

Things are different for probes with electrodes disposed all along the shank because the distance between two consecutive recording sites is huge and the stimulus, for those how are far, can be considered noise. An example of low density channels probe stimulation is reported in *Figure 6.9*.



(a)



(b)

Figure 6.9: Stimulation results for a high density shank steeltrode: a) amplitude, b) SNR

As can be seen, only one channel is responding to the stimulus, all the other just record noise.

Another interesting way to use this characterization is to verify when that delamination are actually happened after an ALT. The procedure is the same used for stimulate the recording site, but, this time, it is used to check where there is the uncovered metal along the trace. For example, in *Figure 6.10*, it is reported a case in which the delamination appears on the section of the trace just close to the electrode itself.

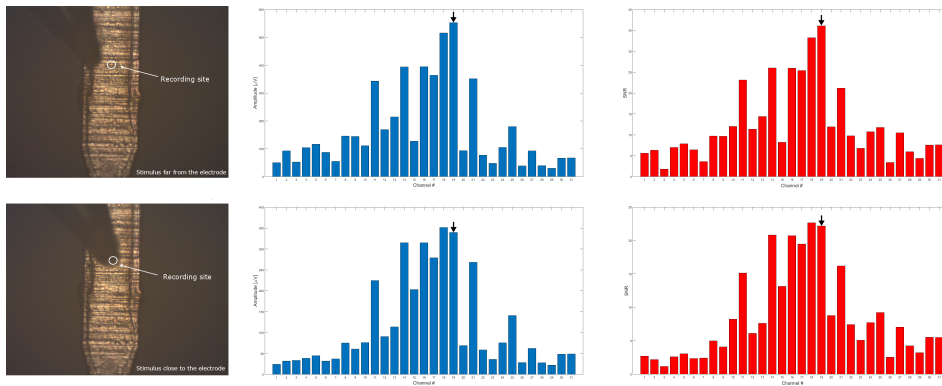


Figure 6.10: Synthetic stimulation to check the trace delamination

The black arrows indicate which is the channel under test. The response of the channel is bigger when the tip of the stimulus is far from the recording site with respect to the case in which they are overlapped. This happens because the delamination have left a section of the trace uncovered so it works as a dummy electrode. Although it is not always easy to phisically identify the delaminations with this methodology, it has been noticed that a consistent number of those happen in proximity to the recording site itself, probably because of the fragility of the Parylene at that interface.

This section concludes the discussion on the characterization of implantable neural probes. As already mentioned, these procedures provide a more clear view on the quality of the implemented devices and give insights to improve the design and the fabrication processes. Once proven that the probe works properly, it can be used to directly record neuronal activity in-vivo on mice and rats (small shank probes) or monkeys (longer shanks) in compliance with the regulations in force on animals treatment in United States of America.

Chapter 7

Conclusions

This thesis work is focused on post-fabrication improvements, as well as on packaging procedures and characterization on different levels of functionality, of implantable neural probes for in-vivo recording. This type of device can be used to study the brain activity more deeply so that new treatments can be adopted for widespread brain diseases such as Parkinson's or Alzheimer's. At the same time, invasive neural recording is the basis for every BML, ranging from the use of robotics arms for neuromuscular disabilitate people to the commercialization of thought-controlled interfaces for paralyzed people, passing through IoT applications.

The design of such devices consists of high density recording sites embedded in an implantable shank ended by a larger back-end for the interfacing with the recording equipment. The back-end is composed by metal pads connected with the recording electrodes through metal traces arranged all along the shank and insulated by a polymer layer.

The main challenges of this technology are:

- using micromachining techniques on different materials other than those normally used in photolithographic processes;
- making devices that are easily implantable and, at the same time, that do not cause damage to the brain tissue;

To provide stiffness, stainless steel is used as a device substrate while a biocompatible polymer called Parylene C is adopted as an insulator for the metal traces. In this way, the device is flexible and rigid at the same time, free to be implanted without the need of external shuttles or coatings. On the other hand, in order to get devices that can float inside the brain synchronized with the micromotions, some completely flexible polymer-made probes are realized using the same photolithographic mask. However, due to the extreme fragility of the flexible version, the latter is mostly confined to characterization tests, whereas the stainless steel type is used for in-vivo measurements.

The probes are released from the wafer using laser cutting along the edges: this operation leaves burrs and impurities in the stainless steel substrate that might scratch the brain tissue during in-cortex implantation, so that post-fabrication processing is requested. The improvements, in terms of substrate roughness, can be obtained performing electrochemical processing on the device, using the so called electropolishing technique. It consists of a charge flow passing between two electrodes immersed in an electrolytic bath. The current promotes metal ions removal from the anode (i.e. the probe) allowing to make the surface smoother. Different electrolyte solutions have been used during this thesis work:

- Oxalic acid in DI water;
- Phosphoric acid and Sulphuric acid mixture.

The two acid configurations have been tested in different current/voltage domains and good results have been obtained using DC voltage in a two steps process for which low frequency roughness peaks are removed in Oxalic acid while high frequency ones are polished in Phosphoric + Sulfphuric acids mixture. Quantitatively it has been proved that this process allows to reduce the roughness of about 50%.

Moreover, using the same polishing process for more time, it is possible to completely remove the stainless steel from a section of the probe in such a way that the final result is a hybrid rigid-flexible probe. This device has the advantage of being easily implantable (because the tip remains stainless steel-based) and, at the same time, it causes small damages because it can move synchronized with the micromotions thanks to the flexible section.

In order to characterize the devices from an electrical point of view, each of them has to be packaged to provide both electrical interfacing and mechanical protection. Two different packaging techniques have been adopted during this work:

- ACF flip-chip bonding for small back-end dimensions;
- ZIF connector-based technique for fast and in series packaging;

The two procedures have been optimized to get a high process yield, thus minimizing the bad-connections fails. Moreover, the second technique has been adapted for flexible probe packaging using Kapton tape to improve back-end stiffness in such devices.

Once the devices are correctly packaged, electrical characterization is necessary to test their functionality before in-vivo operations. That can happen using Electrochemical Impedance Spectroscopy: it allows to measure impedance over a range of frequencies using an electrolyte solution bath to replicate the brain environment (PBS), some electrodes and a potentiostat.

The main challenge here is to correctly interface the high density probe with the equipment in such a way that each electrode of the probe is characterized independently from the other ones. For this purpose, a digitally-controlled interfacing PCB board made up of 32 electromechanical relays has been designed and fabricated. It allows to switch between all the channels making the characterization procedure fast and reliable.

Furthermore, the same PCB board can be used in a tandem configuration to easily characterize crosstalk response between all the possible combinations of probe channels.

Then, some probes are characterized in harsh aging conditions in order to understand which is the corresponding time to failure, thus in terms of device functionality. This procedure is called Accelerated Lifetime Testing. Among the conditions to increase the aging factor, the following ones have been chosen:

- temperature increase up to 60 °C;
- temperature increase up to 60 °C and Hydrogen Peroxide in PBS solution;

In the first case, the temperature of the solution bath accelerates the process in such a way that the metal traces and the Parylene C fail in a shorter amount of time. In this way it is possible to know which is the mean time to failure of the device in a real recording environment: due to the imposed aging conditions, the real time roughly corresponds to the time under stressed conditions multiplied by a factor 5. In this case the first fail has been observed after 40 hours, corresponding to 200 hours of long-term neuronal recording operation.

On the other hand, the Hydrogen Peroxide makes the process even faster than the first case, because it simulates the behavior of Reactive Oxygen Species inside the brain, creating a more aggressive environment. The result is that the first fails have been observed just after 20 hours.

The metal failures consist of channels breaks along the shank, resulting in not working electrodes, whereas the insulation ones are mostly delamination of the polymer above the trace, meaning that the electrode is not able to record only on the exposed sites anymore. By collecting impedance values of the defecting channels it is possible to do a statistical analysis on failures that can help to identify them in further analysis.

As last step, before the in-vivo characterization, a real-stimulus analysis is performed. In this phase, the recording site is stimulated with a fake neuronal signal (represented by a generated sinewave) using as a medium the PBS solution. The signal is then recorded from the probe electrode (if working) and then amplified for the next analysis. Using this procedure one is able to further verify the functionality of each electrode before surgery.

7.1 Future works

The carried out EP processes have shown that good results in terms of surface roughness can be obtained with the two steps procedure presented in *Chapter 2*. However, the obtained results are just a first step to improve the procedure in order to make it less aggressive and more effective. A big further development in this sense could be to verify the functionality of the recording sites as well as the metal traces, and so the probe in general, after the polishing process with EIS and Synthetic characterizations. In particular, this has to be done for each of the two steps of the process, in order to be sure that none of these imply a too aggressive effect on the fragile probe sites. Furthermore, the bubbles appearance on the surface of the stainless steel might be investigated more by performing multiple experiments in different polishing conditions. Based on what has been found so far, one of the most important parameters that can be tuned is the polishing process time: perhaps trying to put the electrodes closer in a controlled way could be useful to speed up the process, thus reducing considerably the time.

For what concern electrical characterization, the measurement setup is now already optimized in one electrode configuration. That means that multiple high density probes can be characterized in series without the need of human control to switch from one electrode characterization to another one. The same considerations are valid for crosstalk characterization setup. However, the latter needs improvements in terms of quantification of crosstalk effect. In fact, so far, just the coupling impedance between two electrodes can be measured easily and this provide limited informations about the introduced noise level during the recording operation. In other words, could be useful quantify the crosstalk in terms of signal on the "victim" trace by making propagate a dummy signal into another trace.

Lastly, more ALTs can be conducted in other aging conditions, even different from the ones presented in this thesis work. That would be useful to increase the number of cases and make a more precise statistical analysis and, in addition, to test the functionality over time of the next generation probes for which, inevitably, material and electrical features will change.

Bibliography

- [1] Susan Young Rojahn. *Brain Chip Helps Quadriplegics Move Robotic Arms with Their Thoughts*. MIT technology Review, May 16, 2012.
- [2] Bashir I. Morshed and Abdulhalim Khan. *A Brief Review of Brain Signal Monitoring Technologies for BCI Applications: Challenges and Prospects*. Journal of Bioengineering & Biomedical Science - The University of Memphis, USA, May 6, 2014.
- [3] *Centre for Neuro Skills, Neuronal Firing*. ©2019. URL: <https://www.neuroskills.com/brain-injury/neuroplasticity/neuronal-firing/>.
- [4] Dr Alan Woodruff. *What is a neuron?* Copyright ©The University of Queensland, Queensland Brain Institute. URL: <https://qbi.uq.edu.au/brain/brain-anatomy/what-neuron>.
- [5] Peter Dayan and L. F. Abbott. *Theoretical Neuroscience*. ©The MIT press, 2001.
- [6] *PhysiologyWeb at www.physiologyweb.com* Copyright ©2000-2019. 2014. URL: https://www.physiologyweb.com/lecture_notes/neuronal_action_potential/neuronal_action_potential_important_features.html#DAMWQMZIODbnlqWpiPzLAix26sS2uWUU.
- [7] *Soft Neural Interfaces for Ultrathin Electronics*. IEEE Nanotechnology Magazine, January 2018.
- [8] *EEG Measures of Cognition*. November 20, 2016. URL: <https://hvmn.com/biohacker-guide/cognition/eeg-measures-of-cognition>.
- [9] M. Teplan. *FUNDAMENTALS OF EEG MEASUREMENT*. Institute of Measurement Science, Slovak Academy of Sciences, Dúbravská cesta 9, 841 04 Bratislava, Slovakia, 2002.
- [10] Rachael Meadows. *Spiritual Evolution: next level of humanity*. May 2, 2019. URL: <http://www.adwenchure.com/spirit-kermit-1-harrison-iis-ted-talk-spiritual-evolution-the-next-level-of-humanity/>.
- [11] *Future Use of MEG*. May 2, 2019. URL: <http://ilabs.washington.edu/future-use-meg>.
- [12] JEFF ZAGOUDIS. *MRI Safety and Technology Updates*. OCTOBER 09, 2019. URL: <https://www.itnonline.com/article/mri-safety-and-technology-updates>.
- [13] *Optimization and Configuration of SQUID Sensor Arrays for a MEGMRI System*, IEEE Trans Applied Superconductivity 23: 1-4, 2013.
- [14] Braginski Alex John Clarke. *Fundamentals and Technology of SQUIDs and SQUID Systems*. [Hardcover] (1stedn), New York, USA, 2006.
- [15] R.K. Thomas. *INTRODUCTION: A Biopsychology Festschrift in Honor of Lelon J. Peacock*. Journal of General Psychology, vol. 120, 1993.
- [16] D; E. Breton Le Bihan. *Imagerie de diffusion in-vivo par résonance magnétique nucléaire*. C R Acad Sci, 1985.
- [17] W; Frahm Merboldt K; Hanicke. *Self-diffusion NMR imaging using stimulated echoes*. Journal of Magnetic Resonance, 1985.
- [18] M C Taylor D G; Bushell. *The spatial mapping of translational diffusion coefficients by the NMR imaging technique*. Physics in Medicine and Biology, 1985.

- [19] *Diffusion Magnetic Resonance Imaging: From Isotropic Diffusion-Weighted Imaging to Diffusion Tensor Imaging and Beyond*. Juntendo Medical Journal, Japan, September 2017.
- [20] Sue McGreevey. *Finding signs of life when it matters most*. July 20, 2017. URL: <https://news.harvard.edu/gazette/story/2017/07/using-fmri-eeg-to-search-for-consciousness-in-icu-patients/>.
- [21] *How to interpret an unenhanced CT Brain scan*. URL: <http://www.southsudanmedicaljournal.com/archive/august-2016/how-to-interpret-an-unenhanced-ct-brain-scan.-part-1-basic-principles-of-computed-tomography-and-relevant-neuroanatomy.html>.
- [22] American Headache Society. *Five Things Physicians and Patients Should Question*. Choosing Wisely, American Headache Society, 6 December 2013.
- [23] D.L.; D.W. Townsend; P.E. Valk; M.N. Maisey Bailey. *Positron-Emission Tomography: Basic Sciences*. Secaucus, NJ: Springer-Verlag, 2005.
- [24] JÜLICH Forschungszentrum. *How does MRI and PET work?* URL: https://www.fz-juelich.de/inm/inm-4/EN/Home/_Fokus/Informationen/artikel.html.
- [25] *Mathematics and Physics of Emerging Biomedical Imaging*. National Research Council (US), Institute of Medicine (US) Committee on the Mathematics, and Physics of Emerging Dynamic Biomedical Imaging. Washington (DC), 1996.
- [26] *On the suitability of near-infrared (NIR) systems for next-generation brain-computer interfaces*. *Physiol. Meas* 25: 815-822, 2004.
- [27] Cheung KC. *Implantable microscale neural interfaces*. Biomed Microdevices, 2007.
- [28] Tresco PA Biran R Martin DC. *The brain tissue response to implanted silicon microelectrode arrays is increased when the device is tethered to the skull*. *J Biomedical Materials Res. Part A*: 169-178, 2007.
- [29] Nicolelis MA Lebedev MA. *Brain-machine interfaces: past, present and future*, *Trends in Neurosciences*. 2006.
- [30] *Electrocorticography*. URL: <https://en.wikipedia.org/wiki/Electrocorticography>.
- [31] *Decoding natural grasp types from human ECoG*, *Neuroimage* 59. Johanson HA, Buonomano, 2012.
- [32] *Single-unit recording*. URL: https://en.wikipedia.org/wiki/Single-unit_recording#cite_note-Geddes-28.
- [33] R. I. Harik Raja N. Khuri Samuel K. Agulian. *Internal capillary glass microelectrodes with a glass seal for pH, sodium and potassium*. *Pflüger's Archiv für die gesamte Physiologie des Menschen und der Tiere* volume 301, 1968.
- [34] *Biopotential Electrodes, Ch. 5, min 12:54*. URL: <https://slideplayer.com/slide/4214704/>.
- [35] F. Solzbacher R. Bhandari S. Negi. *Wafer Scale Fabrication of Penetrating Neural Electrode Arrays*. Biomedical Microdevices, Vol. 12(5).
- [36] *Microelectrode array*. URL: https://en.wikipedia.org/wiki/Microelectrode_array.
- [37] Sam Musallam Mohamad Hajj-Hassan Chodavarapu Vamsy. *NeuroMEMS: Neural probe microtechnologies*. sensors ISSN 1424-8220, 2008.
- [38] Timothy G. Constandinou Katarzyna Szostak Laszlo Grand. *Neural Interfaces for Intracortical Recording: Requirements, Fabrication Methods, and Characteristics*. *frontiers in Neuroscience*, 7December 2017.
- [39] James Yoo Ahuva Weltman and Ellis Meng. *Flexible, Penetrating Brain Probes Enabled by Advances in Polymer Microfabrication*. *micromachines*, 4 October 2016.
- [40] Chong Xie. *Ultraflexible nanoelectronic probes form reliable, glial scar-free neural integration*. *Science advance*, NANO-ELECTRONICS, 15 Feb 2017.

- [41] *Flexible polyimide-based intracortical electrode arrays with bioactive capability*. IEEE Trans. Biomed. Eng., 2001.
- [42] *Development and characterization of in vivo flexible electrodes compatible with large tissue displacements*. J. Neural Eng., 2009.
- [43] K. Gall. *In vivo penetration mechanics and mechanical properties of mouse brain tissue at micrometer scales*. IEEE Transactions on Biomedical Engineering, 2009.
- [44] *Properties: Stainless steel - grade 316 (uns s31600)*. Accessed: 23 December 2019. URL: <https://www.azom.com/properties.aspx?ArticleID=863>.
- [45] *Properties: Silicon, azo materials*. Accessed: 23 December 2019. URL: <https://www.azom.com/properties.aspx?ArticleID=599>.
- [46] Tobias Teichert Zabir Ahmed Jay W. Reddy and Maysamreza Chamanzar. *HIGH-DENSITY STEELTRODES: A NOVEL PLATFORM FOR HIGH RESOLUTION RECORDING IN PRIMATES*. 9th International IEEE/EMBS Conference on Neural Engineering (NER), 2019.
- [47] *Development of an optimized electrochemical process for subsequent coating of 316 stainless steel for stent applications*. Springer Science+Business Media, 2006.
- [48] *Electrochemical and chemical methods for improving surface characteristics of 316L stainless steel for biomedical applications*. Elsevier, 23 January 2013.
- [49] Fengzhou Fanga Wei Hana. *Fundamental aspects and recent developments in electropolishing*. International Journal of Machine Tools and Manufacture, April 2019.
- [50] Machine Modern Shop. *Considerations for Electropolishing Machined Parts*. accessed 29/02/2020. URL: <https://www.mmsonline.com/blog/post/4-considerations-for-electropolishing-machined-parts->.
- [51] T.S. Hahn and A.R. Marder. *Metallography*. 1988.
- [52] Jung-Chou Hung Shuo-Jen Lee Yi-Ho Chen. *The Investigation of Surface Morphology Forming Mechanisms in Electropolishing Process*. International Journal of ELECTROCHEMICAL SCIENCE, 2012.
- [53] *Surface roughness*. accessed 09/03/2020. URL: https://en.wikipedia.org/wiki/Surface_roughness.
- [54] R. G. Kelly J. R. Scully. *An Electrochemical Test for Detecting the Intergranular Corrosion Susceptibility of a Duplex Stainless Steel*. Corrosion- The Journal of Science & Engineering, September 1985.
- [55] H Yugami. *Anisotropic multi-step etching for large-area fabrication of surface microstructures on stainless steel to control thermal radiation*. National Institute for Materials Science, 17 March 2015.
- [56] M. Inman. *A Pulse/Pulse Reverse Electrolytic Approach to Electropolishing and Through-Mask Electroetching*. Surface Technology White Papers, October 2011.
- [57] E.-S. Lee. *Machining Characteristics of the Electropolishing of Stainless Steel (STS316L)*. Adv Manuf Technol, 2000).
- [58] Chi-Chang Hu Chi-Cheng Lin. *Electropolishing of 304 stainless steel: Surface roughness control using experimental design strategies and a summarized electropolishing model*. Elsevier, 14 January 2008.
- [59] Sheng-Yao Lin Jin-Yih Kao and Yih-Sharng Chen. *Surface Processing Technology for 316LVM Stainless Steel Stents*. Journal of Applied Science and Engineering, 2018).
- [60] INTEGRATED CIRCUIT ENGINEERING CORPORATION. *CHIP BONDING AT THE FIRST LEVEL*. accessed 02/10/2019. URL: http://smithsonianchips.si.edu/ice/cd/PKG_BK/CHAPT_09.PDF.

- [61] Masahiro Aoyagi. *Flip-chip Bonding Alignment Accuracy Enhancement using Self-aligned Interconnection Elements to Realize Low-temperature Construction of Ultrafine-pitch Copper Bump Interconnections*. IEEE 64th Electronic Components and Technology Conference (ECTC), 27-30 May 2014.
- [62] Rekha S. Pai. *Flip Chip Bonding Using Sony Anisotropic Conductive Film (ACF) FP1526Y*. 7/29/03.
- [63] *Flip-Chip Technology*. URL: <http://extra.ivf.se/ngl/b-flip-chip/ChapterB1.htm>.
- [64] Young-Ho Kim Sun-Chul Kim. *Review paper: Flip chip bonding with anisotropic conductive film (ACF) and nonconductive adhesive (NCA)*. ELSEVIER Current Applied Physics, 29 May 2013.
- [65] Laura Frisk. *Study of Structure and Failure Mechanisms in ACA Interconnections Using SEM*. Materials Science, 2012.
- [66] Andreas Hierlemann. *Impedance Characterization and Modeling of Electrodes for Biomedical Applications*. IEEE TRANSACTIONS ON BIOMEDICAL ENGINEERING, VOL. 52, NO. 7, JULY 2005.
- [67] E. Warburg. *Ueber das Verhalten sogenannter unpolarisbarer Elektroden gegen Wechselstrom*. Annalen der Physik und Chemie, vol. 67, pp. 493–499, 1899.
- [68] H. Fricke. *The theory of electrolytic polarization*. Philosophical Mag., vol. 7, pp. 310–318, 1932.
- [69] J. E. B. Randles. *Kinetics of rapid electrode reactions*. Discussions Faraday Soc., vol. 1, pp. 11–19, 1947.
- [70] Gustavo Rios. *Nanofabricated Neural Probe System for Dense 3-D Recordings of Brain Activity*. Tech. rep. California Institute of Technology, May 12, 2016.
- [71] Ross M. Walker. *Acquisition of Neural Action Potentials Using Rapid Multiplexing Directly at the Electrodes*. micromachines, 20 September 2018.
- [72] Wikipedia the Free Encyclopedia. *Electroplating*. URL: <https://en.wikipedia.org/wiki/Electroplating>.
- [73] Gamry Instruments. *Electrochemical Impedance Techniques Potentiostatic EIS*. URL: <https://www.gamry.com/application-notes/EIS/potentiostatic-eis-tutorial/>.
- [74] *High efficiency photoelectrochemical water splitting and hydrogen generation using GaN nanowire photoelectrode*. IOPscience-Nanotechnology, 3 April 2013.
- [75] N. A. Nordin; A. J. Jamil; A. S. C. Mat Som; W. F. H. Abdullah; Z. M. Zain; U. M. A Hamid; S. Rani. *Potentiostat readout circuit design for a 3-electrode electrochemical biosensing measurement system*. Tech. rep. IEEE Conference, Shah Alam, Malaysia, 2016.
- [76] Takashi D. Y. Kozai. *A Materials Roadmap to Functional Neural Interface Design*. Advance Fuctional Materials, 19 July 2017.
- [77] S.N. Kukureka D.W.L. Hukins A. Mahomeda. *Accelerated aging for testing polymeric biomaterials and medical devices*. ELSEVIER, Medical Engineering & Physics, 2008.
- [78] Wikipedia the Free Encyclopedia. *Arrhenius equation*. URL: https://en.wikipedia.org/wiki/Arrhenius_equation.
- [79] Cary A. Kuliasha and Jack W. Judy. *In Vitro Reactive-Accelerated-Aging Assessment of Anisotropic Conductive Adhesive and Back-End Packaging for Electronic Neural Interfaces*. IEEE, DARPA sponsored, 2019.
- [80] Cristin G Welle. *Rapid evaluation of the durability of cortical neural implants using accelerated aging with reactive oxygen species*. Journal of Neural Engineering, 28 January 2015.
- [81] *Free radicals and antioxidants in human health: current status and future prospects*. The Journal of the Association of Physicians of India, October 2004.
- [82] *EIS studies of coated metals in accelerated exposure*. Prog Org Coatings, 2003.